THE HENRYK NIEWODNICZAŃSKI
INSTITUTE OF NUCLEAR PHYSICS
POLISH ACADEMY OF SCIENCES

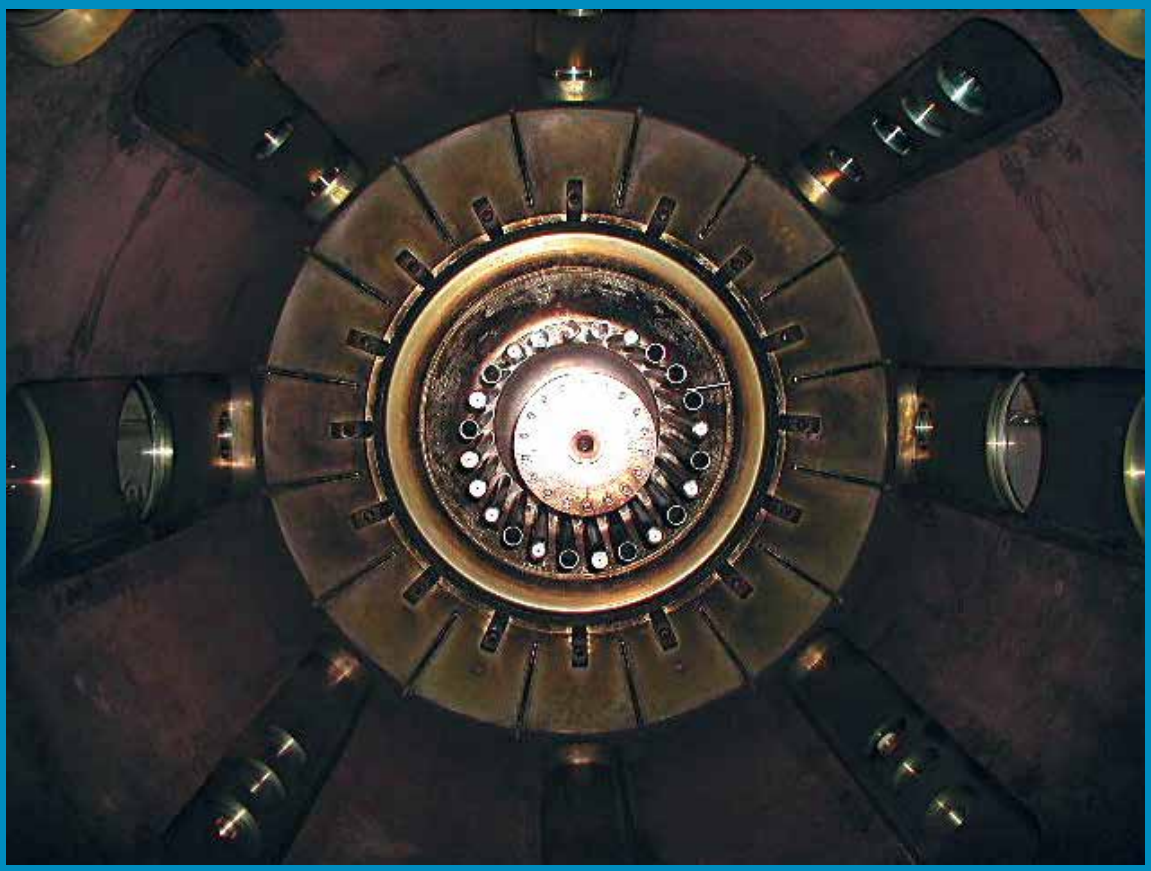

PLASMA-FOCUS
AND CONTROLLED NUCLEAR FUSION

Marek Scholz

PLASMA-FOCUS
AND CONTROLLED NUCLEAR FUSION

Marek Scholz

Translation based on the dissertation entitled "Plasma-Focus and controlled nuclear fusion" ISBN 978-83-63542-24-5, published by the Institute of Nuclear Physics PAN, Kraków 2014

ISBN 978-83-63542-56-6

CONTENTS

INTRODUCTION

The dependence of the binding energy per nucleon on the nucleus mass number known in nuclear physics shows that nuclear energy can *be produced*(emitted) not only in the fission reactions of heavy nuclei, but also in the fusion reactions of light nuclei. In both cases, *the production*(emission) of energy is equal to the increment of the total binding energy. Thus nuclear fusion reactions, in addition to fission reactions, may be the second major source of energy *production* on Earth.

Nuclear fusion reactions take place when light nuclei are brought closer from a distance by nuclear forces, which requires overcoming the electrostatic Coulomb barrier of mutual repulsion of reacting nuclei. As a result, fusion reactions can take place only when the relative kinetic energy E_{kw} of reacting nuclei exceeds the maximum energy of Coulomb barrier $E_{bmax} = Z_1 Z_2 e^2/(4\pi\varepsilon_0 R_0)$, where $Z_{1,2}$ – nucleus mass number, e – elementary charge, and ε_0- dielectric permittivity of vacuum. For characteristic nucleus size $R_0 \approx 5 \cdot 10^{-15}$ m, the energy barrier is equal $E_{bmax} \approx 0.28 \cdot Z_1 Z_2$ MeV. However, due to the tunnel effect, these reactions may occur at much lower relative kinetic energies, E_{kw}, of reacting nuclides than that of the Coulomb energy barrier E_{bmax}. A paper from (Gamow, Teller, 1938) has shown the collision cross-section of the synthesis reaction, taking into account the tunnel effect for energy $E_{kw} < E_{bmax}$.

In the case of hydrogen isotopes, the Coulomb barrier (E_{bmax}) is about 0.28 MeV. This energy, which is much lower when accounting for the tunnel effect, can be provided by an accelerator (beam – target reaction), or may be the result of a very high temperature of the medium, as is found in stars. In the latter case, we are dealing with thermonuclear reactions;

that is, the ones which occur during collisions resulting from thermal motions.

The sub-barrier nature of fusion does not require heating of hydrogen isotopes – deuterium or a deuterium-tritium mixture – to a temperature of 280 keV, which corresponds to about $3 \cdot 10^9$ K (we will specify the temperature in electron-volts and it should be noted that 1 eV corresponds to 11,600 K). The sub-barrier nature of fusion means that the significant rate can be achieved at a much lower energy of thermal motion for deuterium and tritium nuclei, i.e. tens not hundreds of keV (corresponding to a temperature of 10^8 K). Note, however, that even for these "reduced" temperatures, deuterium or a deuterium-tritium mixture is completely ionized, since the ionization potential of hydrogen is just 13.6 eV. Under these conditions, we are dealing with plasma (deuterium or deuterium-tritium), which is a *quasi*-neutral medium containing free electrons and ions behaving collectively.

The average energy of ions in plasma is less than E_{bmax}, but sufficient to ensure that the fusion rate is so high that the produced energy is higher than the energy consumed to generate plasma (i.e. ionize the gas), heat it, and maintain it at a high temperature. In practice, this means that reaching the appropriate temperature of plasma, maintaining it long enough when compared to the average life of reacting particles- in a limited volume with effective thermal insulation – enables the controlled thermonuclear fusion and energy production in such a system.

Confinement of plasma and its insulation from the environment on Earth is much more troublesome than on the Sun or on the other stars, even if we employ fusion reactions occurring in deuterium or a mixture of deuterium and tritium for the production of fusion energy. The pressure of deuterium or deuterium-tritium plasma at a temperature of several tens of thousands of electron-volts, produced as the result of ionization of gas in normal conditions ($n = 2.7 \cdot 10^{25}$ particles/m^3), may amount to up to $5 \cdot 10^{10}$ Pa. Confinement of plasma at such a pressure and temperature using a material wall is virtually impossible. First, the strength of the wall would have to be exceptional for such a large force of pressure; and secondly, the effective thermal insulation becomes problematic in the case of direct contact of plasma with the wall material due to the energy loss resulting from the electron conduction in the contact of plasma with the wall.

It follows that the implementation of controlled thermonuclear fusion on earth will become real if, when keeping temperature at about 10^8 K, we reduce the pressure of plasma to the order of atmospheric pressure, which means that the plasma density should be of the order of $n = 2.7 \cdot 10^{20}$ particles/m^3. Such a low plasma density can be maintained using a magnetic field instead of a material wall. Confinement of plasma inside a strong magnetic field means limiting the mobility of plasma particles in a direction transverse to the field on a microscopic scale; and on a macroscopic scale, plasma, being a diamagnetic material, weakens the magnetic field in the occupied space. In this way gradient of a magnetic pressure holds the plasma in and isolates it from the material wall of the vacuum chamber. In addition, the thermal conductivity of plasma in a magnetic field in a transverse direction is inversely proportional to $(B^2/\mu_0) \cdot \sqrt{T}$, where μ_0 – magnetic permeability of vacuum, which at high values of magnetic induction B and temperature T causes a significant decrease of plasma conductivity, thus making thermal insulation possible.

When applying the effects of a magnetic field on plasma particles, we usually apply two topologies of magnetic field lines. They lead to systems in which the magnetic field lines are open, as in the case of open magnetic traps (mirror, caps, *etc.*) or pinches (θ-pinch, Z-pinch), or closed, as in the case of toroidal systems (tokamak, stellarator, *etc.*).

The concept of magnetic thermal insulation of plasma was tested experimentally for the first time in systems in which the plasma was generated using electric discharge, and confined by the magnetic field originating from the plasma current, with a current of tens of thousands of amperes flowing in cylindrical chambers filled with deuterium, closed by electrodes and with side walls made of dielectric material. The current flowing between the electrodes in such a system initiated and heated a deuterium plasma, and compressed the plasma by the magnetic field, isolating it from the walls of the chamber. This arrangement has been called Z-pinch.

Z-pinch (Fig. 0.1) was, due to its simplicity, intensively studied in the early 50s of the twentieth century in laboratories in the USA, UK, and the former Soviet Union. It has been found during these studies that under certain conditions of deuterium plasma compression, Z-pinch becomes a source of neutrons from fusion reactions of deuterium nuclei, as well as an X-ray source. It seemed that the assumption of a steady nature of this phenomenon, when electrodynamic forces balance the gas-kinetic pressure of plasma in its final stage, was correct. These experiments suggested a quick solution to the problem of a fusion reactor based on linear Z-pinch; especially, considering formula reported by Bennett (Bennett, 1934):

$$I^2=4c^2\,NT \tag{0.1}$$

- where I – current flowing in plasma [MA], N – linear density of plasma [m^{-1}], T – temperature [keV], and c – speed of light [m/s].

Plasma at a density of 10^{23} m^{-3}, through which a current of 1 MA flows, should reach a temperature of about 15 keV. For the temperature the rate of fusion reaches, in the case of deuterium and tritium fusion, the values of the order of 10^{22} m^3/s.

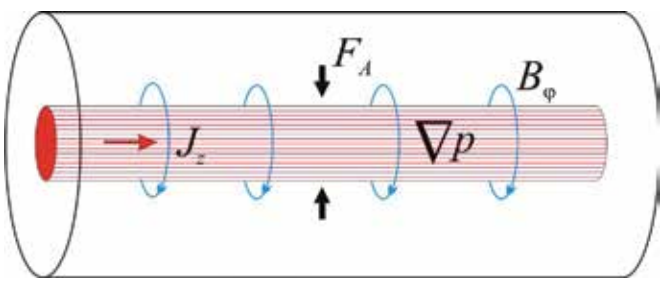

Fig. 0.1. The idea of magnetic confinement of plasma in the Z-pinch system.
F_A – Ampere force, ∇p– pressure gradient in plasma, j_z – z component of the current density vector; B_ϕ – poloidal component of the magnetic field induction vector.

The results of the first experiments in Z-pinch systems, and especially the emission of neutrons (the products of synthesis of deuterium nuclei), suggested that the increase of the current flowing in plasma will further increase the reaction rate, and thus increase the amount of thermonuclear energy produced in fusion. However, further experimental work carried out in these systems has not confirmed this hypothesis, and the results have showed that the increase in current has not resulted in the increased emission of neutrons, which is an indicator of the rate of a thermonuclear reaction. Previous works Anderson et al., (1958); Arcymowich, (1963) list the following main reasons for failure to achieve thermonuclear parameters of plasma and the corresponding fusion rates:

- The emergence of characteristic instabilities (m = 0 or m = 1) resulting in a significant reduction in the lifetime of plasma.
- Low compression and insufficient density of plasma.
- The presence of impurities which have been vaporized from a dielectric chamber wall in plasma, resulting in a significant energy losses from plasma, which then leads to lowering of its temperature, and can lead to repeated electric discharges at the surface of the chamber sidewall, causing a decrease in the current in previously compressed plasma.
- In addition, it was found that the concentration of impurities which evaporated from the dielectric wall of the chamber increased along with increases in current.

In order to solve this problem, a change in the structure of the chamber was proposed, so that the dielectric was replaced with a conductor, e.g. copper. It was assumed that this change would stabilize the plasma in a Z-pinch system, and reduce the presence of impurities from the wall in plasma due to the high thermal conductivity of copper. Since it was not possible to simply replace the chamber wall made of a dielectric which separated the electrodes with a conductor, the dielectric was hidden and moved away from the high temperature plasma while maintaining the characteristic geometry of a Z-pinch, thereby resulting in the structure shown below in Fig. 2.1b. The details of a Z-pinch with metallic walls are shown in Pietrov et al., (1958).

The first experiments (1954 – 1957) carried out at the Kurchatov Institute in Moscow using a system of this design showed a significant increase in the emission of neutrons from deuterium fusion, as compared to the linear Z-pinch. The location of the neutron source was determined using collimators and it was found to be located on the axis of the system in the vicinity of the anode. Furthermore, measurements using magnetic probes showed that the gas discharge starts along the insulator, and the compression of plasma starts at the anode, then extends along the axis of the system and is not strictly cylindrical as in the conventional linear Z-pinch. However, in the end it leads to a configuration of plasma that is typical for such systems. It was noted here that the "cathodic" part of the system hardly affects the phenomenon, and the chamber was divided in two, using only a half in further experiments (Fig. 2.1b). Modification of the linear Z-pinch and testing of plasma compression in a chamber with metallic walls unexpectedly led to the invention of a new type of a system called a non-cylindrical Z-pinch due to the nature of plasma compression. However,

the name Plasma-Focus (PF), derived from the plasma focus formed at the anode, was accepted worldwide.

Parallel to the work carried out by N.V. Filippov at the Kurchatov Institute, a similar plasma focus phenomenon was discovered by J. Mather during research carried out at Los Alamos Institute using a coaxial plasma accelerator which operated at high gas pressure (Fig. 2.1a), the details of which are shown in Mather, (1965).

From that moment on, research on these devices, which later came to be called Filippov or Mather type Plasma-Focus systems, was conducted in different laboratories. The main difference between these two systems lies in the geometry of electrodes; namely, the ratio of the anode diameter to its length, (D/l). In a Filippov-type system $D/l > 1$, while the ratio for Mather geometry is $D/l < 1$. Despite the differences in design, the final characteristics of plasma proved to be very similar as a result of physical processes occurring in these systems.

In the early 1960s, physicists used devices in which they could easily obtain deuterium plasma of high density and high temperature - one of the most intensive fast neutron sources in those days. Moreover, they found that physical processes leading to the formation of a plasma column in Plasma-Focus are very similar regardless of the size of the energy source, which in this case was a capacitor bank; and emission characteristics of plasma significantly depend on the current flowing through plasma. A lot of experimental and theoretical papers were written throughout 50 years of research on plasma produced in PF systems, and the most important results were summarized in various reviews: Bernard et al., (1998); Gribkov and Filippov, (1979); Filippov, (1983); Decker and Wienecke, (1976); Scholz et al., (2004); Sadowski and Scholz, (2008).

Research carried out on PF systems focused on issues related to the physics of the phenomena leading to the generation of plasma with fusion parameters. They tried to find an answer to the question of whether a fusion reactor can be built based on the PF system. Consequently, experiments were conducted which were intended to show that with the increase in current flowing through the plasma, the intensity of fusion reactions increases, e.g. the total emission of neutrons increases in the case of deuterium plasma. A simple Bennett relation (0.1) was a hint here. The size of capacitor banks increased, enabling achievement ofincreasingly intense currents. Although the measurements of anisotropy and the neutron spectrum suggested that the plasma is not in thermodynamic equilibrium, the total neutron emission increased with the fourth power of increase in current; that is, in accordance with formula (0.1). At the end of the 1970s, Plasma-Focus devices began to operate in Europe with a recorded energy of capacitor banks exceeding 0.5 MJ. A Filippov-type device was built at the Kurchatov Institute with a nominal capacitor bank energy of 3 MJ; a system with a nominal capacitor bank energy of 1 MJ was built at the ENEA Institute in Frascati, which operated with two electrode types: Mather and Filippov; while a Mather-type PF device was launched at the University of Stuttgart with a capacitor bank energy of about 0.7 MJ. The results obtained in the course of research using Frascati and Stuttgart systems showed that starting with a certain energy stored in the capacitor bank, i.e. approximately 0.5 ÷ 0.6 MJ, the total emission of neutrons from the plasma focus remained unchanged despite further increases in energy. Such an inhibition of the increase in total neutron emission was ob-

served for the first time in Frascati, and it was thought at the time that the effect was associated with a partial flow of current close to the insulator, which was outside the plasma focus (Gourlan et al., 1978). This was thought to have been the main reason for the inhibition of the increase in total neutron emission from large PF systems. This fact, as well as the finding based on neutron measurements that plasma in the PF system is not in thermodynamic equilibrium, resulted in discontinuation of further development of large PF systems because it was considered not possible to build a fusion reactor with such a configuration. Nevertheless, further researches were done using the Poseidon system at the University of Stuttgart, focusing mainly on the measurement of the emission of neutrons and protons resulting from deuterium fusion reactions. Here too, the inhibition of the increase in total emission of neutrons with increasing energy stored in the capacitor bank was observed. However, changing the conditions of the current flow in the vicinity of the insulator by changing the material of the insulator separating the electrodes showed that it was possible to overcome the effect of saturation of the total neutron emission from plasma (Herold et al., 1989). In addition, a model has been developed describing the conditions for acceleration, confinement and interaction of accelerated deuterons with plasma at the plasma focus based on measurements of proton emission from the (D,D) reaction (Jäger and Herold, 1987).

These experiments have shown that Plasma-Focus systems have not completely exhausted their potential in research related to controlled thermonuclear fusion. Admittedly, the prospect of these systems as energy generation devices seems very limited in the light of current experimental facts, but they enable relatively easy obtainment of the parameters of plasma in which the reactions of fusion of light nuclei occur intensively. This provides an opportunity to study the conditions in which these reactions occur and the emission properties of the products of these reactions in plasma which is not in a thermodynamic equilibrium, as well as the behavior of plasma itself.

The last of the large Plasma-Focus systems, PF-1000, with a capacitor bank energy equal to 1 MJ, was launched at the Institute of Plasma Physics and Laser Microfusion (IPPLM) in Warsaw in the 1990s. Considering the results of the research carried out on systems in Frascati, Stuttgart, and Moscow, the research program was targeted at explaining the phenomena associated with the evolution of deuterium plasma and its impact on the emission of neutrons from plasma, i.e. the course of a deuteron fusion reaction in a plasma focus. The purpose of experiments carried out as a part of this program was to verify results obtained thus far on large PF systems related to the escape of current flowing through plasma; and to show the role of plasma temperature in neutron emission, and the role of epithermal and fast deuterons in the interaction with plasma in the focus. Understanding these processes will enable development, based on a Plasma-Focus device, of intense, pulsed sources of fast neutrons for research related to controlled thermonuclear fusion.

This monograph provides a summary of the experimental work of the author in cooperation with an international team of colleagues, conducted on PF-1000 device.

This textbook shows and summarizes research related to Plasma-Focus systems which will facilitate understanding of important physical processes that determine the behavior of dense conductive plasma confined in Z-pinch geometry. The main objective of this textbook

is to present and explain the role of certain phenomena occurring in plasma generated in a Plasma-Focus which lead to a fusion reaction between light nuclei of hydrogen isotopes. I have also attempted to explain relatively simply the basic topics related to thermonuclear fusion in PF systems, based on experiments conducted using the PF-1000. The nature of nuclear fusion in the PF plasma focus is the main subject of this textbook. Hence the selection of the chapters in the monograph.

The first chapter describes the physical basis for controlled thermonuclear fusion and shows the prerequisites for a nuclear fusion reaction – reaction types, collision cross sections, and rates. In the remainder of this chapter are the basic parameters of the medium in which fusion reactions take place. Physical limitations on the generation of energy from fusion reactions under conditions of magnetic and inertial plasma confinement were estimated based on a zero-dimensional model which takes into account the balance of particles and energy.

The Plasma-Focus system and the physical principles of its operation are described in the second chapter on the basis of experiments and models outlining the behavior of plasma in such a system. The third chapter describes the conditions for a controlled nuclear fusion in a PF device based on the scaling law for PF systems. The fourth chapter is entirely devoted to experimental results obtained in the PF-1000 system and a discussion of these results.

The fifth chapter summarizes the most important topics and problems related to the nature of a fusion reaction in a Plasma-Focus system, as well as final conclusions.

1

PHYSICAL PRINCIPLES OF CONTROLLED NUCLEAR FUSION

Learning the basic conditions under which the controlled thermonuclear fusion of light nuclides can occur, shall enable determination of methods, so that net energy can be produced as a result.

In order to determine the conditions for the production of energy in controlled thermonuclear fusion, let us first consider the fusion reaction itself:

$$A+B\rightarrow(AB)\rightarrow D+E+Q_{AB} \tag{1.1}$$

wherein (AB) is defined as a complex nucleus which decays into D and E. Q_{AB} is the Q -value of the reaction related to the difference in the masses of the products (m_{DE}) and substrates (m_{AB}) of the reaction:

$$Q_{AB}= -(m_{DE} - m_{AB})c^2.$$

The energy of reaction products is determined by kinematics and the nuclear decay energy, with a relatively small share of nuclear excitation and emission of gamma radiation in the process. If the difference of masses is negative ($m_{DE} < m_{AB}$), a predetermined quantity of energy is produced as a result of the reaction - $Q_{AB} > 0$.

Thus, the energy produced per unit of time and unit of volume for a given fusion reaction can be expressed by the following formula:

$$P_f = w_{AB}\, Q_{AB} \ , \tag{1.2}$$

where w_{AB} is the reaction yield expressed by the number of reactions per unit of time and unit of volume, and P_f is the power produced in the unit of volume.

The reaction yield is proportional to the density of colliding particles n_A and n_B, the collision cross-section per reaction σ, and the relative velocity of the particles v_r, defining the stream of colliding particles:

$$w_{AB} = \sigma(v_r)\,(1+\delta_{AB})^{-1}\, n_A\, n_B\, v_r \ , \tag{1.3}$$

where δ_{AB} is the Kronecker delta and is 1 for reactions between identical particles.

Relationship (1.3) describing the reaction yield reflects the nature of binary collisions of two particles (nuclei in this case), where the collision cross-section is a proportionality coefficient for a given velocity v_r, in a very simplified way, assuming that the reacting particles have the same velocity and a specified direction of motion. In the general case, according to the kinetic theory, reacting particles in the described ensemble do not have equal velocities, but the probability of occurrence of velocity within certain limits $(\vec{v}, \vec{v} + d\vec{v})$ is described as the distribution function of $f(\vec{v})d^3v$, which may be different for each type of particle. In this case, densities $n_{A,B}$ in formula (*1.3*) are functions of velocity expressed by $n_{A,B}(\vec{v}_{A,B}) = n_{A,B} f_{A,B}(\vec{v}_{A,B})$, where $f_{A,B}(\vec{v}_{A,B})$ satisfies the normalization condition: $\int_{vA,B} f_{A,B}(\vec{v}_{A,B})\, d^3 v_{A,B} = 1$.

Following by extension of eq. (1.3) for binary reactions over the corresponding velocity spare, we get the general expression for the reaction yield:

$$w_{AB} = (1+\delta_{AB})^{-1}\, n_A\, n_B \int_{vA}\int_{vB} \sigma_{AB}(v_r)\, v_r\, f(\vec{v}_A)\, f(\vec{v}_B)\ d^3 v_A\, d^3 v_B \ , \tag{1.4}$$

where $v_r = |\vec{v}_A - \vec{v}_B|$.

Calculation of the reaction yield in binary collisions of particles A, B, based on relationship (1.4), requires knowledge of the collision cross-section, as it depends on the relative velocity of the colliding particles, as well as knowledge of velocity distributions of these particles. However, it should be noted that the integral in formula (1.4) represents product $v_r\sigma_{AB}$, properly averaged by all components of particle velocities:

$$\langle \sigma v_r \rangle_{AB} = \int_{vA}\int_{vB} \sigma_{AB}(v_r)\, v_r\, f(\vec{v}_A)\, f(\vec{v}_B)\ d^3 v_A\, d^3 v_B \ , \tag{1.5}$$

often defined as the reaction yield coefficient.

Assuming that the reacting particles are in thermal equilibrium, i.e. are described by the Maxwell energy distribution function:

$$F(E) = C \cdot \frac{E^{1/2}}{(kT)^{3/2}} exp\left(-\frac{E}{kT}\right) \quad , \tag{1.6}$$

where C is a constant, and E is their relative kinetic energy, we can find the reaction rate coefficient using formula (1.5) by integrating the product of the collision cross-section and the relative energy of particles in the whole range of the Maxwell energy distribution $0 < E < \infty$:

$$\langle \sigma v_r \rangle_{\mathrm{AB}} = \int_0^\infty \sigma(E) E^{1/2} F(E) dE \quad . \tag{1.7}$$

In order to calculate the integral in formula (1.7), necessary is the knowledge of the relationship between the collision cross-section and energy. If there are no resonances in the energy range which interest us, the most important factor in determining the resulting relationship of the collision cross-section and energy is the probability of a tunnel transition through the potential barrier. Gamow has shown (Gamow and Teller, 1938) that the collision cross-section σ, caused by a tunnel effect, for energy E less than the maximum energy required to overcome the potential barrier E_{max}, is:

$$\sigma(E) = \frac{C_1}{E} exp\left(-\frac{\pi M^{1/2} Z_{\mathrm{A}} Z_{\mathrm{B}} e^2}{\sqrt{2}\, \varepsilon_0 h E^{1/2}}\right) \quad , \tag{1.8}$$

where ε_0 – dielectric permittivity of vacuum, h – Planck's constant, M - reduced mass:

$$M = \frac{m_{\mathrm{A}} m_{\mathrm{B}}}{m_{\mathrm{A}} + m_{\mathrm{B}}} \quad , \tag{1.9}$$

where the maximum energy of the potential barrier is given by:

$$E_{max} = \frac{Z_{\mathrm{A}} Z_{\mathrm{B}} e^2}{4\pi \varepsilon_0 R_0} \quad . \tag{1.10}$$

For the characteristic nuclear size $5 \cdot 10^{-15}$ m, the energy of the Coulomb barrier is $E_{max} \cong 0.28\, Z_A Z_B$ [MeV], which for hydrogen isotopes, i.e. deuterium and tritium, is 280 keV.

By substituting (1.6) and (1.8) to formula (1.7), we have got the expression for the reaction rate coefficient as:

$$\langle \sigma v_r \rangle_{AB} = \frac{const}{T^{3/2}} \int_0^\infty exp\left(- \frac{\pi\, M^{1/2}\, Z_A\, Z_B\, e^2}{\sqrt{2}\, \varepsilon_0\, h\, E^{1/2}} - \frac{E}{kT} \right) dE \quad . \tag{1.11}$$

The integrand in (1.11) is the product of two functions, one increasing with energy, derived from permeability of the potential barrier, and the other decreasing, derived from the Maxwell energy distribution. It follows that the integrand in the expression (1.11) has a maximum. By differentiating the integrand (1.11), one can find the energy E_M for which the reaction rate coefficient is at the maximum:

$$E_M = \left(\frac{\pi\, Z_A\, Z_B\, e^2\, M^{1/2}\, kT}{2\sqrt{2}\, \varepsilon_0 h} \right)^{2/3} \quad , \tag{1.12}$$

where E_M is expressed in Joules.

For the reaction between deuterium and tritium, by expressing the temperature T of deuterium and tritium ions in keV, we can express (1.12) in the following form:

$$E_M \cong 6.6 \cdot T^{2/3}, \text{ where } E_M \text{ is expresed in [keV].} \tag{1.13}$$

If the ions have a temperature of 1 keV, then energy E_M, at which the reaction rate coefficient is at the maximum, will be 6.6 keV; and for the temperature of 10 keV, the maximum reaction rate coefficient occurs at an energy of about 31 keV. Relative energy for which the fusion reaction rate is the highest exceeds the average energy of particles in the Maxwell distribution $(3/2)kT$, and therefore it is in the "tail" of the Maxwell distribution, but it is much smaller than the maximum energy barrier (1.10). This fact is simple in its physical meaning: for collisions with a relative energy of reacting ions of $E << E_M$, which occur much more often, the permeability of the potential barrier is small; but collisions in which $E >> E_M$, for which barrier permeability occurs more often, are rare. Based on these, it follows that collisions of particles with energy less than the energy of the Coulomb barrier (sub-barrier) essentially contribute to the rate of thermonuclear reaction, since the Coulomb barrier permeability is different from zero for small relative energies of the colliding ions. Thus, fusion can occur at temperatures below the Coulomb potential barrier. Assuming the Maxwell distribution of reacting particles, one can find the reaction rate coefficient as it depends on the temperature of ions in the reaction.

Fig. 1.1. shows the reaction rate coefficients for the three basic fusion reactions of (D,D), (D,T), (D, ^{3}He) calculated using data published in (Huba, 2009). Characters <> express averaging after the Maxwell distribution.

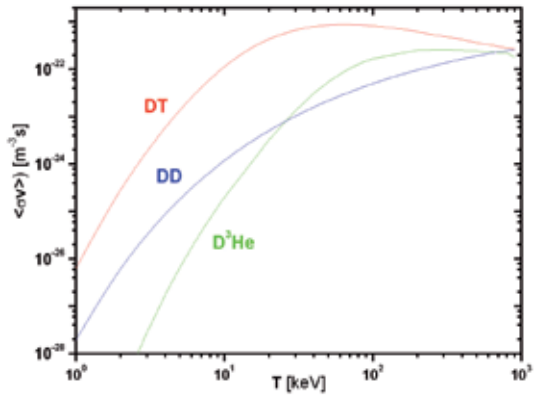

Fig. 1.1. The reaction rate coefficient as a function of ion temperature for reactions of (D,D), (D,T), (D, ^{3}He).

It can be seen that the highest reaction rate coefficient occurs for deuterium-tritium reactions in an energy range of 10 to 100 keV, which in terms of absolute temperature gives a range from 10^8 K to 10^{10} K. At these temperatures, matter exists only in a plasma state and is entirely ionized, being a mixture of positive ions and electrons of such a density that Coulomb forces (long-distance) determine their statistical properties. One can tell in short that plasma is a *quasi*-neutral mixture of positively and negatively charged particles that behave collectively.

Specific thermonuclear systems can vary in methods of creation, confinement, and heating of plasma. However, regardless of the method, fusion reactions initiated in plasma should progress at a rate such that the resulting energy production is higher than the energy used for creation, heating, and confinement of plasma. The system in which this occurs produces net energy, and is called a thermonuclear reactor. This being the case, one can specify plasma parameters, for which net energy production will take place, based on the energy balance of the fusion system. Such a criterion for plasma parameters was formulated for the first time by J.D. Lawson (Lawson, 1957) for a cyclically operating system which maintains plasma in volume V and temperature T within one cycle of duration τ_C.

When defining the criterion, Lawson assumed that the energy of fusion products E_f entirely leaves plasma without affecting its internal energy; and that this energy decrease during the cycle, τ_C , results from radiation only, primarily through bremsstrahlung radiation, for which plasma is transparent, except for processes related to e.g. thermal conductivity. He further assumed that the energy from external sources E_{ex} is used to raise the internal energy of plasma E_t to an appropriate level and maintain it despite losses caused by emission during the cycle, τ_C :

$$E_{exAB} = E_{tAB} + E_{rAB} \ , \tag{1.14}$$

where AB is a type of fusion reaction (e.g. (D,T) – deuterium-tritium reaction).

After the cycle, all the remaining energy of plasma is transferred outside, meaning the system returns to its initial state. The requisite for continuous operation of such a system is the periodicity cycles, which means that the part of the energy transferred outside ($E_f + E_{ex}$) in the course of one cycle will be transformed with an efficiency of η ($0 < \eta < 1$) into energy directly used to initiate the next cycle of system operation, i.e.:

$$\eta\,(E_{f\mathrm{AB}}+E_{\mathrm{exAB}}) \geq E_{\mathrm{exAB}}\ . \tag{1.15}$$

In order to determine plasma parameters for which condition (1.15) is satisfied, it is further assumed that all kinds of plasma particles are in thermal equilibrium in an ideal fusion system (temperature is the same for all types of particles). Furthermore, effects of spatial profiles of particle density in the plasma can be neglected.

The amount of energy produced in a fusion reaction in volume V and time τ_C can be expressed based on (1.2), (1.4), and (1.5), using the following relationship:

$$E_{f\mathrm{AB}} = \frac{n_{\mathrm{A}}\, n_{\mathrm{B}}\, \langle\sigma v_r\rangle_{\mathrm{AB}}\, Q_{\mathrm{AB}}\, V\, \tau_C}{1+\delta_{\mathrm{AB}}}\ , \tag{1.16}$$

where the coefficient $(1+\delta_{\mathrm{AB}})^{-1}$ takes into account the reaction between identical particles.

Using the expression for concentration of fuel ions at low burn-up:

$$n_f = n_{\mathrm{A}} + n_{\mathrm{B}}\ , \tag{1.17}$$

the relationship (1.16) can be represented as:

$$E_{f\mathrm{AB}} = \alpha_{\mathrm{AB}}\, n_f^2\, \langle\sigma v_r\rangle_{\mathrm{AB}}\, Q_{\mathrm{AB}}\, V\, \tau_C\ , \tag{1.18}$$

where:

$\alpha_{\mathrm{AB}} = 1/2,\ n_f = n_{\mathrm{A}} = n_{\mathrm{B}}$ for A = B ,

$\alpha_{\mathrm{AB}} = \xi(1 - \xi),$ for A ≠ B ,

$\xi = n_{\mathrm{A}}/n_f$.

$E_{f\,\mathrm{AB}}$ is expressed in [J], V in [m^3], n_f in [m^{-3}], Q_{AB} in [J], and σv_{r} in [m^3/s] and is the function of temperature (Fig. 1.1).

Bremsstrahlung, is the primary contributor to losses associated with energy radiated from plasma. The radiated power per volume unit of plasma is given by (Huba, 2009):

$$P_{brAB} = b_{br}\, n_e \sqrt{T_e}\, \sum_i n_i Z_i^2 \quad , \tag{1.19}$$

where b_{br} = 1.62·10^{-38}, n_e – electron concentration, T_e – electron temperature of plasma, n_i – concentration of ions with a charge status of Z_i; in this case, i = A, B. If we use expression for the amount of fuel (1.17), the assumption regarding thermal equilibrium of charged plasma particles and quasi-neutrality (n_e=$\sum_i n_i Z_i$), the expression for the energy radiated from plasma in volume V and time τ_C shall be expressed as:

$$E_{brAB} = b_{br}\, \beta_{AB}\, n_f^2 \sqrt{T}\, V \tau_C \quad , \tag{1.20}$$

where:

$\beta_{AB} = [\xi Z_A + (1-\xi)Z_B][\xi Z_A^2 + (1-\xi)Z_B^2]$ for A ≠ B ,

$\beta_{AB} = Z_A^3$, for A = B,

E_{brAB} is expressed in [J], n_f in [m^{-3}], and T in [eV].

The internal energy of plasma, taking into account the expressions (1.17) as before and the assumption of thermal equilibrium is equal to:

$$E_{tAB} = \chi_{AB}\, \frac{3}{2} n_f\, kTV \quad , \tag{1.21}$$

where:

$\chi_{AB} = 1 + \xi Z_A + (1-\xi)Z_B$, for A ≠ B ,

$\chi_{AB} = 1 + Z_A$, for A = B ,

n_f is expressed in [m^{-3}], and kT in [J].

By substituting (1.18), (1.20), and (1.21) to (1.15) and making a simple transformation, we can obtain the relationship between density, confinement time, and plasma temperature which shows for what values of these quantities the fusion system begins to generate energy in subsequent repeated cycles:

$$n_f \tau_c \geq \frac{\chi_{AB}\, \frac{3}{2} kT}{\eta(1-\eta)^{-1}\, \alpha_{AB}\, \langle \sigma v_r \rangle_{AB}\, Q_{AB} - b_{br}\, \beta_{AB} \sqrt{T}} \quad . \tag{1.22}$$

For plasma which is in thermal equilibrium, the reaction rate coefficient $\langle \sigma v_r \rangle$ is a function of temperature, as shown in Fig. 1.1. Consequently, the right side of the inequality (1.22), which is called the Lawson criterion (Lawson, 1957) , depends on temperature and makes sense only within the range of temperatures for which the denominator of the right hand side of inequality (1.22) is greater than zero. In addition, there is no explicit dependence on the characteristic size of plasma, but it can be introduced into this inequality by confinement time τ_C.

Fig. 1.2 represents product $n_f \tau_C$ as a function of temperature T for the two coefficients η and three types of fuel consisting of:

a mixture of deuterium and tritium 50/50 ($\xi = 1/2$), in which there is one reaction:

$$D + T \rightarrow n(14.1\ MeV) + {}^4He(3.5\ MeV)\ ,$$

a mixture of deuterium and helium ^{3}He 50/50 ($\xi = 1/2$), in which there is one reaction:

$$D + {}^3He \rightarrow p(14.7\ MeV) + {}^4He(3.67\ MeV)\ ,$$

deuterium, in which there are two reactions, with approximately equal probability:

$$D + D \rightarrow T(1.11\ MeV) + p(3.02\ MeV)\ ,$$

$$D + D \rightarrow {}^3He(0.82\ MeV) + n(2.45\ MeV)\ .$$

The parameters involved in relationship (1.22) needed to calculate the foregoing fusion reactions are shown in Table 1.1.

Table 1.1. Lawson criterion parameters for the three types of reactions.

Fuel	ξ	α_{AB}	β_{AB}	χ_{AB}	Q_{AB} [J]
(D,D)	-	½	1	2	$1.18 \cdot 10^{-12}$
$(D_{1-\xi}, T_\xi)$	½	¼	1	2	$2.82 \cdot 10^{-12}$
$(D_{1-\xi}, {}^3He_\xi)$	½	¼	3¾	2½	$2.94 \cdot 10^{-12}$

From Fig. 1.2, it follows that the right side of inequality (1.22) has a minimum for a given temperature of fuel, and efficiency η of transformation of energy derived from plasma at the end of the cycle into energy directly used in the initiation of the next fusion cycle. The absolute minimum of this function is the minimum value of $(n_f \tau_C)_{min}$ that we must provide so that the system starts generating energy. We can see that the minimum value of the product depends significantly on the type of fuel, and that it occurs for different temperatures for a given fuel type at a given efficiency of η. Furthermore, for lower values of the η coefficient, the minimum value of the product $(n_f \tau_C)_{min}$ increases.

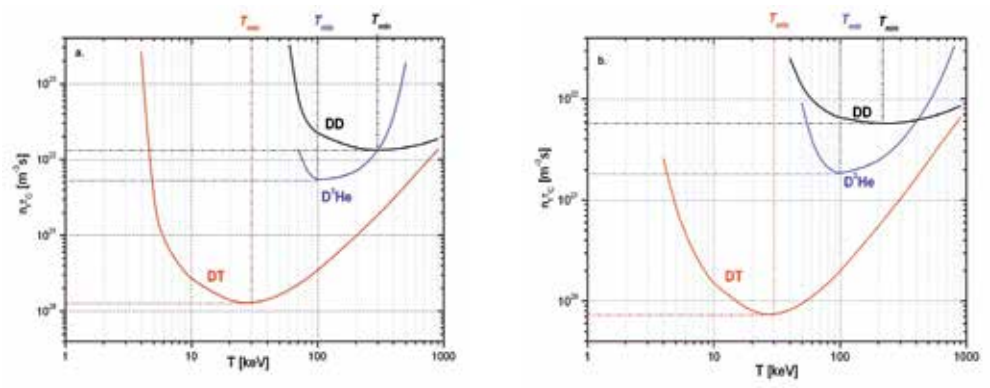

Fig. 1.2. Product $n_f \tau_C$ as a function of temperature for (D,D), (D,T), (D,³He) reactions and coefficients: a) $\eta = 0.2$ and b) $\eta = 0.3$.

Using Fig. 1.2, we can express figures $(n_f \tau_C)$min and corresponding temperatures for three types of reactions, and two coefficients η in a table.

Table 1.2. The temperatures at which $n_f \tau_C$ reaches the minimum values for (D,T), (D,³He), (D,D) reactions and two different values of η.

Reaction	η	T_{min} [keV]	$(n_f \tau_C)_{min}$ [m^{-3}s]	η	T_{min} [keV]	$(n_f \tau_C)_{min}$ [m^{-3}s]
(D,T)	0.2	30	$1.26 \cdot 10^{20}$	0.3	30	$7.27 \cdot 10^{19}$
(D,³He)		100	$5.2 \cdot 10^{21}$		100	$1.8 \cdot 10^{21}$
(D,D)		300	$1.33 \cdot 10^{22}$		220	$5.72 \cdot 10^{21}$

It can be seen that there is an optimum temperature of plasma for which the product of density and the time of its confinement is minimal, depending on the composition of the plasma. The criterion for the production of energy in the fusion system, as shown in graph

Fig. 1.2 and Table 1.2, for temperatures where $n_f \tau_C$ assumes the minimum, means that the system will produce net energy from nuclear fusion if plasma of a given density is sustained at an adequate temperature for such a time Δt that $n\Delta t \geq n_f \tau_C$. It is clear that the easiest way to meet this criterion is to use the mixture of deuterium and tritium as a fuel.

J.D. Lawson, who was the first to derive this criterion, assumed that the fusion system would operate in pulses, but cyclically with a specific cycle time related to the density of confined plasma at a sufficiently high temperature. This criterion can be applied to both systems which sustain low-density plasma during a long period of time, which is characteristic for so-called systems with magnetic plasma confinement; and systems with inertial confinement of plasma of enormous density, though sustained for a very short time. However, as shown in Table 1.2, plasma must still be at a sufficiently high temperature in both cases. This is why the graph now shows the relationship between tempearure and products $Tn_f \tau_C$ or $p_f \tau_C$ where p_f is the pressure of plasma. The condition for above mentioned products can be obtained by multiplying the expression (1.22) on both sides by kT. For example, Fig. 1.3 shows relationship $p_f \tau_C$ and the temperature for reactions (D,D) (D,T), and (D,^{3}He), and coefficient $\eta = 0.3$.

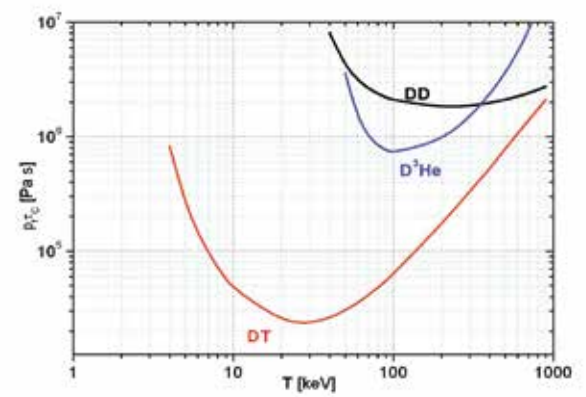

Fig. 1.3. Lawson criterion for the product of the gas-kinetic pressure of plasma and the confinement time as dependent on temperature for three types of reactions and coefficient $\eta = 0.3$

Thus, the condition for production of net energy in a fusion system is defined by the product of the gas-kinetic pressure of plasma and the time of its confinement. Fig. 1.3 shows that in the case of fuel, which is a mixture of deuterium and tritium, for a cycle lasting one second and energy transformation efficiency $\eta = 0.3$, the system begins to generate fusion energy in subsequent, repetitive work cycles if the fuel pressure reaches a quarter of the atmospheric pressure at a temperature of about 30 keV. Cycle time, or the time of plasma sustainment, is associated not only with the escape of particles carrying energy out of the fusion system, but also with the duration of thermonuclear fuel burn-up, it means the kinetics of fusion.

Therefore, it is worth taking a look at the course of fusion reaction kinetics regardless of how we heat and confine the plasma ions. As with deriving the Lawson criterion, suppose a zero-dimensional model in which we neglect the spatial distribution of plasma ions, assum-

ing that they have a uniform distribution in space. With these assumptions, the change in the amount of plasma ions in time is described by the continuity equation:

$$\frac{dn_i}{dt} = (S_i^+ - S_i^-) + (w_i^+ - w_i^-) \quad , \tag{1.23}$$

where n_i – the concentration of ions of a given type S_i^+, S_i^- that are, respectively, the streams of ions flowing in and out of a predetermined volume of plasma, and w_i^+ and w_i^- are the reaction yields, resulting in the emergence and reduction of particles in this volume, respectively. The *i* coefficient is A or B, respectively, so that the relationship (1.23) is in fact a system of differential equations.

If streams of ions flowing in and out of a given plasma volume balance one another: $S_i^+ = S_i^-$, and in the case of the (A,B) reaction: $w_i^+ = 0$, the equations in (1.23) for both A and B ions take the following form:

$$\frac{dn_{\mathrm{AB}}}{dt} = -w_{\mathrm{AB}}^-(t) = -n_{\mathrm{A}}(t)\, n_{\mathrm{B}}(t)\, \langle \sigma v_r \rangle_{\mathrm{AB}} \quad . \tag{1.24}$$

By summing up the equations in the system of equations (1.24), we obtain the equation for the concentration of fuel ions in plasma:

$$\frac{d}{dt}(n_{\mathrm{A}} + n_{\mathrm{B}}) = -2n_{\mathrm{A}}(t)\, n_{\mathrm{B}}(t)\, \langle \sigma v_r \rangle_{\mathrm{AB}} \quad . \tag{1.25}$$

By using the expression (1.17) describing the concentration of fuel ions, we can write the expression (1.25) as:

$$\frac{dn_f}{dt} = -2\alpha_{\mathrm{AB}} \langle \sigma v_r \rangle_{\mathrm{AB}}\, n_f^2(t) \quad , \tag{1.26}$$

where, as previously:

$\alpha_{\mathrm{AB}} = 1/2$, $n_f = n_{\mathrm{A}} = n_{\mathrm{B}}$ for A = B,

$\alpha_{\mathrm{AB}} = \xi(1 - \xi)$, for A ≠ B,

$\xi = n_{\mathrm{A}}/n_f$.

Equation (1.26) is valid in the considered volume of homogeneous plasma under equilibrium conditions for flows $S_i^+ = S_i^-$, for time $0 < t < t_b$, where t_b is the total burn-up time of the fuel ions. The solution to equation (1.26) for a constant temperature of plasma in time, i.e. constant $\langle \sigma v_r \rangle$ has the following form:

$$n_f(t) = \frac{n_{f0}}{1+2\alpha_{AB}\langle \sigma v_r \rangle_{AB} n_{f0} t} \quad , \tag{1.27}$$

where $n_{f0} \equiv n_f(0)$ is the concentration of fuel at the initial moment, $t = 0$.

Equation (1.27) describes the change in the concentration of fuel ions over time as a result of fusion. The amount of energy generated as a result of fusion per unit volume, corresponding to concentration in time $0 < t < t_b$, and for a constant fuel temperature may be expressed by (1.2), (1.4), (1.5), and (1.17), using the following relationship:

$$E_{fAB} = \alpha_{AB}\langle \sigma v_r \rangle_{AB} Q_{AB} \int_0^t n_f^2(\tau) d\tau \quad . \tag{1.28}$$

By integrating the above expression, taking into account (1.27), we obtain:

$$E_{fAB}(t) = Q_{AB} \frac{\alpha_{AB}\langle \sigma v_r \rangle_{AB} n_{f0}^2 t}{1+2\alpha_{AB}\langle \sigma v_r \rangle_{AB} n_{f0} t} \quad . \tag{1.29}$$

The approach to the Lawson criterion, i.e. the production of net fusion energy in a system, can be slightly modified using the above relationship by introducing the definition of energy multiplication coefficient G, which is equal to the ratio of the density of the energy produced by fusion E_{fAB}, to the initial internal energy density of the fuel in the system:

$$G = \frac{E_{fAB}(t)}{\chi_{AB} n_{f0} \frac{3}{2} kT} \quad , \tag{1.30}$$

where, as previously:

$\chi_{AB} = 1+\xi Z_A+(1-\xi) Z_B$ for $A \neq B$,

$\chi_{AB} = 1+Z_A$ for $A = B$.

The initial internal energy is the energy of fuel heated to temperature T at the moment of starting the thermonuclear burn-up process. The capability of net energy production in the fusion system enables us to determine by how much the energy from fusion exceeds the internal energy of fuel in the form of plasma when the burn-up process starts. The boundary condition $G = 1$ specifies the "*break-even*" point of the system from the viewpoint of net

energy production. Neither of the existing fusion systems, both with magnetic and inertial plasma confinement, have yet reached this condition.

Usually the energy multiplication condition is defined more rigorously by taking into account energy loss during burn-up:

$$G = \frac{E_{f\mathrm{AB}}(t) - E_l(t)}{\chi_{\mathrm{AB}}\, n_{f0} \frac{3}{2} kT} \quad , \tag{1.31}$$

where E_l mainly denotes, as before, losses due to bremsstrahlung radiation from plasma described in formula (1.19). By using expression (1.17) for the amount of fuel and assuming thermal equilibrium of charged plasma particles, the expression for energy radiated per unit volume of plasma in time *t*, resulting from bremsstrahlung radiation, can be expressed as:

$$E_l = E_{br\mathrm{AB}}(t) = b_{br} \beta_{\mathrm{AB}} \sqrt{T} \int_0^t n_f^2(\tau) d\tau \quad , \tag{1.32}$$

where, as previously:

$\beta_{AB} = [\xi Z_A + (1-\xi) Z_B][\xi Z_A^2 + (1-\xi) Z_B^2]$ for A ≠ B,

$\beta_{AB} = Z_A^3$, for A = B.

After integrating (1.32), we obtain:

$$E_{br\mathrm{AB}}(t) = \frac{b_{br}\, \beta_{\mathrm{AB}}\, \sqrt{T}\, n_{f0}^2\, t}{1 + 2\alpha_{\mathrm{AB}} \langle \sigma v_r \rangle_{\mathrm{AB}}\, n_{f0}\, t} \quad . \tag{1.33}$$

By substituting (1.29) and (1.33) for (1.31), we get the expression for the effective energy multiplication coefficient:

$$G = \frac{[Q_{\mathrm{AB}}\, \alpha_{\mathrm{AB}} \langle \sigma v_r \rangle_{\mathrm{AB}} - b_{br}\, \beta_{\mathrm{AB}} \sqrt{T}] n_{f0}\, t}{(1 + 2\alpha_{\mathrm{AB}} \langle \sigma v_r \rangle_{\mathrm{AB}}\, n_{f0}\, t) \frac{3}{2} \chi_{\mathrm{AB}} kT} \quad . \tag{1.34}$$

We can use formula (1.34), as in the case of the Lawson criterion, to find the condition for achieving "*break-even*" by giving *G* a value of one and making simple transformations to obtain the following relationship:

$$n_{f0} t = \frac{\frac{3}{2} \chi_{\mathrm{AB}} kT}{\alpha_{\mathrm{AB}} \langle \sigma v_r \rangle_{\mathrm{AB}} [Q_{\mathrm{AB}} - 3\chi_{\mathrm{AB}}\, kT] - b_{br}\, \beta_{\mathrm{AB}} \sqrt{T}} \quad , \tag{1.35}$$

where the parameters α, β, χ, Q in relationship (1.35) for (D, T), (D, D) and (D, ^{3}He) fu-

sion reactions are shown in Table 1.1. Just as in relationship (1.22), the right side of (1.35) is a function of temperature, so that the condition for „*break-even*" can be shown on a graph as a function of temperature for the three selected fusion reactions as before (Fig. 1.4).

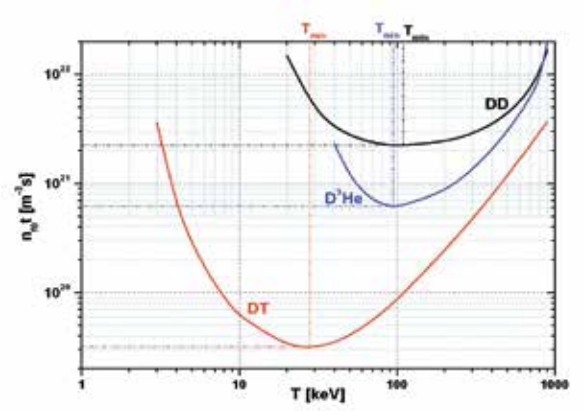

Fig. 1.4. The „break-even" (G = 1) condition for (D,D), (D,T), and (D,³He) fusions as a function of plasma temperature

The figure shows that in the same way as for the previously derived Lawson criterion (1.22), we have different minimum value of product $n_{f0}\,t$ for each reaction at a given temperature. The minimum values $(n_{f0}\,t)_{\min}$ required to achieve „*break-even*" for the three selected reactions are, respectively:

(D,D) $(n_{f0}\,t)_{\min} = 2.23 \cdot 10^{21}$ [m^{-3}s] at a temperature of $T_f = 110$ keV;
(D,^{3}He) $(n_{f0}\,t)_{\min} = 2.16 \cdot 10^{20}$ [m^{-3}s] at a temperature of $T_f = 95$ keV;
(D,T) $(n_{f0}\,t)_{\min} = 3.17 \cdot 10^{19}$ [m^{-3}s] at a temperature of $T_f = 28$ keV.

Both the Lawson criterion and *G* condition associated with the multiplication of energy in a fusion system show that production of energy in the system requires an optimum fuel temperature, for which the product of fuel confinement time to its density is minimal. The density of the fuel, and therefore its pressure, is lower if we can maintain it at this temperature for a longer period, allowing the highest level of burn-up; that is, enabling as many fusion reactions as possible to occur. The derived relationships also show what kind of fuel is necessary in order to make meeting these criteria as easy as possible.

The problem of maintaining fuel at a proper density and a temperature of several tens of thousands of electron-volts is closely connected with its burn-up, described by the kinetics of fusion reactions. Taking this into consideration, we can achieve appropriate fuel burn-up not only by isolating it and keeping it away from the walls of the reactor chamber for an adequate time, but also by relaxing its confinement and allowing it to expand freely, if only it has an appropriate density, size, and temperature at the beginning of the explosion. The specific "Lawson criterion" for the production of energy in such a fusion system, connecting these

three values, can be derived using relationship (1.30), which after substitution with (1.29) and simple transformations, will take the following form:

$$n_{f0}t = \frac{G\,\chi_{AB}3kT}{2\alpha_{AB}\langle\sigma v\rangle_{AB}Q_{AB}\left(1-\frac{G\,\chi_{AB}3kT}{Q_{AB}}\right)} \quad . \tag{1.36}$$

Assuming that time t in the formula is the time of fuel expansion $t_{ex} = r_s/\ _{ex} = r_s/\sqrt{3kT/\overline{m}_f}$, we can write condition (1.36) as:

$$n_{f0}r_s = \frac{G\,\chi_{AB}3kT\sqrt{3kT/\overline{m}_f}}{2\alpha_{AB}\langle\sigma v\rangle_{AB}Q_{AB}\left(1-\frac{G\,\chi_{AB}3kT}{Q_{AB}}\right)} \quad , \tag{1.37}$$

where r_s is the initial radius of the compressed fuel, v_{ex} is the expansion rate, $\overline{m}_f = m_A\,\xi + m_B\,(1-\xi)$ (for A ≠ B) and $\overline{m}_f = m_A$ (for A = B) is the averaged mass of fuel particles, excluding the mass of an electron, and T is the temperature of the plasma.

For the $G = 1$ condition ("*break-even*"), we can find the relationship between the product of the concentration and the size of the compressed fuel as it corresponds to the temperature (Fig. 1.5).

This method of plasma "confinement", wherein we allow for free expansion of plasma at an appropriate density, size, and temperature, during which the appropriate fuel burn-up takes place, is called inertial plasma confinement.

Fig. 1.5 shows the "*break-even*" condition for a system with inertial plasma confinement. In contrast to previously derived criterion (1.35), losses resulting from bremsstrahlung radiation of plasma were omitted here.

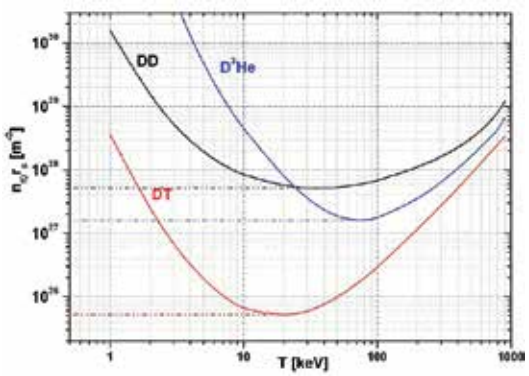

Fig. 1.5. The "break-even" (G = 1) condition for (D,D), (D,T), and (D,³He) fusions as a function of plasma temperature for the inertial plasma confinement

Fig. 1.5 shows, like in the previous one, that for different types of fuel at a predetermined temperature, we obtain the minimum values of product $n_{f0}\,r_s$, which in the case of a mixture of deuterium and tritium will be $n_{f0}\,r_s = 5.18\cdot10^{25}$ m^{-2}, and in the case of deuterium fuel will be $n_{f0}\,r_s = 5.2\cdot10^{27}$ m^{-2}.

These considerations of fusion systems can be summarized by saying that the key processes leading to the production of net energy are: first, ionization and heating fuel to a high temperature in order to ensure a favorable reaction rate; and second, confinement of fuel for a period of time long enough to obtain a net energy yield from the system. The boundary condition for such systems, called "*break-even*", shows the relationship between the concentration of fuel particles, confinement time, and temperature (Fig. 1.4, 1.5). It follows that for plasma maintained for 1 s at dozens of keV, the particle concentration should be of the order of $10^{19} \div 10^{21}$ m^{-3}, as shown in Fig. 1.4. In contrast, in the case of inertial confinement of plasma of size r_s = 1 mm, the concentration of plasma particles should be of the order of $10^{28} \div 10^{30}$ m^{-3}, and the time of confinement at a temperature T of 10 ÷ 30 keV would be about 10^{-9} s.

These considerations show two ways to achieve the goal of producing net energy from a thermonuclear fusion reaction. In the first, we achieve such a concentration and temperature of plasma that intensive fusion reactions take place in it during hydrodynamic expansion. This method is called inertial confinement. In the second, plasma at a temperature of several dozens of keV is isolated from the material walls and maintained for a relatively long time (a few seconds), but with a significantly lower concentration of particles. The range of concentrations and time of confinement of plasma particles for these two methods is schematically shown in Fig. 1.6.

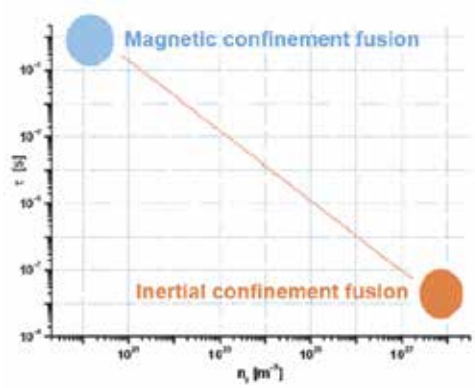

Fig. 1.6. Magnetic and inertial plasma confinement. The range of densities and confinement time of plasma

We can keep the plasma away from the material walls using a magnetic field. This is related to the fact that plasma state is a state of moving charged particles, electrons and ions. The magnetic field for plasma confinement can be generated by a system of current conductors (e.g. as in a stellarator) and it can be generated by the current flowing into a plasma (e.g. Z-pinch), or a superposition of the magnetic field generated by the plasma current and field produced by the system of current conductors (e.g. tokamak). This method is called magnetic plasma confinement.

An important indicator of the confinement of plasma in a magnetic field is the ratio of the plasma kinetic pressure $p_{kin} = \chi_{AB}\, n_f kT$ to the pressure of the magnetic field $p_{mag} = B^2/2\mu_0$, where μ_0 is the magnetic permeability of a vacuum. This ratio is defined as β which is a

measure of how efficiently the magnetic field maintains plasma particles, being in thermal motion, in a given volume, which can be expressed as:

$$\beta_{max} \frac{B^2}{2\mu_0} \geq \frac{3}{2} \chi_{AB} n_f kT \quad , \tag{1.38}$$

where $\chi_{AB}=1+\xi Z_A+(1-\xi)\, Z_B$ for $A \neq B$,

$\chi_{AB}=1+Z_A$ for $A = B$,

n_f is expressed in [m^{-3}], and kT in [J].

In this way, the maximum pressure of plasma is determined by the achievable magnetic field.

The simplest system of magnetic confinement of plasma is the pinch, where the magnetic field of the current in plasma causes compression and confinement.

2

PHYSICS OF THE PLASMA-FOCUS SYSTEM

The concept of magnetic plasma confinement was examined experimentally for the first time in systems in which plasma was produced by an electrical discharge in gas. It was confined by the magnetic field coming from the plasma current at tens of thousands of amperes. Electric discharges were conducted in cylindrical chambers in which the current flowed along the z axis of the cylinder (hence the name – Z-pinch). The side walls of the cylinder were made of a dielectric in these first experiments. The idea was quickly abandoned because of the achieved plasma parameters and a low emission of neutrons from (D,D) fusion reactions. The chamber design was changed by placing the insulator away from the plasma using metallic (conductive) side walls of the cylinder (Pietrov et al., 1958). Thus, a new system was made in which the emission of neutrons from plasma located in the vicinity of the anode increased significantly. The cathode part of this system had not affected the phenomenon, so it was abandoned. The system was called a non-cylindrical Z-Pinch due to the nature of plasma compression, but the name Plasma-Focus (PF), derived from the plasma focus formed at the anode, was adopted in literature. A similar phenomenon of plasma focusing was discovered by J. Mather (Mather, 1965) when using a Marshall-type gun (coaxial plasma accelerator). From that moment on, research on these two types of devices, which later came to be called Filippov (Filippov et al., 1962) or Mather type Plasma-Focus systems, were conducted in different laboratories.

2.1. PLASMA-FOCUS PRINCIPLE OF OPERATION

A typical arrangement of Plasma-Focus (PF), regardless of whether it is a Filippov or Mather type of system, consists of the following basic elements (Fig. 2.1):

Capacitor bank with the capacity of C_0, which stores electrical energy.

Electrical circuit containing low-inductive spark gaps, *Is*, and cables between the bank and the current collector.

An anode (1) separated from a cathode (2) by a cylindrical insulator (3) in the vacuum chamber (4).

A vacuum chamber often is used as the cathode in the Filippov system. The chamber, after reaching a high vacuum (of the order of 10^{-3} Pa), is filled with different types of gases depending on the nature of the experiments. In experiments relating to thermonuclear fusion, the chamber is filled with deuterium, and sometimes a low admixture of an inert gas (e.g. argon) is added for diagnostic purposes.

The PF system can be represented as an RLC circuit, in which the electrical energy initially stored in the capacitor bank, with a capacity of C_0, changes into the magnetic field energy of the current during shaping, separation from the insulator, and acceleration of the current sheath along the electrodes.

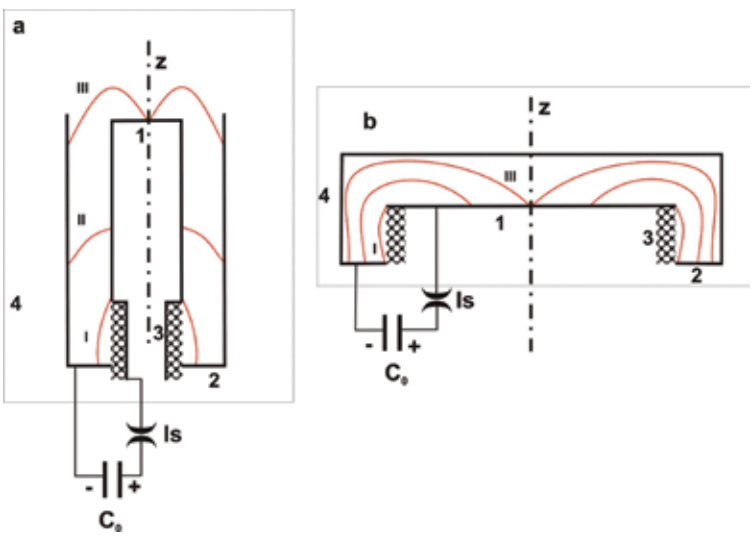

Fig. 2.1. Diagram of Mather (a) and Filippov (b) type Plasma-Focus (PF) systems;
1 – anode, 2 – cathode, 3 – insulator, Is – spark gap, C_0 – power supply (capacitor bank).
I – discharge phase, II – acceleration phase (Mather-type system only), III – radial movement of the layer and creation of the plasma focus.

After triggering of the spark gap (Is, Fig. 2.1), voltage from the power source, i.e. the capacitor bank, grows on the electrodes causing electrical discharge in the gas along the insulator where the plasma layer is formed and wherein increases the current of the electrical discharge (phase I). An current sheath is formed, then detaches from the insulator under the Ampere force and ionizes and sweeps the gas like a snow-plow while accelerating along the electrodes. This phase (II) of the phenomenon is characteristic of the Mather type of electrodes and does not occur in the Filippov system. In this phase, current builds up, and if the electrodes of the system (the load) are matched to the power source, the current reaches its maximum after the current sheath reaches the end of the anode. This is where the axial component of the current density in the sheath begins forming the azimuthal component of the magnetic field B_θ. Field B_θ causes movement of this part of the current sheath towards the axis of the electrodes (phase III), which results in compression and heating of the plasma. The plasma focus is formed on the axis of the anode with a high particle concentration of 10^{19} particles/cm^3, heated to a high temperature of the order of one keV. In this phase, the current density j_z reaches a value of more than 10^7 A/cm^2, then results in the development of current instabilities, an anomalous increase in resistivity of plasma, and a decrease of current. It is followed by a rapid dissipation of the magnetic energy of the current into plasma. Characteristic times related to the dynamics of the final stage of this phenomenon take values from several to hundreds of nanoseconds. Dissipation of the magnetic energy and the associated space-time dynamics of the current sheath are correlated with the emergence of accelerated charged particles, electrons and ions, hard X-ray pulses, as well as neutron radiation pulses if the working gas is deuterium.

The equivalent electrical circuit of the Plasma-Focus device, taking into account its components and allowing for an approximate description of its processes, is shown in Fig. 2.2 (Scholz et al., 2004).

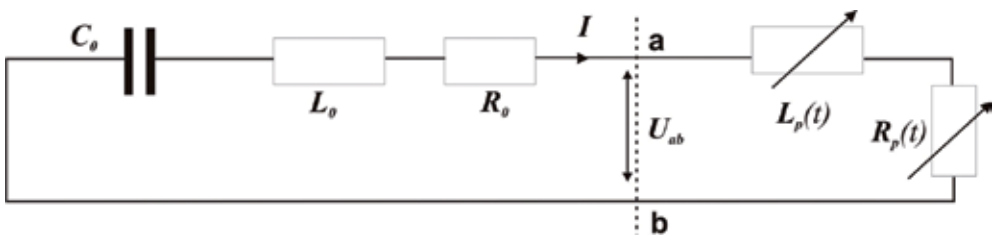

Fig. 2.2 The equivalent electrical circuit for the discharge in Plasma-Focus. U_{ab} voltage between electrodes, C_0, L_0, R_0, capacitance, inductance, and resistance of the power source, respectively, Lp– inductance related to the movement of the electric current sheath, R_p – plasma resistivity in ohms.

According to the generalized Ohm's law, equations describing current and voltage waveforms in such a circuit can be formulated by the following expressions:

$$U_0 - \frac{1}{C_0}\int I\,dt - L_0\frac{dI}{dt} + R_0 I = U_{ab}(t) \quad , \tag{2.1}$$

where I – discharge current, R_0 – resistance internal resistance of the power source, C_0 – capacitance of the capacitor bank, and U_0 – capacitor bank charging voltage. L_0 represents the sum of inductances of the capacitor bank, collector, and the anode-insulator junction, and U_{ab} is expressed by the formula:

$$U_{ab} = \frac{d(L_p I)}{dt} + R_p I \quad , \tag{2.2}$$

where R_p is the resistivity of the current sheath, and L_p – inductance related to the movement of the electric current sheath along the electrodes, ranging from 0 to L_{pmax}.

This description merely shows that a PF system consists of a power source (points a, b), and a load i.e. electrodes. The voltage U_{ab} varying in time is the voltage on the electrodes of the PF. Typical voltage and current waveforms in the PF system are shown in Fig. 2.3.

The effective transfer of energy from the power source to the load (electrodes) with the moving electric current sheath (which should create a plasma focus with parameters enabling fusion reactions), has to match the parameters of the source and the load.

a)

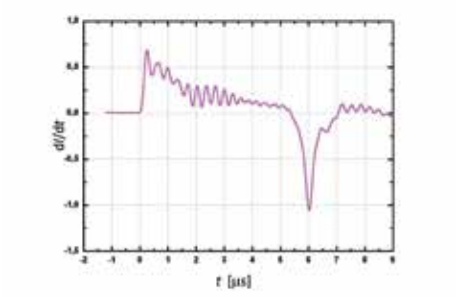

b)

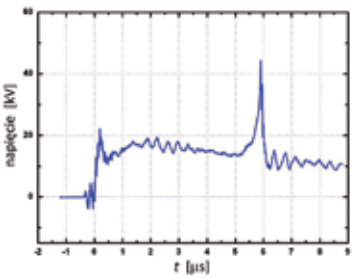

c)

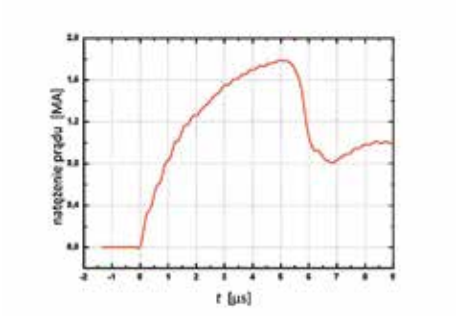

Fig. 2.3 Typical voltage and current characteristics of a discharge in a Plasma-Focus,
a) a derivative of the discharge current (relative units),
b) the voltage across the electrodes,
c) the discharge current.

The matching condition for the Mather-type PF can be formulated, assuming that the current in the circuit reaches a maximum when the radial compression starts in the electric current sheath. The condition formulated in this way seems to be a good approximation because first, the compression phase of the electric current sheath lasts much shorter than the phase of its acceleration along the electrode; and second, the final plasma parameters according to the Bennett relationship represented by formula (0.1) depend on the square of current.

The time for which there is maximum discharge current is equal to one-fourth of the period, and is expressed as:

$$\tau_m = \frac{T}{4} = \frac{\pi}{2}\sqrt{L_0 C_0} \quad . \tag{2.3}$$

On the other hand, the beginning of a radial acceleration of the current sheath is equal to the time it takes to reach the end of the electrodes, namely:

$$\tau_{ac} = \frac{l}{v_{CS}} \quad , \tag{2.4}$$

where l is the length of the electrodes, and v_{CS} – the mean speed of the electric current sheath which can be described by the relationship: $v_{CS} = a_{CS}\tau_{ac}$, where a_{CS} – the mean acceleration of the sheath. Assuming that the mean acceleration is proportional to the pressure of the magnetic field pushing the electric current sheath, and inversely proportional to the mass of gas completely swept by the sheath (a snow-plow model), it can be expressed as:

$$a_{CS} \cong const\ \frac{B_\theta^2}{p_0\, l} \cong const\ \frac{I_m^2}{r_A^2\, p_0 l} \quad , \tag{2.5}$$

where I_m– the amplitude of the discharge current, r_A – the radius of the anode, and p_0 is the initial pressure of the working gas in the vacuum chamber.

By substituting expression (2.5) for (2.4), and assuming, according to the matching condition $\tau_m = \tau_{ac}$, and expressing the current amplitude by $I_m = U_0(C_0/L_0)^{1/2}$, we obtain:

$$\frac{U_0^2\, C_0^2}{r_A^2\, p_0\, l^2} \cong const \quad . \tag{2.6}$$

The matching condition, now expressed by relation (2.6), combines the parameters of the power source (U_0 and C_0), the geometry of the load (r_A and l), and the pressure of the working gas p_0. The capacity of the capacitor bank and the geometry of the electrodes are usually fixed in PF systems because it is difficult to change these components. It is much easier to adjust the charge voltage or the working gas pressure. However, in practice, the working gas pressure can only be changed in a very limited way. Regardless of the energy of the capacitor

bank in existing PF devices, the pressure of the working gas in these systems ranges from one to a maximum of $1.33 \cdot 10^3$ Pa. After exceeding these pressures, the plasma compression collapses, and the density and temperature of the plasma in the PF focus rapidly drop. This is related to the phenomenon of gaseous breakdown in the electric field, which should lead to the creation of a uniform and symmetrical electric current sheath along the insulator separating the electrodes of the PF system.

Although matching condition (2.6) is approximate, it allows us to draw some conclusions; namely, that we can obtain the matching condition only for a small range of power source parameters and gas pressure within the particular geometry of the electrodes of the system. In addition, the variable inductance of the system associated with the velocity of the current sheath cannot be less than the inductance set by the geometry of the electrodes.

Condition (2.6) enables matching of the power source parameters (capacitor bank) to inductance of the load (geometry of electrodes), so that we can reach the maximum value of the amplitude of the current flowing in the system. The role of variable inductance of electrodes can be shown by transforming equations (2.1) and (2.2) into:

$$\left(L_0 + t\frac{dL}{dt}\right)\frac{dI}{dt} + \left(R_0 + \frac{dL}{dt}\right)I + \frac{1}{C_0}\int I\,dt = U_0 \quad , \tag{2.7}$$

where dL/dt is a derivative of the inductance and for the cylindrical electrodes of the PF system equals:

$$\frac{dL}{dt} = \frac{\mu_0}{2\pi} v_z ln\left(\frac{r_K}{r_A}\right) \quad . \tag{2.8}$$

In equation (2.8), r_K is the radius of the cathode, and v_z – velocity of the electric current sheath along the system electrodes. The Bessel function of the first kind is the solution to equation (2.7) (Mather, 1965) assuming that $R_0 = 0$.

This paper shows on the chart (Fig. 2.4) $I(t)/I_m$ versus reduced time $t/2\pi\sqrt{L_0 C}$, wherein $I_m = U_0\sqrt{C/L_0}$ (Formula 2.5) shows that as the value of $(dL/dt)/(2\sqrt{L_0/C}$ increases, the ratio $I(t)/I_m$ decreases; that is, the smaller the value of dimensionless parameter $(dL/dt)/(2\sqrt{L_0/C}$, the greater the amplitude of the current we can obtain in the system. In conclusion, it seems that for a given fixed derivative of inductance dL/dt, an increase in amplitude of the current in the circuit can be obtained by reducing inductance L_0.

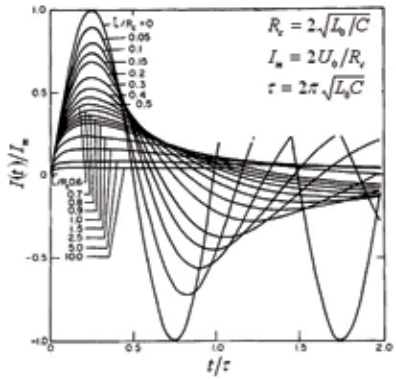

Fig. 2.4 The normalized current waveform $I(t)/I_m$ versus a dimensionless variable describing time t/τ, for different values of parameter L/R_c, where $L=dL/dt$, calculated using equation (2.7),(Mather, 1965).

Unfortunately, it turns out that in practice, this method aimed at increasing the amplitude of the current in the PF system does not, in fact, ensure that the final plasma parameters are consistent with the Bennett relation. This is due to the fact that no distinction was made in many experimental studies between the total current from the power source flowing in the system, and the current flowing in the pinch (plasma focus) during the phase of its maximum compression, the latter being used in the laws for scaling Z-pinch systems. The total current is usually measured using a Rogowski coil in the device's collector, i.e. before the electrodes in the experiments, and is not necessarily equal to the current in the plasma focus region. Measurements using magnetic probes showed (Gourlan et al., 1978) that a substantial part of the current can flow out of the plasma focus, e.g. remain at the insulator (Fig. 2.5), or flow outside the current sheath during its movement through the channels caused by repeated gaseous breakdowns between the electrodes.

It can be concluded on this basis that PF system optimization is not just about choosing parameters of the power source and electrodes so that the amplitude of the total current flowing through the system is at its maximum, but about organizing the course of initial phases of discharge so that the total discharge current flows into the plasma focus during its maximum compression. Unfortunately, due to the variety of processes associated with the formation of a current sheath, there is no single theoretical model to describe a situation in which the total current in the PF system flows through the plasma focus. The solution to this problem is based rather on experimental knowledge and experience gained as a result of years of research done on these devices.

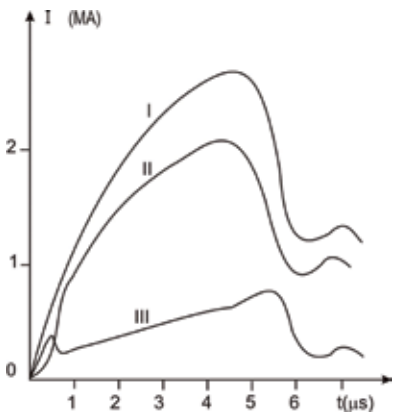

Fig. 2.5 The flow of current between the electrodes of the PF system in Frascati, I – total current in the system, II – reverse current, III – insulator surface current (Gourlan et al., 1978).

Analysis of Eq. (2.7) shows that during the breakdown and formation of the electric current sheath, $L \cdot dI/dt$ dominates, where $L = L_0$, and $I \cdot dL/dt$ during the phase of acceleration and radial compression. This results in a sheath velocity of the order of tens of thousands of m/s, a current at about 1 ÷ 2 MA, and a voltage between the electrodes at kilovolts in the acceleration phase. During compression, with a significant increase in velocity of up to several thousand m/s, there is a sudden voltage spike which is associated not only with inductance, which varies in time, but also with the increase in resistance induced by the development of kinetic instabilities in the plasma focus. At the same time, dissipation of current energy occurs, resulting in a significant jump in the current derivative and decrease in its value. The occurrence of distinct peaks (Fig. 2.3) in the current and voltage characteristics is one of the basic criteria which indicates a good transition of energy to the plasma focus in the PF device.

To sum up, we can say that achieving a high density and temperature of plasma in the focus means that the current sheath will be at its maximum velocity before the final pinching, and the whole allowable current in the PF system will flow in the plasma focus; that is, until achieving a maximum transformation efficiency of the electricity stored in the capacitor bank into kinetic energy of the sheath and the magnetic field around the focus. It seems that this is a prerequisite for the occurrence of thermonuclear reactions with great intensity in the plasma focus. It should be noted, as shown in the experiments, that achieving this condition requires the course of formation and acceleration of the current sheath be optimal with regard to structure, final velocity and efficiency of gas sweeping.

2.2. FORMATION OF THE CURRENT SHEATH

Basic processes leading to the formation of the conductive current sheath can be represented using a description of the characteristic phenomena for a discharge in gases. It should be noted that the electrical gaseous breakdown occurs within a specific geometry of electrodes (insulator length <10cm), for pressures ranging from $1.3 \cdot 10^2 \div 1.0 \cdot 10^3$ Pa, and voltage at the capacitor bank of over 16 kV, which is well above the voltage resulting from Paschen's law.

At the beginning of the discharge process, after the spark gap operation, and after voltage appears at the electrodes, the electrode geometry determines the electric field distribution in the gas between the electrodes. Initially, the value of this field is the largest on the cathode – insulator boundary (Fig. 2.6), and even though gas ionization with an electric field takes place in the whole area, development of the ionization wave is the fastest along the insulator, causing the formation of a small layer of ionized medium with a low degree of ionization and cylindrical symmetry, short-circuiting the cathode and anode (Scholz et al., 2005).

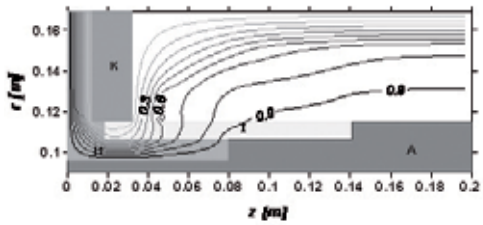

Fig. 2.6 Distribution of equipotential lines of the electric field potential between the electrodes of the PF-1000 system (IPPLM). A –anode, K – cathode, I – insulator (Scholz et al., 2005). The values indicated on equipotential lines were normalized to the anode potential. The cathode potential is equal to zero.

Resistance of this short-circuiting layer of the electrode decreases with increasing concentration of electrons n_e, caused by gas ionization. This increase in the concentration of electrons in the layer can be described using a simple model in which the change in the number of electrons N_e in time per unit of length of the layer is described by the formula (Braginski, Migdal, 1958):

$$\frac{dN_e}{dt} = \frac{\tilde{R}I^2}{\varepsilon} \quad , \tag{2.9}$$

where $\tilde{R}$ – resistance per unit length of the electric current sheath, I – the current in the sheath, and ε is the mean energy required to ionize one atom with the release of one free electron.

In (Braginski, Migdal, 1958) it is assumed that ε = 100 eV which is also the average value of energy necessary for the ionization of one hydrogen atom (which comprises the energy utilized for ionization (13.6 eV)), excitation, and mean energy required for heating the electron to the temperature of plasma. Resistance $\tilde{R}$ is related to N_e as in: $\tilde{R} = \frac{m_e}{e^2 N_e \tau_{ea}}$, where m_e, e is the mass and charge of the electron and τ_{ea} is the time between the electron--atom collisions.

As the result of ionization and increase in N_e, there is a sudden drop in resistance $\tilde{R}$, which lasts from dozens to hundreds of nanoseconds depending on the scale of the device. Consequently, thin conductive plasma layer appears near the surface of the insulator, which detaches from the insulator under the Ampere force and moves with the acceleration along the electrodes. During its movement, the electric current sheath ionizes and sweeps the working gas filling the vacuum chamber as a result of the resonant charge exchange. In the ideal case, the azimuthally homogeneous plasma layer should form with a uniform current distribution. In reality, this ideal description of the processes is highly simplified, because it is affected by the nature of the insulator–cathode junction, the kind of insulator material, the nature of the insulator–anode connection, etc. All these design elements affect the distribution of electric fields and the course of gas ionization. One can try to influence them by using, for example, a cathode in the shape of a blade resulting in accumulation of an electric field right at the cathode (Borowiecki and Czekaj, 1985).

In order to find the optimal conditions for formation of the electric current sheath, various insulator materials have also been used, e.g. borosilicate glass or Al_2O_3. It was found that an aluminum oxide insulator provides good results, especially when a thin layer of material from the electrodes is deposited on it during discharge, resulting in equalization of the potential on the surface of the insulator, which leads to a more uniform current sheath. It is difficult to introduce all the nuances to one model of the current sheath formation; therefore, experimental knowledge is used when designing PF devices and choosing the parameters of the insulator–electrode node, which causes structures of individual systems varying greatly from each other.

Formation of the current filament is one of the most important processes occurring during creation of the current sheath. Filippov (Kolesnikov et al., 1966) and Bostick (Bostick et al., 1969) showed that there are brightly lit fibers in the electric current sheath (Fig. 2.7).

Formation of radial filaments in the electric current sheath in a PF is observed in early stages. Sometimes this structure remains until the creation of the plasma focus, affecting plasma parameters. Increasing the pressure of the working gas causes the filament structure to become very clear at high pressures (Fig. 2.7).

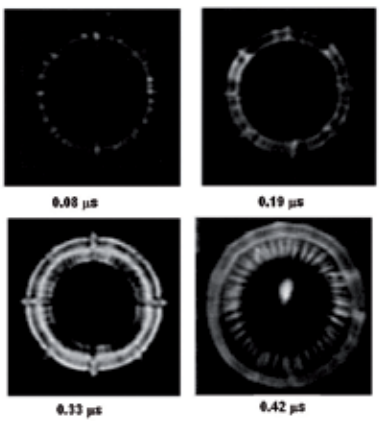

Fig. 2.7 Images of the electric current sheath in a PF in the visible light from the front of electrodes at different moments in time (unpublished photographs from PF-20, IPPLM, courtesy of K. Tomaszewski)

Description of the formation of the filament structure of the current sheath, based on the ionization instability model during electric gaseous breakdown in the space between electrodes, has been shown in Vikhriev, Braginski (1980). According to this model, the appearance of such a structure at the initial stage of discharge is caused by a non-linear increase in the heterogeneity of the initial electron concentration as a result of a two-stage ionization, i.e. ionization from the excitation level. If two-stage ionization is not at work here (for electron concentration $n_e << 10^{13}$ cm^{-3}), the ratio of the electron concentration to the mean concentration in the selected area of the layer does not change in time, i.e. the relative heterogeneity of concentration is constant:

$$\frac{\tilde{n}_{e1}}{n_{e1}} = \frac{\tilde{n}_{e0}}{n_{e0}} \quad , \tag{2.10}$$

where n_{e0} – mean electron concentration at time t_0, and n_{e1} – at time t_1. If the electron concentration exceeds 10^{13} cm^{-3}, and the frequency of collisions is high enough for ionization to occur from the excitation level, the mean energy required to ionize one atom is defined only by the ionization energy. The relative heterogeneity of the concentration described by formula (2.10) can be obtained by integrating gas ionization equation (2.9) for different values of ε:

$$\frac{\tilde{n}_{e1}}{n_{e1}} = \left(\frac{\tilde{n}_{e0}}{n_{e0}}\right)^{\varepsilon_0/\varepsilon_1} \tag{2.11}$$

where, as before, for hydrogen there is: ε_0 = 100 eV, and ε_1 = 13.6 eV.

The heterogeneous appearance of electron concentration during the electric breakdown in hydrogen at the initial stage of discharge is a natural phenomenon associated with an avalanche increase in the number of electrons due to ionization in the electric field. Heterogeneity of electron concentration is constant until the ionization processes begin from the excitation level (2.10). The average concentration increases from 10^8 cm^{-3} at the completion of the breakdown process, and resistance drops per unit length of the layer, to a value of 10^{13} cm^{-3}, when a sudden ionization increase. If the relative value of heterogeneity is 1.3 at this time then, after exceeding a concentration of 10^{13} cm^{-3}, it will assume the value of approx. 6 (for $\varepsilon_0/\varepsilon_1 \approx 7$, in accordance with (2.11)). With sufficient initial disturbance of the electron concentration, heterogeneities of ionization degree of a high amplitude may develop, which result in the formation of filament structure in the current sheath. Due to the change in the nature of electron collisions from electron–atom to Coulomb collisions, further increase in the degree of ionization slows down the growth of heterogeneity of the electron concentration in the current sheath.

The characteristic spatial step of the concentration disturbance was determined in Vikhriev, Braginski (1980) and based on Fourier analysis of the disturbance. Damping and levelling of the degree of ionization for short-wave harmonics occurs as a result of diffusion processes (diffusion of particles); and the characteristic step for which there is a levelling of the ionization degree is expressed by relationship $\delta_D=(2D_a\, t)^{1/2}$, where D_a – the ambipolar diffusion coefficient and t – characteristic time of the process. In contrast, long-wave harmonics are damped due to diffusion of the magnetic field, which defines the characteristic step of levelling heterogeneities in the electron concentration according to relationship $\delta_c=(2D_c\, t)^{1/2}$, where diffusion coefficient D_c is defined by Coulomb conductivity σ_c, $D_c=1/(\mu_0\, \sigma_c)$. Thus, there is a range of harmonics for $\delta_c > \delta_D$ in which the disturbance of homogeneity increases due to lack of damping. However, over sufficiently long time period, diffusion processes lead to smoothing and homogenizing of electron concentration in the electric current sheath, and the filament structure of the sheath does not appear (Fig. 2.8).

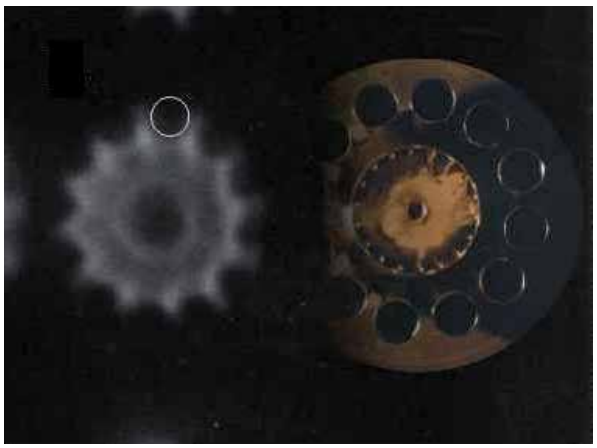

Fig. 2.8 A photograph made along the z axis of electrodes during convergence of the electric current sheath to the axes of the PF-1000 system (IPPLM) captured using a high-speed camera. View of the electrodes alongside. The white circle indicates one of the cathode bars. Shutter speed 0.5 μs, deuterium pressure in the chamber $5.32 \cdot 10^2$ Pa. (M. Scholz, M. Borowiecki, photograph not published)

The fact that in some cases the current sheath retains the filament structure until the end of the plasma focus formation process is due to the fact that the current's own magnetic field, whose intensity increases in the filament, compresses the filament to form a pinch in the equilibrium. Thus, the structure of separated filaments, appearing as a result of a disturbance in the homogeneity of the electron concentration of the current sheath in the gaseous electric breakdown phase, can be maintained even after the creation of a plasma focus (Fig. 2.9).

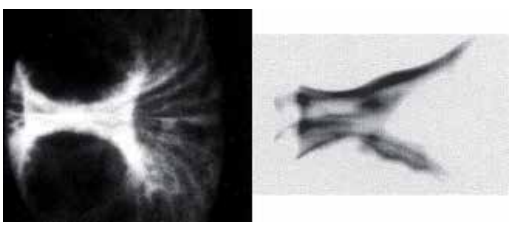

Fig. 2.9 Images in visible light made using a high speed camera from the side in two different experiments on the PF system, showing the fibrous structure during the collapse of the electric current sheath and at the maximum compression (Sadowski, Scholz, 2008)

In conclusion, the two processes of diffusion and increase of current in a single filament affect the final structure of the current sheath. Thus, the circuit parameters which determine the rate of current increase and electrode–insulator geometry, which affects the heterogeneity of the electric field, or heterogeneity of the degree of ionization, determine the formation of the current sheath. In addition, this formation process of the sheath depends on the type of gas; e.g. the use of a molecular gas, in which the amount of energy required to ionize one atom is greater than in the case of monatomic gas, facilitates formation of the filament structure in the sheath (Khautiev et al., 1999).

Deuterium, which is commonly used in experiments using Plasma-Focus systems, is a molecular gas and thus is conducive to the filament structure of the current sheath, which is often observed in the experiments (e.g. Bernard et al., 1975).

The filament structure of the current sheath is closely related to its azimuthal symmetry; that is, the uniformly azimuthal current distribution in the layer. Ensuring azimuthal symmetry is highly important in the formation of the current sheath, due to the subsequent phases of discharge development in a Plasma-Focus system; namely, the sweeping of gas during acceleration of the sheath, and a symmetrical compression of plasma in the last phase of the phenomena leading to formation of the plasma focus. It follows that the formation of a symmetrical and uniform current sheath significantly affects the parameters of the plasma focus. Therefore, it seems appropriate to look for ways to generate such a current sheath. One of the ways to make the electric breakdown symmetrical and homogeneous may be the pre-ionization of gas at the surface of the insulator, e.g. by doping with a radioactive isotope. Tritium added to deuterium may provide for such a pre-ionization. Unfortunately, the number of experiments in PF systems working with a mixture of deuterium and tritium is negligible, which does not allow us to draw firm conclusions on the homogenise of the current sheath. Another way to properly shape the sheath may be to profile the distribution of gas by pulsed injection of an appropriate amount of gas into the space between the electrodes, in the vicinity of the insulator, or at the ends of electrodes. However, there is very little experimental data due to the significant complexity of the experiment, and therefore complex data analysis, resulting from the influence of additional variables on the phenomenon such as gas injection valve parameters, synchronization between the valve opening time, voltage application time across the electrodes, *etc*. Despite this, it seems that in the case of Plasma-Focus systems with a power source energy of 1 MJ, shaping the current sheath by profiling the gas distribution via injection between electrodes is very promising.

In summary, it can be concluded that the process of gas ionization in the electric field, which increases in time and whose spatial distribution is defined by the geometry of the insulator-electrode node, creates the current sheath and determines its properties, azimuthal symmetry, homogeneity, and degree of ionization at the initial moment when it detaches from the insulator and when the sheath begins its movement along the electrodes. The process of detachment of the current sheath from the insulator occurs with the increase in current due to the Ampere force which acts directly on electrons carrying the current. Under this force, the electrons in the sheath begin to move, dragging the plasma ions. The Ampere force acts on plasma ions through the electric field arising from a small offset of electrons relative to ions, and then it acts on the gas molecules as the result of collisions of ions in the gas. The velocity of the ions is then reduced by the force of friction in the gas. The total force acting on a unit length of the current sheath can be expressed by the following formula:

$$F = 2\pi r_A \frac{B^2}{\mu_0} \quad , \tag{2.12}$$

where r_A – radius of the anode.

Ion velocity relative to the particles of the working gas in the initial stage of formation may be determined based on their kinetic energy achieved at the mean free path, due to the process of resonant charge exchange λ_{ex}:

$$v_i = \left(\frac{2F\lambda_{ex}}{m_i N}\right)^{1/2} , \tag{2.13}$$

where N is the number of particles per unit length of the electric current sheath, and the mean free path for the resonant charge exchange is determined by a collision cross section σ_{ex} (for hydrogen $\sigma_{ex} \approx 3 \cdot 10^{-15}$ cm^2).

There may be gas molecules behind sheath ions which move with a velocity of v_i, which can affect the electric strength to gaseous breakdown in the vicinity of the insulator at the maximum compression of plasma and shunted current out of the plasma focus.

As the number of ions increases during ionization, they initiate a directed movement of working gas molecules as a result of collisions. Hence, the condition for the permeability of the electric current sheath to gas particles can be expressed as follows:

$$\frac{N\sigma_{ex}}{2\pi r_A} \geq 1 . \tag{2.14}$$

If N reaches a value which enables satisfaction of the above inequality, the current sheath becomes undiscerning to the molecules of the working gas, and capable of transferring the pressure of the magnetic field to particles. One can say that a "magnetic piston" is created, capable of sweeping the gas. Due to the fact that the current in the sheath increases very rapidly, such an undiscerning sheath reaches a velocity greater than the speed of sound at the beginning of its movement along the electrodes, which leads to the formation of a shock wave in the gas. In this manner, a structure is moving along the electrodes in the Mather system, which is called the current sheath and consists of a shock-wave and a magnetic piston; that is, the plasma layer pushed by the pressure of a magnetic field. The mean free path for the process of resonant charge exchange is small enough for the range of gas operating pressures, so that gas ionization and its sweeping takes place at the front of the shock wave, which can lead to a gradual increase in weight of the sheath, and which does not increase proportionally to the mass of the swept gas. The efficiency of gas sweeping is one of the important conditions affecting the formation of a plasma focus of suitable density and temperature. Residual gas or partially ionized plasma remaining behind the sheath, caused by poor sweep efficiency (e.g. because of its filament structure), can lead to a decrease in dielectric strength of the space between the electrodes behind the sheath, and thus the appearance of a shunt effect outside the plasma focus, which significantly reduces compression of plasma in the focus. Due to fundamental difficulties in carrying out the measurements, there are almost no reliable experimental data about the density of gas or partially ionized plasma which remains after the transition of the electric current sheath.

2.3. ACCELERATION OF THE CURRENT SHEATH

At the moment when the current sheath becomes opaque to gas particles and a "magnetic piston" is created, sweeping of the working gas and acceleration of the current sheath begins under the pressure of the magnetic field. Sweeping of gas, the dynamic properties of the electric current sheath during acceleration along the electrodes, and compression can be described by a simple model of a two-dimensional *snow-plow* (Basque et al., 1968). In this model it is assumed that the well-conducting layer has no internal structure (zero-dimensional approximation). It is symmetrical relating to the z axis of the system and does not depend on the φ angle, and its motion is described by the trajectory of points on the (r,z) plane located on the surface of the current sheath (Fig. 2.10).

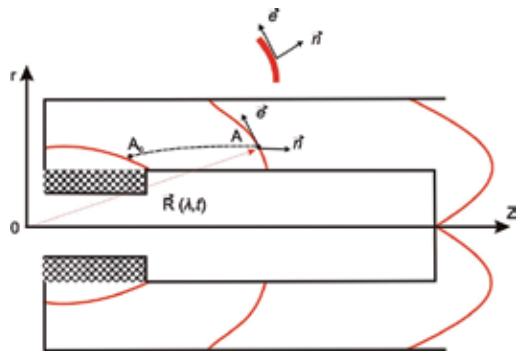

Fig. 2.10. Coordinate system of the two-dimensional snow plow model. A - point of the electric current sheath defined by coordinate λ along the layer, A_0 - the initial position of the A point at the insulator, $\vec{e}_\tau = \frac{\partial \vec{R}}{\partial \lambda} / \left|\frac{\partial \vec{R}}{\partial \lambda}\right|$ - vector tangent to the layer surface, $\vec{n} = e_\tau \times e_\varphi$ - normal vector

$\overrightarrow{OA} = \vec{R}(\lambda, t) = \vec{e}_r r(\lambda, t) + \vec{e}_z z(\lambda, t)$ vector is a function of coordinate λ and t. $\vec{R}$ vector for $t = const$ determines the shape of the sheath, and for $\lambda = const$ describes the trajectory of the layer point. The velocity of the sheath element is determined by the following equation:

$$\vec{v} = \frac{\partial \vec{R}}{\partial t} \quad . \tag{2.15}$$

The length of element $d\lambda$ is equal to $(\partial \vec{R} / \partial \lambda) d\lambda$, and therefore the mass of element dm of the current sheath, corresponding to element dm can be obtained from the following equation:

$$\frac{d}{dt}\left(\frac{dm}{d\lambda}\right) = 2\pi \rho_0 r (\vec{n} \cdot \vec{v}) \left|\frac{\partial \vec{R}}{\partial \lambda}\right| \quad , \tag{2.16}$$

where ρ_0 – initial density of the working gas filling the chamber, and the equation for movement of element $d\lambda$ of the current sheath is given by:

$$\frac{d}{dt}\left(\frac{dm}{d\lambda}\frac{\partial \vec{R}}{\partial t}\right) = \frac{\mu_0}{4\pi} I^2 \frac{1}{r}\vec{n}\left|\frac{\partial \vec{R}}{\partial \lambda}\right| \quad , \tag{2.17}$$

where I is the total current flowing between the electrodes.

Joining the initial conditions to the above equations: $R(\lambda,t=0) = const\cdot(dm/d\lambda)$, $v_r(0) = v_z(0)$ and the equation of electrical circuits (2.1) and (2.2), we can use the equation of motion to calculate the velocity of the sheath, its shape, and hence $L_p(t)$ – inductance associated with the movement of the current sheath along the electrode. In this way, we can calculate both the current $I(t)$ flowing through the layer and the voltage $U_{ab}(t)$. The two-dimensional snow-plow model can therefore be used to determine the condition for the adjustment of circuit parameters to the movement of the current sheath, without the additional assumption made by Mather (Mather, 1971) in his paper that the inductance associated with the movement of the layer $L_p(t)$ is a linear function of time (see equation 2.7). Based on this model, we can also calculate the time sequence of the current and voltage for given parameters of the generator, geometry of electrodes, and the working gas pressure; as well as compare them to oscillograms of the current registered using the Rogowski coil (Fig. 2.11), or voltage registered using a voltage divider.

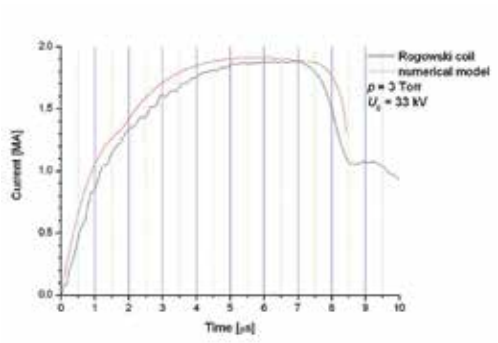

Fig. 2.11. Current measured using the Rogowski coil (black line) and calculated from the 2D snow-plow model (red line). (2D snow-plow model calculations courtesy of R. Miklaszewski)

Furthermore, such a model enables determination of the velocity of the electric current sheath (v_z) along the electrodes of the system, and the radial velocity (v_r) versus time (Fig. 2.12) or the sheath shape.

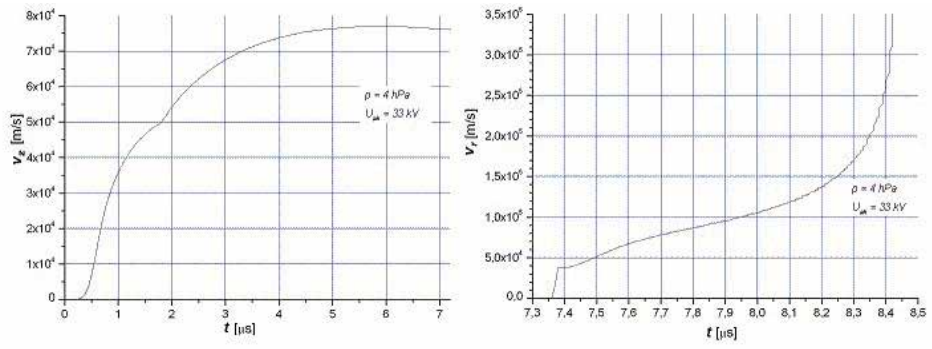

Fig. 2.12. Velocity of electric current sheath v_z and v_r versus time calculated from the 2D snow-plow model. (2D snow-plow model calculations courtesy of R. Miklaszewski)

Velocity v_z of the current sheath along the electrodes was measured with several magnetic probes arranged in the space between electrodes at different distances from the insulator (Mather, 1971; Bernard and Coudeville, 1976). This allows comparison of the measurement results with the results of calculations based on the snow-plow model. On the other handt, velocity of radial compression calculated from the snow-plow model can be verified using a streak camera which records the image of plasma glow through a slot (Chapter 4, Fig. 4.13), so one can visualize the radial movement of the current sheath (Fig. 2.13).

Due to the fact that the magnetic field between the electrodes varies as $1/r$, the part of the sheath near to the anode moves faster than the part of the sheath which is closer to the cathode, hence the characteristically slanted shape of the sheath, which also shows the two-dimensional snow-plow model. A slant of the current sheath causes the swept working gas to flow along the layer towards the cathode wherein, if solid, the excess mass of gas is collected. Firstly, this results in a slowing of the movement of the sheath as well as lower velocity; and secondly, can cause gas remaining behind the layer to undergo electric breakdown, shunting the primary current flowing through the sheath, and thus through the plasma focus of the PF system (Fig. 2.5).

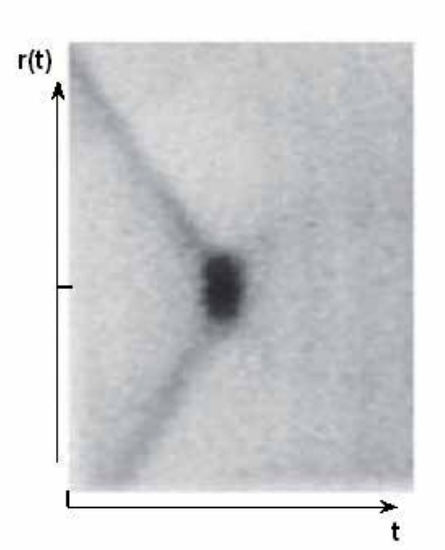

Fig. 2.13. Image showing the radial movement of the electric current sheath recorded with a fast streak camera in visible light. PF-20, IPPLM, working gas pressure 133 Pa, U_0 = 30 kV. (M. Borowiecki, unpublished photograph)

In order to avoid this problem, the cathode is typically composed of rods (Chapter 4, Fig. 4.3), allowing the free flow of gas outside the space of electrodes during movement of the electric current sheath.

Calculated and measured velocity of the current sheath along the electrodes v_z varies with time (Fig. 2.12), and ranges between 10^6 cm/s to 10^7 cm/s at the end of the electrodes, depending on their length and geometry. When the part of the sheath close to the anode extends beyond the edge of electrodes, the current density component j_z appears, resulting in the creation of component B_θ of magnetic field induction. It causes this part of the sheath to start moving radially toward the axis of the electrodes of the PF system (Fig. 2.10). Gas, which was ionized and swept by the sheath as it moved along the electrodes, is no longer swept to the axis, and is not subject to radial compression. Most of the mass moves further in the direction of its current sheath movement (along the *z* axis). This enables avoidance of a situation in which a most of the dopant, e.g. from the insulator or other structural elements present in close proximity to the electrode–insulator node, reaches the plasma focus. Thus, one of the assumptions associated with structural changes in linear Z-pinch systems leading to the formation of Plasma-Focus systems is satisfied.

The radial movement of the current sheath starts when the sheath reaches the end of the electrodes. If the matching between power source (capacitor bank) and load (electrodes) is good, the current reaches its maximum value. Movement of the current sheath in the radial direction starts with an initial velocity of zero. Then, the sheath rapidly accelerates, reaching a radial velocity v_r of several times 10^7 cm/s (Fig. 2.12) shortly before reaching the electrodes. The process of radial compression of the layers in the PF system lasts from dozens to hundreds of nanoseconds depending on the radius of the anode. The shape of the sheath in the PF system during radial compression is not cylindrical (as in the linear Z-pinch, see Introduction, Fig. 0.1), and is somewhat curved. The size of the curvature determines the mass outflow, geometry (length), and the plasma focus parameters.

In a two-dimensional snow-plow model, we can estimate the amount of energy transferred from the capacitor bank to the accelerator by determining $L_p(t)$ from equation (2.2) using the following relationship:

$$W_{ab} = \int IU_{ab}dt = \frac{1}{2}L_pI^2 + \frac{1}{2}\int \frac{dL}{dt}I^2dt + \int R_pI^2dt \quad , \tag{2.18}$$

where R_p – resistance of the current sheath, L_p – inductance associated with its movement, I – the intensity of the total current flowing through the electrodes. We can use (2.18) to determine the distribution of electricity initially stored in the capacitor bank among various types of energy in the accelerator system. Three components of this equation describe, respectively, the energy accumulated in the magnetic field: $L_pI^2/2$ kinetic energy related to the movement of the layer: $\int\frac{dL}{dt}I^2\,dt/2$ and ohmic heating energy $\int R_pI^2dt$.

Based on the snow-plow model, we can fairly accurately estimate the primary current-voltage waveforms measured in a PF system for a given geometry of electrodes, as well as the initial pressure of the working gas, which allows us to choose the inductance of the system, the geometry of the electrodes, and the pressure of the working gas in such a way that the current flowing in the PF system reaches its maximum at the moment of maximum compression.

However, the two-dimensional snow-plow model, despite its advantages, has very significant limitations, the most important being its inability to determine the internal structure of the current sheath during acceleration and compression, and its inability to determine the parameters of the plasma focus (pinch).

2.4. STRUCTURE OF THE CURRENT SHEATH

As noted in Section 2.2, the movement of the current sheath takes place in the working gas filling the vacuum chamber of a PF system. Due to the fact that the sheath becomes undiscrening to gas particles at the beginning of its movement (see condition 2.14), and both the current and the related magnetic field pressure increase very rapidly, the movement of the sheath is supersonic from the very beginning, leading to formation of a shock wave in the gas.

Mean free paths for the resonant charge are exchanged and elastic collisions in the gas for the pressure range used in the PF are very small, therefore the inert gas is compressed and heated at the shock front. Thus, the current sheath can be ideally defined as a complex spatial structure between undisturbed inert gas and a "magnetic piston," consisting of a dense and hot neutral layer, ionization layer, and plasma layer, through which current flows, and behind which there is vacuum (or very thin plasma) with a magnetic field. Note that this

perfect image of the current sheath does not necessarily agree with the experimental image, especially with the radial filaments existing in the sheath (Fig. 2.7).

Both, measurements made with magnetic probes used to determine the structure of the "magnetic piston," and measurements made with high-speed cameras, spectrometry, and interferometry, providing information about the parameters of the plasma in the layer, are used as diagnostics to measure the structure of the current sheath. Usually, these two types of diagnostics, e.g. magnetic probes and interferometry, are used separately. They were used simultaneously only in a few cases (Krauz et al., 2012).

As noted earlier (Section 2.3), measurements made using a magnetic probe were taken in the space between electrodes. Several probes spaced along the electrodes determine the speed of the current sheath and compare, e.g. with the results of calculations based on the snow-plow model. However, the electric current flowing in the sheath was determined more often by integrating the signal measured by the probe, which confirmed, as described in (Gourlan et al., 1978), that part of the current flows outside the sheath (Zadrożny, 1990).

Measurements made using magnetic probes (Borowiecki et al., 1984; Krauz et al., 2011; Ananin et al., 1978) showed that the distribution of current density is relatively broad (1÷2 cm), and sometimes has two peaks (Fig. 2.14) . If a part of the current flows at the shock front, and in the primary part of the plasma skin layer (in the so-called "magnetic piston"), a sheat structure is not proper formed due to initial processes in the vicinity of the PF system insulator, and significantly affects the sweeping of the working gas, causing a low density and temperature of the plasma focus.

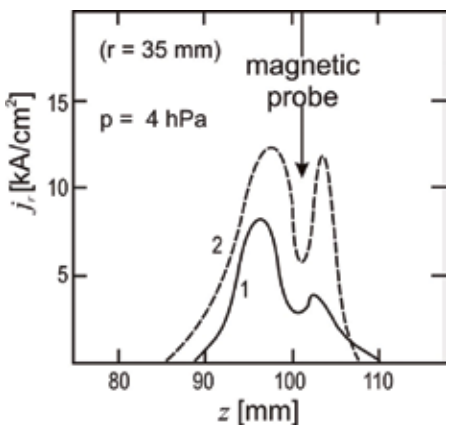

Fig. 2.14. Current density distribution in the electric current sheath: 1) without the insert modifying the electric field distribution at the insulator 2) with the insert (Fig. 12 from: Borowiecki et al., 1984)

The concentration of particles in the plasma layer was determined by interferometry, usually when the layer approached the electrode axis. The specific concentration of particles in the layer, typical of many systems, was about $10^{17} \div 10^{18}$ cm^{-3}, with the width of the plasma layer being of the order of 1 cm, depending on the initial pressure of the working gas and the current intensity. An example of an interferogram and the distribution of plasma particle concentration is shown in Fig. 2.16.

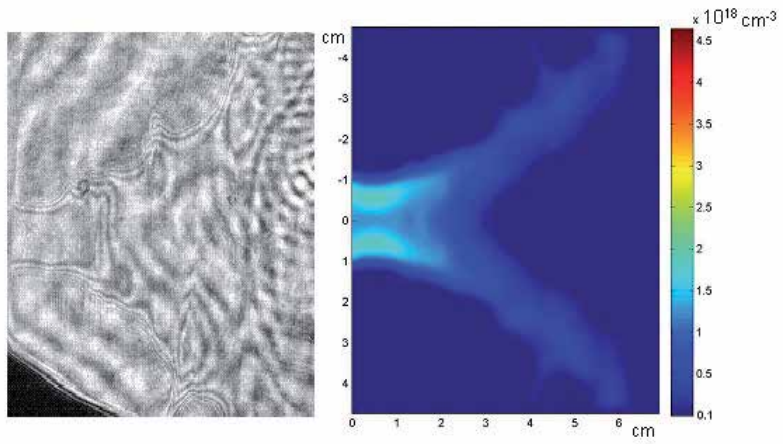

Fig. 2.15. Interferogram of the electric current sheath and a 22 ns electron concentration distribution before the electric current sheath reached the axis of the system. The anode surface is on the left side of the interferogram. PF-1000 system, IPPLM. (M. Paduch, P. Kubes, M. Scholz, unpublished photograph)

In order to compare the structure of the current sheath obtained via measurements using magnetic probes and interferometry with the results of computer modeling of the structure, computer codes were developed for solving equations of fluid non-ideal magnetohydrodynamics (MHD) which account for the geometry of the Plasma-Focus system (Potter, 1971; Dyachenko and Imshennik, 1974; Vikhriev and Braginski, 1980; Maxon and Edellman, 1978; Stępniewski, 2004). MHD equations are both continuity equations describing the law of conservation of mass, momentum, and energy, and also the equation of magnetic field diffusion derived from Maxwell's equations. These partial equations are stored in the cylindrical symmetry according to the geometry of electrodes in the Plasma-Focus system, assuming the homogeneity of the medium regarding the angular variable ϕ and further supplemented with the circuit equation and the equation describing ionization kinetics (Stępniewski, 2004). Braginski transport coefficients (Braginski, 1963) were used in the equations.

By solving this system of equations, we obtain spatial distributions at given time t, plasma density $\rho(r,z,t)$, velocity components $v_r(r,z,t)$ and $v_z(r,z,t)$, electron temperature $T_e(r,z,t)$, and ion temperature $T_i(r,z,t)$ in the plasma. In order to solve these equations, additional boundary conditions are assumed that are specific to the PF system, as well as initial conditions describing density, velocity, and the ion and electron temperature of plasma at the initial time $t = 0$. Examples of distributions of density and ion temperature in the plasma layer, prior to its reaching the electrode axis, obtained through numerical calculations, based on the model described in (Stępniewski, 2004), are shown in Fig. 2.16.

The results of calculations shown in Fig. 2.16 indicate that plasma density in the layer is in the range of $10^{17} \div 10^{18}$ particles per cm^{-3}, and distribution of electron temperature in the layer has a value corresponding to the energy of 10 to 60 eV. The measured and calculated

electron concentration of the plasma in the electric current sheath is more or less consistent. The calculated maximum electron temperature of the plasma in the current sheath during movement first in the *z* direction, and then in the *r* direction along the electrodes (see Fig. 2.10) is equal to several dozens of electron-volts. There is virtually no experimental study describing the measurements of the electron temperature during its movement along the electrodes. A few spectrometric measurements presented in (Skrzeczanowski, 1990) show that just after the formation of the electric current sheath, at the initial moment of its movement (a small distance from the insulator), the temperature of plasma corresponds to an energy of about 3 eV, and in the position before to the end of the electrodes it reaches about a dozen electronvolts.

Attempts to comprehend the physical processes leading to the formation of the current sheath, the creation of its structure, the impact of this structure on the sweeping of the working gas and final velocities of the sheath at a given electrode geometry, and parameters of the capacitor bank were aimed at understanding what their impact is on the parameters of the plasma focus (pinch). The properties of the current sheath can ultimately lead to formation of the pinch, in which maximum values of density and temperature are achieved.

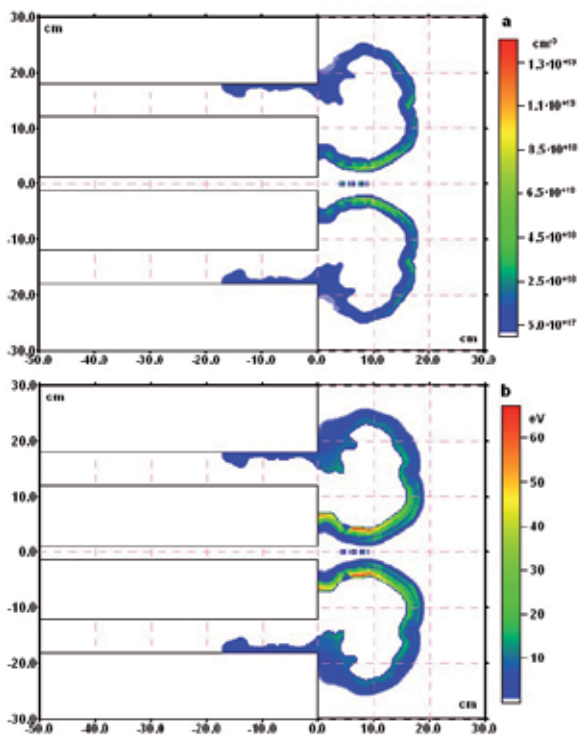

Fig. 2.16. Distributions of density (a) and the electron temperature (b) in the plasma layer prior to its reaching the axis of the PF-1000, IPPLM system, obtained from the model described in (Stępniewski, 2004)

2.5. PLASMA FOCUS

After the current sheath, whose shape differs from cylindrical (see Fig. 2.16), reaches the electrode axis of the PF system, the formation and shaping phase of the plasma focus begins. Since the very beginning of PF systems, this is the phase for which extensive study has been carried out regarding plasma parameters in the focus and the radiation, both in a wide range of the electromagnetic spectrum and corpuscular, with particular emphasis on the emission of neutrons from fusion (D,D) reaction. Basic plasma parameters and radiation from the plasma focus, integrated over time, were obtained in these first experiments on PF systems. Plasma density at its focal point, its temperature, and the lifetime of the focus were most interesting from the viewpoint of fusion. These values are related to the Lawson criterion (see Chapter 1), and their measurement enables specification of how far we are from break-even at a given current flowing through the plasma focus. Due to the lack of recording capabilities using nanosecond resolution with the techniques available at that time (late 1950s and early 1960s), the location of emission of soft X-rays from hot plasma integrated over time was measured using a *camera obscura* with a beryllium or aluminum filter, and the total emission of neutrons from reaction (D,D) was measured using silver counters. The image from the *camera obscura* enabled estimation of the size of the plasma focus (e.g. Fig. 2.17), and the total emission of neutrons enabled estimation of the number of deuterium nuclei fusion reactions in plasma was measured by absolute calibrated neutron counters.

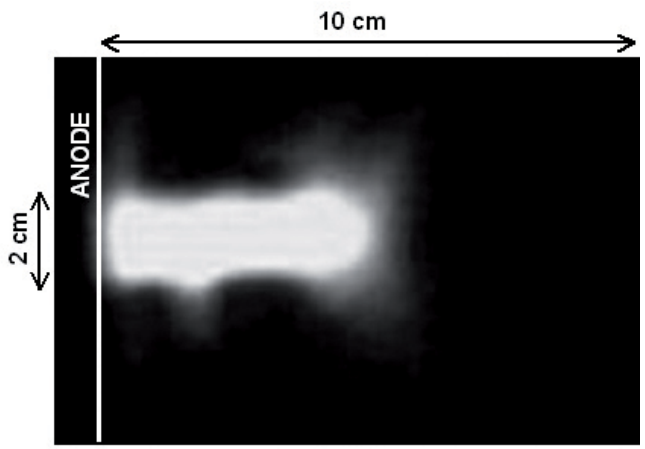

Fig. 2.17. Image of the plasma focus using an X-ray frame camera in the XUV range (energy of recorded quanta: a window of 0.2 ÷ 0.3 keV and above 0.6 keV), exposure time 2 ns, 10 ns before the maximum compression. (Scholz, 2008)

It was assumed that plasma in the focus was in equilibrium with the magnetic field at a certain time interval, and its parameters could be described by the Bennett relationship [see Introduction, formula (0.1)]; that is, a relationship between the linear concentration, temperature, and current flowing in plasma. Assuming that parameters of plasma in the focus satisfy relation (0.1) at a certain period of time, we can use the fusion reaction yield formula [see Chapter 1, formula (1.4)] in order to find the relationship between the total emission of neutrons from reaction (D,D), and the intensity of the current flowing through the plasma focus in the form of:

$$Y_n = \frac{1}{(4c)^4} \frac{l}{\pi r_p^2} \tau \frac{\langle \sigma v_r \rangle_{DD}}{T^2} I_p^4 \quad , \tag{2.19}$$

where l and r_p are, respectively, the length and radius of the plasma focus, T is its temperature, τ is the lifetime of plasma in equilibrium, and I_p is current intensity in the plasma focus.

We can estimate the number of (D,D) reactions occurring in plasma based on the total emission of neutrons and thus, know the reaction heat and the total energy that has been emitted as a result of these reactions. It follows from equation (2.19) that the number of reactions in plasma depends on the fourth power of the current in the plasma focus. It is the scaling law for Plasma-Focus systems, which is a criterion similar to the Lawson criterion, showing that the number of fusion reactions, and the energy emitted as a result of these reactions in a single discharge, increases to the fourth power of the current intensity in plasma. Moreover, the number of fusion reactions also depends on the size of the plasma focus (length, radius), the lifetime of the focus balance, and the temperature of plasma (if the particles in plasma assume Maxwell's distribution of velocity). The maximum current in the PF system is determined by the parameters of the capacitor bank (capacity, inductance, and charging voltage), and the change in inductance of electrodes caused by the movement of the layer *dL/dt* (see Fig. 2.4). It follows that, given the appropriate parameters of the capacitor bank and the match of the electrodes to them according to the criteria described in Section 2.1, we can design the PF layout according to the scaling law, where the $G = 1$ criterion indicating the break-even point of the system from the viewpoint of energy production from fusion will be met [Chapter 1, formula (1.30)]. In addition, we can easily verify the designed and built system experimentally by measuring the current, the total emission of neutrons, geometric dimensions of the plasma focus, and its temperature. Measurements of the total emission of neutrons relative to the current in the PF device built in Limeil (Bernard, Coudeville, 1976), for currents in the range of 40 to 2500 kA, showed that the total emission of neutrons is proportional to the current during the lifetime of the plasma focus to the power of 3.3 : $Y_n I^{3.3}$ (Fig. 2.18).

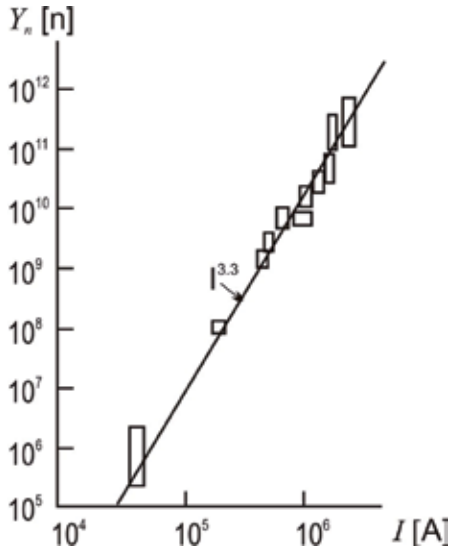

Fig. 2.18. The total emission of neutrons versus current. (Bernard, Coudeville, 1976)

Experiments with deuterium carried out in the 1960s and early 1970s using Plasma-Focus systems fostered hope that the modification of the linear Z-pinch system to the PF configuration would allow building a fusion reactor. All the more, that at the measured level of total neutron emission of the order of $10^9 \div 10^{10}$ n/discharge, the duration of the neutron emission was 100 ns, and the estimated concentration of plasma particles in the focus was $2 \cdot 10^{19}$ cm^{-3} (Mather, 1965; Filippov et al., 1962).

Neutron emission levels at this concentration of plasma particles suggested that the plasma temperature in the focus corresponded to the energy of a few keV. In order to verify the parameters of the plasma focus in the PF (especially the temperature), measurements of the spectrum of neutrons emitted along the PF axis using nuclear emulsions, anisotropy of neutron emission using scintillation probes, and the spatial distribution of the neutron emission source using a set of collimators were taken in addition to the measurement of the total emission of neutrons Y_n.

Measurements of isotropic neutron emissions from the focus presented in (Mather, 1965) led to the hypothesis of a *quasi*-steady fusion plasma in the focus. In (Filippov et al., 1962; Bernstein et al., 1969; Mather, 1971), in addition to isotropic neutron emission, the energy spectrum of neutrons emitted along the axis from the PF system was measured at the same time (see Fig. 2.19).

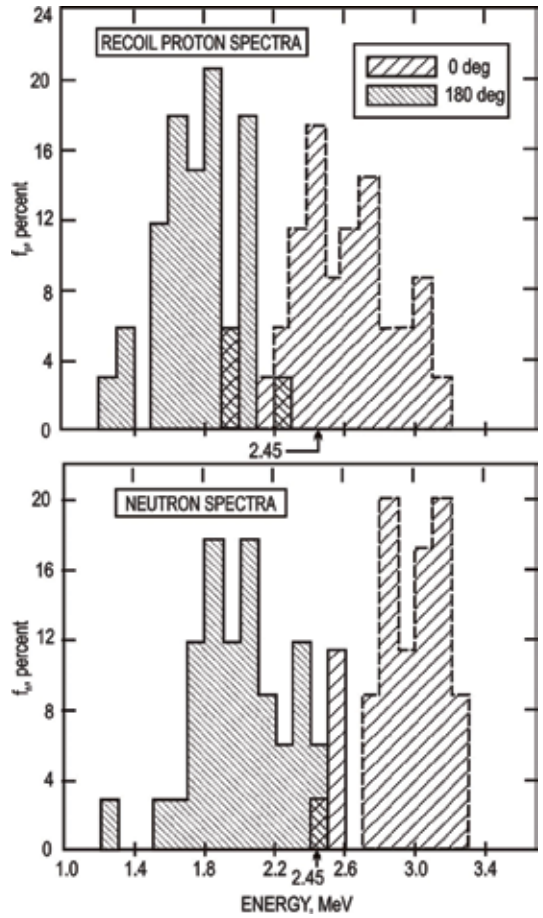

Fig. 2.19. Neutron energy spectra obtained using nuclear emulsions along the axis of the Plasma-Focus electrodes (Bernstein et al., 1969)

Measurements of the spectrum of neutrons using nuclear emulsions showed an average shift of neutron energy emitted along the axis at about 400 keV, which corresponds to the velocity of the center of mass of fusing deuterons, equal to $1.6 \cdot 10^8$ cm/s. Isotropic emission of neutrons from the focus was measured in the same experiment. This leads to the conclusion that reacting deuterons have an isotropic distribution of energy in the center of mass of the system, and the center of mass moves along the axis with a velocity of the order of 10^8 cm/s. Based on these experimental facts, it was assumed that we were dealing with a moving "drop" of fusion plasma, in which intense (D,D) reactions occur. This model of neutron production from the fusion reaction was called *moving-boiler*. In order to verify this hypothesis, data regarding length l of the plasma focus, obtained in these experiments from the images taken using the *camera obscura* in the range of soft X-rays and integrated over time, was correlated with the distance traveled by the "drop" of fusion plasma during neutron emission (approx. 100 ns) at a velocity of the order of 10^8 cm/s. And so, paradoxically, the length of the plasma focus measured using the images was about 5 cm (approximately, for Fig. 2.17), and the distance the "drop" will travel along the PF axis during neutron emis-

sion was about 10 cm. This in turn would imply that intense neutron emission occurs only at the beginning of the "drop" movement.

Very high velocity of the center of mass, 10^8 cm/s, obtained from the measurements of the neutron energy spectrum along the PF axis (e.g. Bernstein et al., 1969) corresponds to the kinetic energy of deuterons at about 40 keV/deuteron. This, in turn, proves the lack of isotropy of the plasma focus. It turned out that the plasma homogeneity in the focus, which was observed in the images, e.g. from the *camera obscura*, is insufficient to explain the observed emission of neutrons.

As the result of these discrepancies, the shift in the energy spectrum of neutrons emitted from the (D,D) reaction was explained, in addition to the *moving-boiler* hypothesis, by assuming that deuterons accelerated to high energies in the plasma focus collide with deuterons in the plasma. This in turn led to the conclusion that the reactions from fusion of deuterium nuclei do not occur in thermal plasma, i.e. the production of neutrons in the plasma focus is not a fusion. This hypothesis began to dominate after presentation of the spectrum of neutron energy measured perpendicular to the axis of the PF system in (Bernstein, Hai, 1970). The extension of the measured spectrum enabled estimation of the ion temperature corresponding to an energy of 20 ÷ 50 keV based on (Lehner, Pohl, 1967). In the case of fusion plasma at this ion temperature, the total emission of neutrons should be two orders of magnitude higher than the emission measured in this experiment.

Homogeneity of the plasma focus in the PF system visible in the images from cameras in various spectra where deuterons are accelerated by accelerative processes, as well as low anisotropy of neutron emission measured from the focus - and thus an attempt to determine the nature of the neutron emission – have given rise to intensive experiments aimed at understanding the processes occurring during the lifetime of the plasma focus in PF systems. Significant progress in this area of research was made in the 1970s in relation to the use of nanosecond recording techniques and development of diagnostic methods based on the use of laser technology, as well as high-speed image sensors in visible and X-ray ranges.

The overall picture of the phenomena occurring during the lifetime of the plasma focus is basically the same for most PF devices, and the experimental results obtained with the PF-150 system (about 50 kJ, 30 kV) operating in IPPLM in 1973÷1998 will be used to present these results. In a series of papers, the detailed picture of the evolution of the plasma focus was shown based on analysis of the shape, density, and temperature of plasma obtained via four-frame interferometry using a ruby or neodymium laser with a pulse duration of 2÷3 ns (Sadowski, Scholz, 2008; Kasperczuk, 1984), a four-frame "Quadro" camera in the visible range with a shutter speed of 1 ns (Paduch et al., 1992), and an X-ray *camera obscura* for soft X-rays with a shutter speed of 1 ns (Volobuyev et al., 1988). It has been shown that the evolution of the plasma focus (pinch) can also be broken down into several phases. Fig. 2.20 shows the dynamics of the plasma focus in soft X-rays (from the *camera obscura*), visible light (from the "Quadro" camera), and based on interferograms.

a)

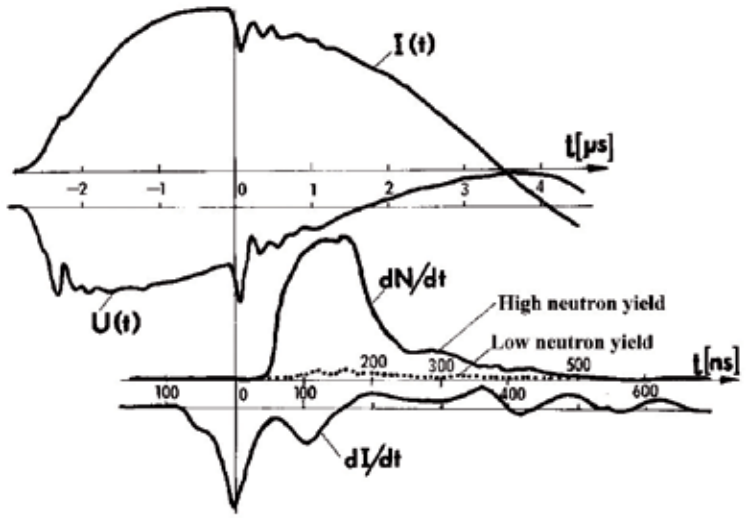

b)

X-ray still camera [ns]

Fast optical still camera [ns]

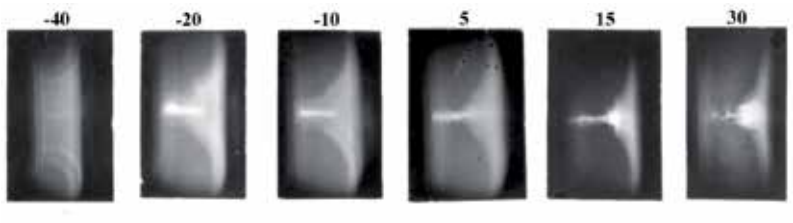

Interferograms [ns]

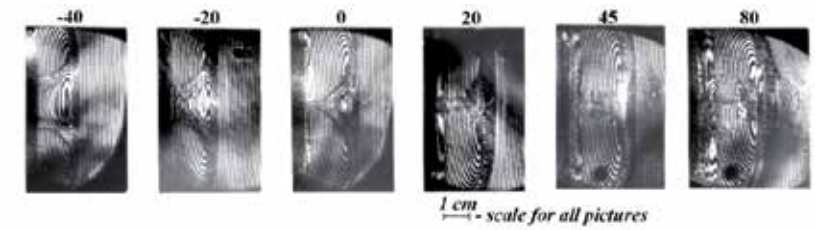

Fig. 2.20. The evolution of the plasma focus in PF shown by various diagnostic methods: a) Typical oscilloscopy waveform; b) Typical image of implosion and pinch of plasma(spatial scale applies to interferograms only). [Fig. 5 shown in (IPPLM, 1996)].

It was conventionally assumed that time $t = 0$ corresponds to the minimum of derivative dI/dt, identical to the moment of maximum compression (2.20). After the collision of shock waves of the layer on the electrode axis of the PF system, the phase of radial compression of the gas in front of the shock front of the current sheath switches to the first phase of plasma focus formation, i.e. radial compression of plasma, at a velocity of about $4 \cdot 10^7$ cm/s ($-20 < t < 0$ ns), during which the derivative of the current reaches its minimum. Already in this stage, plasma begins to emit soft X-rays from a cylindrical area. In some systems, weak pulses coming from the neutron emission were measured in this phase. In the next 20 ns ($0 < t < 20$ ns) is the maximum compression phase during which, according to the interferometric data, the electron concentration of plasma reaches the values of $(2 \div 3) \cdot 10^{19}$ cm^{-3} for the minimum focus radius of the order of 1.5 mm. The same radius of the focus in the soft X-ray is obtained from the *camera obscura* behind a beryllium filter with a thickness of 50 μm. If thinner filters are used, the radius of the focus is greater, which means that there is a core in the plasma focus with a high electron concentration and temperature surrounded by a plasma coating with lower concentration and temperature. After the phase of maximum compression, there is an increase in the radius of the plasma focus, a respective decrease of electron plasma concentration, and the system switches to the so-called *quiet phase* which lasts about $20 \div 30$ ns with a constant radius of the focus. In this phase, the electron plasma concentration decreases at a constant radius, which indicates axial movement of the plasma with a high velocity of about $2 \cdot 10^8$ cm/s (Fig. 2.21).

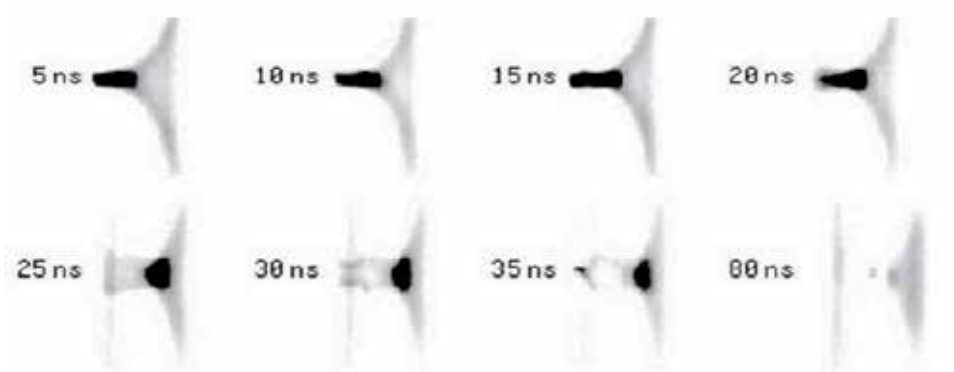

Fig. 2.21. The sequence of images taken in visible light using a four-frame camera with a shutter speed of 1 ns illustrating the temporal dynamics of the plasma focus, in particular the plasma outflow along the axis of the focus (unpublished photographs by K. Tomaszewski)

Next comes the unstable phase when m = 0, in which instability appears within approx. 20 ns, leading to the creation of constrictions along the plasma column (Fig. 2.22b), which can be regarded as a re-pinching of the plasma. The temperature in the constriction can reach the order of a single keVs.

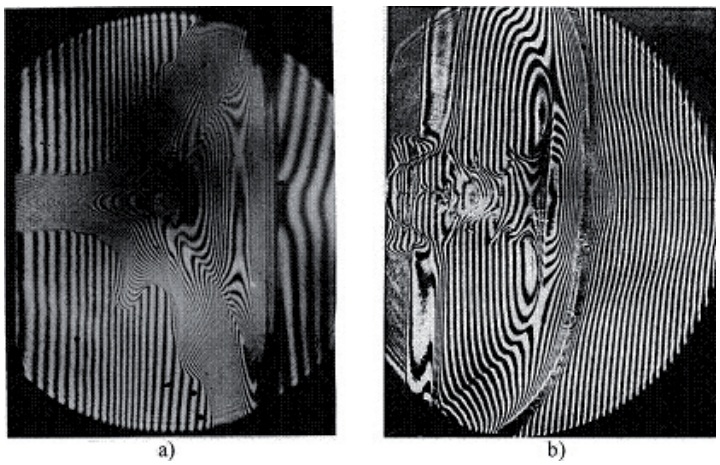

Fig. 2.22. Examples of interferograms showing: a) (quiet phase) of the focus, b) unstable phase of the focus (instability m = 0) [Fig. from the dissertation (Pokora, 1980)]

Pulses of hard X-rays are observed during this phase, which may indicate that some mechanisms appear which accelerate electrons and ions to high energies. A neutron emission pulse has a fast rising edge, sloping trailing edge and reaches the maximum for t of about 100 ns. The pulse width at half height is about 200 ns. The emission of neutrons reaches its maximum in the last development phase of the plasma focus: the phase of its destruction ($t > 100$ ns).

It can be seen that the plasma focus (pinch) has a complex space-time structure with continuously changing parameters, and the maximum temperature and density of plasma can be separated in time.

Below is the order of the individual phases of plasma focus evolution mentioned above:

i. Compression phase ($t < 0$).

ii. Stable (quiet) phase, during which plasma expands to twice its minimum radius.

iii. Unstable phase, during which instabilities develop when m = 0, and there is re-pinching of the plasma focus.

iv. Decay phase, during which the destruction of the plasma focus results from the interruption caused by the instability of m = 0.

This breakdown is clearly visible for PF systems of medium and high electricity accumulated in the capacitor bank ($W_b > 20$ kJ), and typical for most systems. There are differences which apply only to spatial and temporal characteristics, such as the minimum radius, length, or duration of the focus, and the duration of phases ii. ÷ iv., which can vary from 30 ns for PF with an energy of 20 kJ, to 250 ns for an energy of 0.5 MJ.

The nature of the evolution of the focus [items: i., ii.] with two plasma pinches is characteristic of Filippov-type PF systems and Mather-type systems with high energy of the capacitor bank (Poseidon in Stuttgart) and (PF-1000 in Warsaw). Two pulses of hard X-rays and two neutron pulses (Schmidt et al., 2006) corresponding to these pinches have been often observed in these systems.

Similarly, differences exist in length l of the plasma focus along the z axis of the electrodes and depend on the shape of the end of the internal electrode, which is the anode. In the case of a semispherical end of the anode, the length of the focus is smaller than in the case of a flat "head." This is due to the fact that the current sheath in the radial compression of the gas is not cylindrical and has a radius of curvature (see Fig. 2.16), which depends primarily on the geometry of the ends of electrodes. The non-cylindrical nature of compression of the electric current sheath in a PF system is an important feature of this device and determines the nature of the phenomena occurring in the plasma focus to a large extent. In particular, one of the consequences of this phenomenon is the emergence of the axial movement of plasma that may result in the emergence of a cumulative plasma beam outflowing from the plasma focus (Fig. 2.23). This effect may be a consequence of the transformation of the kinetic energy of a radial motion of the current sheath, pinched at a velocity of $(3 \div 5)\cdot 10^7$ cm/s, into the kinetic energy of the plasma beam along the axis of the plasma focus.

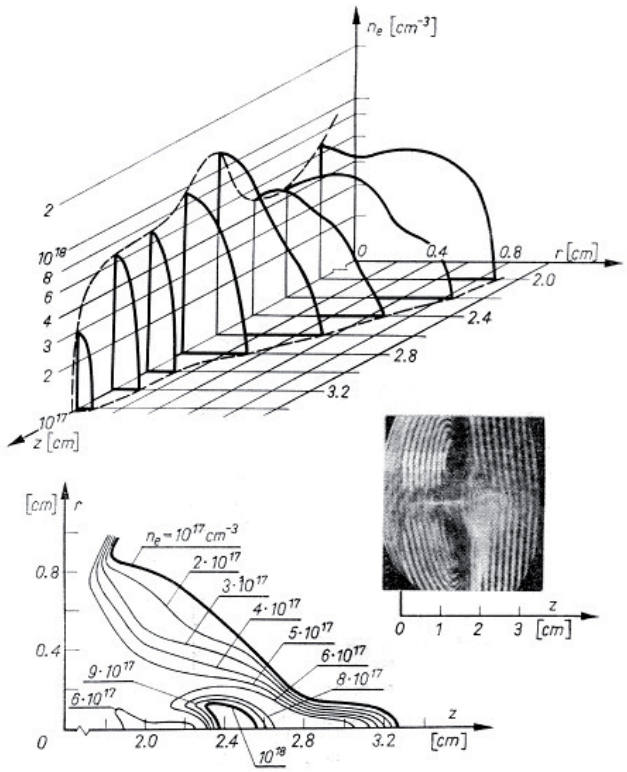

Fig. 2.23. Spatial distribution of electron concentration showing the outflow of the plasma beam 3.2 cm from the anode surface. Deuterium pressure $p_0 = 1.2 \cdot 10^3$ Pa. (Fig. 6 in Denus et al., *1977)*

Firstly, this phenomenon results in a decrease of plasma concentration along the plasma focus, which stimulates the development of both magnetohydrodynamic (e.g. m = 0) and kinetic instabilities; and secondly, in the formation of an ion beam with an energy of 10 keV, as well as the creation of a dense plasma target, which in turn may significantly affect the process of (D,D) reactions in plasma and thus the related emission of neutrons.

The process of creating the plasma focus is clearly visible on waveforms of the current and voltage derivative (Fig. 2.3) as distinct extreme values. The presence of clearly distinguishable extreme (maximum and minimum) values on waveforms of the current derivative and voltage pulse shows that the plasma focus is formed in the PF system with parameters allowing for an intensive process of nuclear fusion. Unfortunately, this is not a sufficient condition. The intensity of (D,D) reactions, and thus the level of total emission of neutrons from the plasma focus is affected both by the magnetohydrodynamic phase, which is associated to a large extent with the initial conditions of formation and acceleration of the current sheath; as well as the phase where the magnetohydrodynamic description does not work, which is related to the emergence of phenomena associated with the rapid outflow of plasma from the focus (a decrease in its density), which leads to the development of kinetic instabilities. Unfortunately, a complete description of these phenomena does not exist, and the differences in the observed behavior of plasma in the case of different devices is due to the characteristics

of these systems, which affect the process of initial phases which form the structure of the current sheath, its shape (curvature radius), and kinetic energy.

It should be noted that the maximum values of the electron temperature, ion temperature, and electron concentration determined by spectroscopic methods (Czekaj et al., 1981; Paduch et al., 1992), interferometrically (Kasperczuk, 1984), or using the *Thomson scattering* effect (Bernard, Coudeville, 1975) are independent of the energy of the capacitor bank in a PF system and are as follows: 100 eV < T_{emax} < 2 keV; 300 eV < T_{imax} < 1.5 keV; $5 \cdot 10^{18}$ cm^{-3}< n_{emax} < $5 \cdot 10^{19}$ cm^{-3}.

Experiments conducted from the 1960s to the 1980s made it possible to understand how the plasma focus (pinch) is created in Plasma-Focus systems, enabled measurement of its density, temperature, lifetime, and sizes. Depending on the energy stored in the capacitor bank, the structure and size of the current sheath and the volume of plasma in the focus changed; whereas its temperature and density changed only slightly. Moreover, the total neutron yield for (D,D) fusion calculated on the basis of measured focus parameters was only about 1% of the total number of neutrons emitted from the focus measured in different experiments on PF systems.

Experiments have also shown that the plasma in the focus is not in thermal equilibrium. On the contrary, both macro- and microscopic instabilities develop in it. However, the most important finding was that despite the lack of thermal equilibrium of plasma and its low temperature, we can obtain a relatively high yield of deuterium fusion reactions in plasma.

3

THE YIELD OF A D-D FUSION REACTION IN THE PLASMA-FOCUS SYSTEM

The emission of neutrons from the plasma focus is the main indicator of the (D,D) fusion reaction yield in the Plasma-Focus system. The amount of neutrons generated in a (D,D) fusion reaction in volume V and during the lifetime of the plasma focus τ, assuming that plasma is in equilibrium at this time, can be expressed by the relationship (2.19), which corresponds quite well to the experimental data in a wide range of current intensities in plasma (see Chapter 2, Fig. 2.18).

Numerous experiments done throughout the 1960s, 70s, and 80s on Plasma-Focus systems with different energy sources (capacitor banks), ranging from a few to several hundreds of kJ, and using deuterium as a working gas, showed a promising relationship between the total number of emitted neutrons and the energy of the capacitor bank supplied to these systems. Such energy scaling for various systems is summarized in Fig. 3.1.

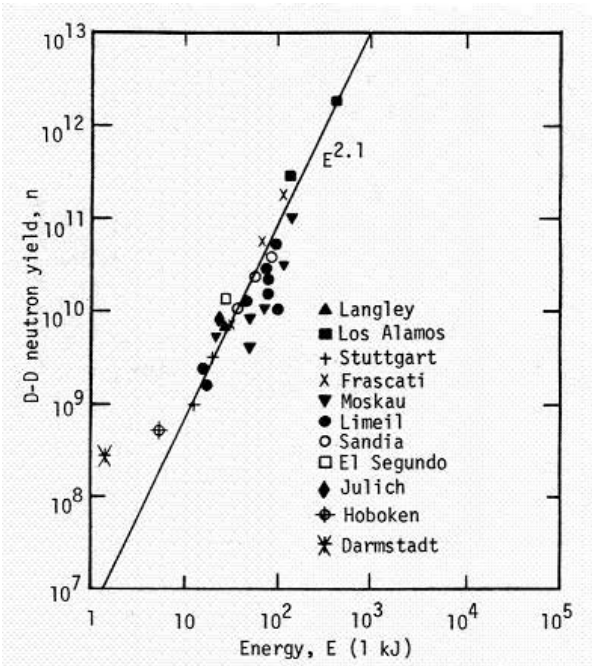

Fig. 3.1. Scaling law for the total emission of neutrons as a function of energy supply from capacitor banks collected in 1975. (Michel et al., 1974)

The relationship of the total emission of neutrons from a (D,D) reaction can be approximated by the following formula: (Michel et al., 1974)]:

$$Y_n \approx 10^7 W_0^2 , \tag{3.1}$$

where Y_n – the total number of neutrons in a discharge in a full solid angle, and W_0 – the energy of the capacitor bank expressed in kJ.

Large Filippov and Mather-type Plasma-Focus systems with nominal energy of the capacitor bank ranging from hundreds of kJ to 1 MJ were extensively studied in Los Alamos, Limeil, Frascati, Stuttgart, and Moscow from the early 1970s to late 1990s.

These systems were built in order to verify experimentally the scaling law which relates the total emission of neutrons as a measure of the (D,D) fusion reaction yield to the intensity of current in the system. This law was derived from numerous experiments on systems with energy less than 0.5 MJ and is expressed as

$$Y_n \sim W_0^{1.7\div2.5} \sim I_0^{3.5\div5} \sim I_p^{4\div5}, \tag{3.2}$$

where Y_n – the total emission of neutrons in a discharge, W_0 – energy of the capacitor bank in [kJ], I_0 – total current in [MA] flowing in the circuit of the PF system, most often measured in the collector of the device using a Rogowski coil, I_p – intensity of current flowing in the plasma focus at the moment of neutron emission from the plasma.

Formula (3.2) shows that the neutron emission increases along with the increase of energy in the capacitor bank, and the current flowing in the plasma focus, attesting to the deuterium nuclei fusion reaction yield in the focus. The experimental relationship expressed by formula (3.2) for PF systems with capacitor bank energies in the range of 1÷500 kJ, and a maximum current amplitude in the range of 0.07 ÷ 2.5 MA, allows calculation of the capacitor bank energy at which the energy delivered to plasma equals the energy emitted as the result of nuclear fusion reactions, i.e. at which the condition $G = 1$ is fulfilled.

Equation (3.1) shows that the properly working Plasma Focus system should emit 10^{11} neutrons per 100 kJ of energy stored in the capacitor bank in one discharge. In large PF systems with a power source of 0.5 MJ and higher, the maximum number of neutrons from the (D,D) reaction in plasma achieved for a current of 2 MA was in the range of $(6 \div 8)\cdot 10^{11}$ (Bernard et al., 1975; Brzosko et al., 1987). Given that the volume of plasma in large PF systems is approximately 20 cm^3, we obtain the neutron emission yield per unit volume at the level of about $3\cdot 10^{10}$ n/cm^3 from a (D,D) reaction.

It follows from the scaling law (3.1) that the number of neutrons from a (D,D) reaction emitted from the plasma focus per 1 kJ of energy stored in a capacitor bank is about 10^7, and means that PF is the system in which fusion reactions of deuterium nuclei occur very intensively at a relatively low energy supplied to the system.

Considering a (D,T) fusion reaction, which is more efficient, the scaling law gives about 10^9 neutrons per each kJ of energy stored in the capacitor bank. This directly corresponds to the number of reactions, with the energy emitted in each reaction equal to $Q = 2.82\cdot 10^{-12}$J. Taking this into account, we can use the scaling law and the condition $G = 1$, for which the energy produced in (D,T) fusion reactions in plasma is equal to the energy stored in the capacitor bank W_0, to show that $G = 1$ can be already achieved for $W_0 \approx 400$ kJ. Also, the physics of processes in a PF system allow, with proper technological and technical preparation of the power source, operation at a frequency of discharges of the order of one or several Hz. These facts led to the conclusion in the initial stage of research performed on the PF systems that the construction of the reactor based on a Plasma-Focus device would be simple.

Experiments carried out on systems with a nominal power supply source energy of 1 MJ (i.e., in excess of 400 kJ) in Frascati and Stuttgart showed that the increase in energy of the power source, and accordingly the total current in the system in accordance with the experimental scaling law, does not increase the total emission of neutrons from the plasma focus beyond this point. Beginning with certain energy values of 0.5÷0.6 MJ, the total emission of neutrons does not grow as provided as scaling law. Instead, it enters a saturation, and even drops with further increase in capacitor bank energy. It should be noted that the increase in capacitor bank energy in all these PF systems, confirming the scaling law, was caused by an increase in the charge voltage U_0, but not an increase in its capacitance C_0.

The problem of inhibiting the increase in the total emissions of neutrons (the reaction yield) with an increase in capacitor bank energy and the total current in the PF system was initially encountered for an energy of about 100 kJ. It turned out that it was related to the repeated electric discharge on the surface of the insulator, which occurred during the acceleration of the plasma layer and increase in the circuit inductance. This was reflected in the dynamics of the compressed plasma sheath and, consequently, in the parameters of the plasma focus. The modernization of the insulator–electrode node structure in PF systems enabled an increase in the total emission of neutrons as energy of the capacitor bank increased to a level of 0.5 MJ.

Understanding the processes and phenomena occurring in a PF and their relationship with the design of these systems (operating in conditions of very high power densities of the order of dozens of GW), and then linking this to the law of scaling of the increase in the total emission of neutrons from nuclear fusion, has become a key problem for PF systems. A number of studies were done on PF systems to this end from the early 1970s to the late 1990s in order to discover the causes of the inhibition of intensity of (D,D) nuclear reactions in the plasma focus of the device. It was assumed in the course of this research that the processes occurring in the PF system generate the plasma focus at a high temperature T and density n, maintained for a period of τ which is long enough for the reactions occurring in it to be considered as thermonuclear fusion. This assumption would confirm the scaling law which relates the total emission of neutrons from the plasma focus Y_n to the current intensity, or energy contained in the capacitor bank, represented by equation (3.2).

On the other hand, the total value of neutron emission Y_n, estimated based on the results of measurements of density n, temperature T and the lifetime τ of the plasma at the plasma focus, was significantly less than measured. In addition, the neutron emission showed the spatial anisotropy of intensity and energy, the widening of the neutron spectrum measured perpendicular to the axis of electrodes, and the Doppler shift of neutron energy spectrum towards higher energies measured along the axis of the electrodes in the direction from the anode of the PF system. The "anomalous" properties of the emission of neutrons from the PF plasma focus, from the viewpoint of the nature of the occurring (D,D) reactions, indicate that the nuclear reaction (D,D) takes place as a result of the interaction of deuterons accelerated to an energy of several dozens of keV with either deuterium plasma, the gas filling the experimental chamber, or both. This in turn implies an entirely different relationship between Y_n and the total current or capacitor bank energy than represented by formula (3.2). In order to properly interpret the results of measurements of neutron emission from a (D,D) reaction from the PF system, it was assumed that the plasma focus in which the fusion reactions take place is moving at a high velocity along the axis of electrodes of the PF system, the so-called *moving boiler* model. The Doppler shift of the neutron energy spectrum and the anisotropy of the intensity of their emissions was explained in this way.

Difficulties in interpretation of the course of nuclear reactions in the plasma focus resulted partially from the fact that experiments on Filippov and Mather-type systems were conducted with electrodes, which often were not matched to the power supply [see Chapter 2, formula (2.6)], and partially from the state of experimental technology, which in the initial study period did not enable obtainment of measurement results with a time resolution

at the level of nanoseconds. With the advent of technology capable of measuring time with nanosecond resolution and an understanding the fact that the PF system should include electrodes (load) adequately matched to the energy source (capacitor bank), it was possible to carry out a series of experiments that included measurement of essential parameters which could affect the course of fusion reactions and the total emission of neutrons from the plasma focus all during one discharge. This allowed systematic examination of processes leading to the creation of the plasma focus wherein the nuclear reactions, (D,D) in this case, occur in the PF system. As a result, a collection of experimental facts was gathered which can explain the mechanisms leading to the resolution of problems related to the course of nuclear reactions in the focus of the PF system.

For large Plasma-Focus devices with a capacitor bank energy of more than 100 kJ and currents of the order of MA, measurements using scintillation probes usually showed two neutron pulses of varying amplitudes (Schmidt et al., 2006). An example of such a discharge is shown in (Rys. 3.2).

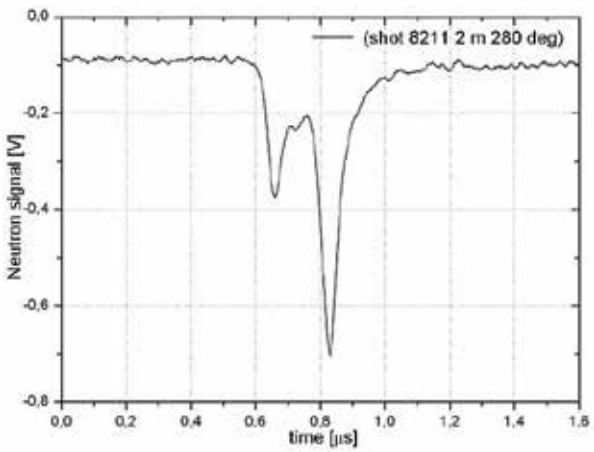

Fig. 3.2. Neutron signal registered in the PF-1000 system using the scintillation probe obscured with 0.5 cm layer of lead. The probe was perpendicular to the plasma focus at a distance of 2m (Discharge No. 8211, unpublished result)

The first neutron pulse, constituting only a part of the total neutron emission, appears at the end of the compression phase, probably at the time of contact of the shock wave on the axis of the electrodes. The neutron group corresponding to this pulse is emitted during the quiet phase of the plasma focus stage. Scintillation probes positioned end-on and side-on to the axes of the electrodes record first pulses as they occur almost simultaneously (Doppler shift is small). They have the same nature and shape of a Gaussian curve. This attests to a small anisotropy of emission of this group neutrons, and their energy determined using the time of flight method for the deuterium system was 2.45 MeV. We can assume that this group of neutrons also includes such neutrons that emerge in fusion reactions as the result of the heating of plasma in the focus with the shock wave first, then with the adiabatic com-

pression of plasma. The yield of this emission for a (D,D) reaction is described by a formula derived from the relationship shown in Chapter 1, formula (1.3):

$$Y_n = \frac{1}{4} n^2 \langle v_r \sigma_{DD} \rangle V\tau \ , \tag{3.3}$$

where n – plasma density, $\langle v_r \sigma_{DD} \rangle$ – thermonuclear reaction rate averaged over the Maxwell's distribution of deuterium ion velocities in plasma, V – volume of the plasma focus, τ – time of maintaining fusion plasma parameters in the focus.

The neutron emission value calculated using formula (3.3) for the measured values of temperature corresponding to an energy of 0.3 ÷ 1 keV, a density of about 10^{19} cm^{-3}, a volume of ≥ 10 cm^3 (in large PF systems), and time to maintain the focus $\tau \leq 100$ ns is small and comprises only a part of neutrons from the first pulse.

The basic neutron pulse coming from the second group of neutrons emitted from the focus is characterized by a steeper rising edge than the first one, and it appears when the unstable phase of the focus starts and the plasma density is several times smaller in relation to the maximum (in the maximum compression phase). There is not only anisotropy of the energy spectrum of emitted neutrons here, but also anisotropy defined as the ratio of emission of neutrons measured parallel to electrode axis to the emission measured perpendicular to this axis. The anisotropy coefficient defined in this way is greater than one. The value of the anisotropy coefficient varies depending on the development of the m = 0 instability, and it is smaller for the plasma focus with one neck than for the one where there are more necks. A detailed study of the neutron emission area performed by means of a special neutron pinhole camera showed that the spatial distribution of this emission approximately coincides with the area of the plasma focus (Fig. 3.3). This shows that only a small portion of the (D,D) reaction takes place outside of the plasma focus in the surrounding working gas (deuterium) of low density.

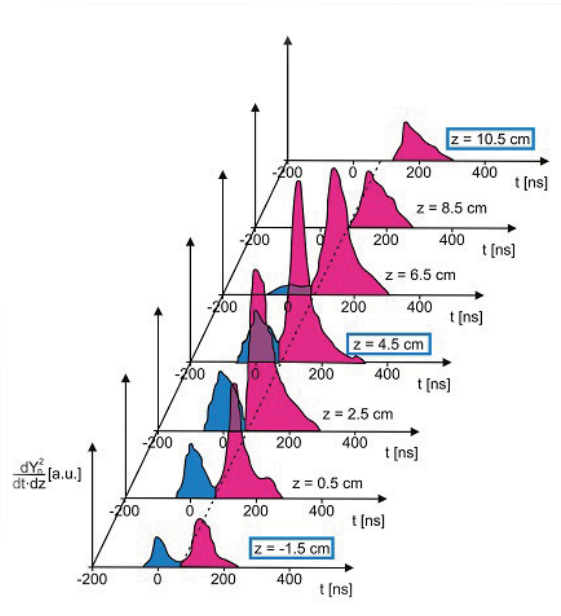

Fig. 3.3. Signals from the neutron pinhole camera made for a single discharge. The spatial resolution along the axis was $\Delta z = 2$ cm, the temporal resolution was about 20÷30 ns. The first pulse occurs only up to a distance of 6.5 cm from the anode. The second pulse is shifted by 40 ns for $z = 10$ cm with respect to $z = 0$ cm (anode surface). (Schmidt et al., 2006, Fig.4)

In order to determine the mean kinetic energy of deuterons in nuclear reactions, the ToF (*Time of Flight*) method was applied using scintillation probes positioned at different distances. The energy spectrum of emitted neutrons as a function of time during the evolution of the plasma focus was estimated (Schmidt et al., 2006), using the deconvolution methods described, e.g. in (Vlad, 1984; Schmidt and Herold, 1987).

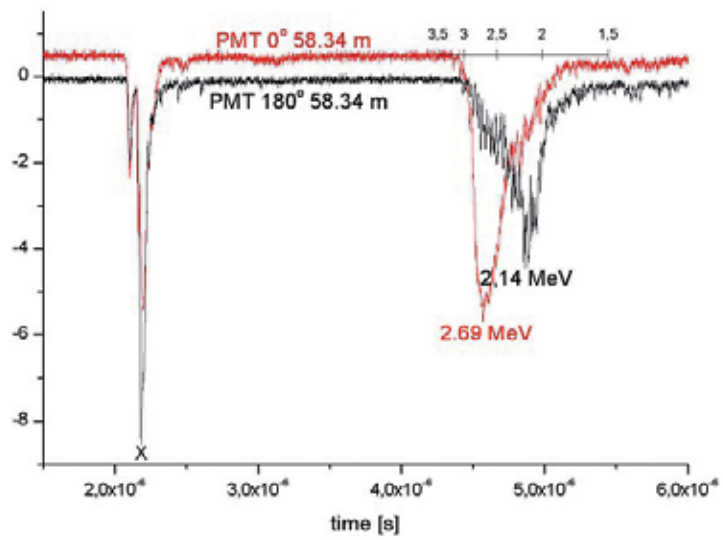

Fig. 3.4. Signals from scintillation probes positioned along the electrode axis of the PF-1000 system at angles of 0° and 180° (Chapter 4, Fig. 4.6) and at a distance of 58.34 m from the surface of the anode. Discharge No. 5649, $p_0 = 467$ Pa, $U_0 = 27$ kV, $Y_n \approx 1.56 \cdot 10^{11}$ n/pulse (Scholz, 2008)

Fig. 3.4 shows signals from scintillation probes positioned parallel to the electrode axis of the PF-1000 system at angles of 0° and 180° (Chapter 4, Fig. 4.6), and at a distance of 58.34 m from the end of the anode. They come from the pulse of a hard X-ray and a neutron pulse emitted from the plasma focus. The characteristic Doppler shift of the signal is visible, indicating the movement of the center of mass of the system in which (D,D) reactions occur. If deuterons in the plasma focus are at a temperature of the order of 1 keV, the observed Doppler shift indicates the presence of a group of fast deuterons. The estimated mean energy of the beam of such fast deuterons for this discharge (Fig. 3.4) is about 60 keV. Doppler shift is different for different discharges and the mean energy of a group of fast deuterons estimated to a good approximation varies in the range of 20÷150 keV.

In summary, we can say that the measurements of neutron emission from plasma, research on anisotropy of this emission, and time and energy characteristics at various points in the plasma focus stage showed that (D,D) reactions in plasma have the nature of fusion only to a limited extent. This is because the ionic temperature of plasma is too low. On the other hand, a group of fast deuterons with energies from a dozen to more than a hundred thousand of electron-volts, which interacts with the low-energy plasma ions, significantly impacts the fusion. The presence of these fast deuterons does not explain well the amount of the total emission of neutrons from the focus due to the short duration of their confinement in the plasma focus. This results from a simple estimation which enables assessment of the ratio of fast deuterons to the total number of deuterons in the focus based on the measured emission of neutrons. It is assumed that fast deuterons with a mean energy of about 50 keV will fly only once by a focus with a length of about 8 cm, in which the average concentration of ions is equal to 10^{18} cm^{-3}. If, on average, the total emission of neutrons for a large PF system is at 10^{11}, we can use the formula $N_b = Y_n/(\sigma_{DD} n_D l)$, where σ_{DD} – collision cross-section for the fusion reaction, n_D – concentration of deuterons in the focus, l – length of the focus, to show that the ratio of fast deuterons to the total number of deuterons in the focus for these parameters is just a few percent. This value is far too high, unless we take into account the possibility of confining this group of deuterons in the focus for a longer period of time due to their cyclotron motion in the magnetic field, which causes the path l of such ions in plasma to be greater than the size of the focus.

This conception on the role of ions of medium kinetic energy (10÷150 keV) in interacting with low-energy plasma deuterons during a (D,D) nuclear reaction in the plasma focus became dominant in the interpretation of experiments on different systems. It has been expressed most consistently in the GPM (*Gyrating Particle Model*) model shown in (Jäger and Herold, 1987), based on experimental data obtained on the Poseidon device in Stuttgart. Deuterons in this model move on a spiral in a cyclotron motion in the magnetic field of the plasma focus. The mechanism of acceleration of these ions has not been completely defined yet. The cyclotron motion of medium-energy deuterons makes the time of their confinement in the focus much longer than in the case of a single traversing of the focus length. The cyclotron radius of these ions is of the order of the diameter of the plasma focus, and they can make several rotations during which they interact with the hot plasma focus, as with a target. The result is an interesting system in which a group of deuterium ions of medium energy (10÷150 keV), interacting with the plasma target of a temperature corresponding to an energy of the order of a thousand of electron-volts, causes high intensity

nuclear reactions, as evidenced by the total emission of neutrons. In addition, this group of ions, due to the fact that the collision cross-section for the Coulomb collisions in plasma is significantly larger than the cross-section for fusion, heats the electron and ion component of plasma which leads to an increase in the intensity of fusion, and thus to a further increase in the share of neutrons in the total emission. Heating the particles of the plasma focus with fast ions is similar in nature to heating the plasma in tokamaks with a beam of neutral atoms.

In summary, we can assume that a large group of deuterium ions with energies of dozens of thousands of electron-volts, which is difficult to measure directly using current diagnostic methods, and whose presence can be inferred indirectly (e.g. by measuring the spectrum of accelerated electrons with energies of 100 keV, which should be accompanied by the emission of hard X-rays), is responsible for (D,D) fusion reactions in the pinch of the PF system. Hence, neutron pulses are usually preceded by hard X-ray pulses, as shown in Fig. 3.5.

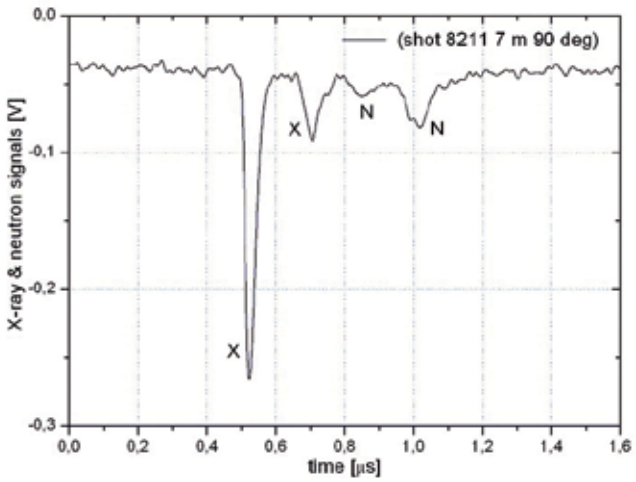

Fig. 3.5. Signals of hard X-rays and neutrons from the PF-1000 registered by a scintillation probe placed perpendicular to the plasma focus at a distance of 7 m (Discharge No. 8211, unpublished result)

It seems reasonable to assume that this group of electrons should be accompanied by a group of accelerated ions of similar energy because of the *quasi* neutrality of plasma. In the presence of a strong magnetic field with induction of about 100 T, ions of this group will move along complex trajectories, confined despite their energy in the plasma focus for a time long enough to significantly increase the intensity of the (D,D) fusion reaction by repeatedly colliding with deuterons in plasma. The observed Doppler shift of the neutron spectrum towards higher energy for emissions along the focus axis away from the anode suggests that the magnetic field has a more complex geometry, and in addition to the induction component B_θ there is also the B_z component of the field. The presence of this component and the appearance of the filaments described in Section 2 in the focus may lead to complex closed configurations of the magnetic field in which ions with energies of dozens of keV are confined in the plasma focus.

If the nature of the reaction of deuterium nuclei fusion in the plasma focus entails the interaction of deuterons accelerated to an energy of several dozens of keV with a plasma target, the intensity of the reaction will depend both on the parameters of this group (beam) of deuterons, and the parameters of the plasma focus (target). At the same time, the number of ions with energies of dozens of keV confined in the focus and its vicinity by the magnetic field of the current should increase along with the increase of the total current in the focus, leading to a higher total emission of neutrons.

Neutron measurements were supplemented by measurements of the angular distribution and energy spectrum of protons from the second reaction channel using trace detectors (CR39 or PM355) integrated over time (Jäger and Herold, 1987; Malinowska et al., 2008). The role a group of deuterons with energies of dozens of keV, confined by the magnetic field and interacting with the plasma focus, can play in the (D,D) fusion reaction at the plasma focus of a PF was confirmed in these measurements, as it was in the case of neutron measurements.

According to this description, the intensity of a (D,D) fusion reaction in the focus, and thus the value of the total neutron emission, is associated with the total number of accelerated deuterons, their mean kinetic energy, plasma density in the focus, and its electron temperature. Although the emission of neutrons is not of fusion nature, and though we do not know the causes of acceleration of deuterons in the focus to an energy of several dozens of keV, we can say that there is no physical reason for the inhibition of the total neutron emission as it has been shown in the results of experiments carried out on large PF systems. In contrast is the question of whether the nature of the fusion reaction in the focus can be the premise for designing the PF system as a fusion reactor producing energy from thermonuclear fusion.

We should still address an important issue related to the empirical scaling law shown in (Fig. 3.1); namely, the relationship between the total neutron emission and the energy of a power source, i.e. the electric energy stored in the capacitor bank (formula 3.1). Such a scaling makes sense from the viewpoint of the relationship between energy emitted in nuclear fusion and energy supplied to the system. However, it seems that the relationship between the value of neutron emission and the total current in the pinch (formula 3.2) is more physically explicable. It should be noted that the total current in the PF system does not mean the total current flowing through the plasma focus, as mentioned in the previous chapter. Typically, the total current in the circuit, instead of the current in the focus (pinch), was measured in various Plasma-Focus systems. It was not a big problem in small PF systems with energies of several dozens of kilojoules, where these currents were almost identical. However, as shown by experiments on the system with an energy level of the order of a megajoule performed in Frascati, the whole current recorded in the system does not flow through the plasma focus (Gourlan et al., 1978). Shunting of the total current in the PF circuit observed in the Frascati system has been associated with the efficiency of sweeping of the working gas with the current sheath moving from the insulator to the electrode axis. If the structure of the current sheath formed in the initial phase of the phenomenon is such that a part of the working gas remains in the vicinity of the insulator, then current shunting begins due to the repeated electric gaseous breakdown. This may especially occur in large PF

systems (capacitor bank energy $W_0 > 0.5$ MJ), and in situations where impurities other than deuterium gas are present in a vacuum chamber, which substantially affects the electrical gaseous breakdown and the formation of the current sheath. This happens most often when, after replacing an insulator, the system requires so-called training, or multiple discharges in order to release oxygen and nitrogen absorbed on its surface and bring on the emission of neutrons.

As we can see, the problem of shunting the total current in the PF system out of the plasma focus (pinch) increases with the increase of capacitor bank energy, and it is closely related to a number of phenomena occurring during the formation and acceleration of the current sheath before the formation of the plasma focus. Although it is a prerequisite for scaling the neutron emission with the current, it has been rarely studied in the past.

4

EXPERIMENTAL RESEARCH ON THE COURSE OF FUSION IN THE PF-1000 SYSTEM

As emphasized in the previous section, the main problem investigated in PF systems has related to explain the causes of the saturation of the total neuron emission growth, i.e. the saturation of the rate of fusion in the plasma focus. Furthermore, researchers began to have serious doubts as to the fusion nature of the reaction. Systematic research on PF systems with energy of the power source above 0.5 MJ in Frascati, on the „Poseidon" system in Stuttgart, or on the PF-3 at the Kurchatov Institute, led to a unification of views on the course of the thermonuclear fusion reaction in the plasma focus. It became clear that with an increase in the power source energy is a growing problem of effective sweeping of the current sheath and the total current flowing through it towards the axis of the PF system, so that all current generated in the system flows in the plasma focus. It seemed that this problem may be closely related to proper shaping of the current sheath, the process of its acceleration, and compression on the electrode axis. With this in mind, a number of facilities started systematic research using various PF systems in order to study the conditions under which the current sheath is correctly formed, so that the final result is the plasma focus (pinch), wherein fusion reactions occur extensively. Due to the fact that deuterium was the working gas in these experiments, the total emission of neutrons was a measured value which characterized the intensity of reactions taking place in the plasma focus. The results of this research helped to determine the conditions under which the current sheath is formed correctly, what should

be its proper structure, and how to optimize the design of the electrodes and insulator in order to create these conditions.

The second chapter, which describes physical processes in the operation of PF systems, shows some of the aspects of the problem, which can be systematized as a reminder.

Firstly, there is the question of current shunting, or its flow outside the plasma focus, encountered for the first time in the Frascati system when using a miniature Rogowski coil placed near the cathode, and then confirmed using magnetic probes, both in the PF-3 system at the Kurchatov Institute in Moscow, as well as in the PF-150 at the Institute of Plasma Physics and Laser Microfusion in Warsaw. These measurements showed that during compression of the working gas, i.e. the motion of the current sheath towards the axis of the system, part of the current flows outside the sheath, mostly in the plasma generated during the ionization of residual working gas that has not been completely swept during detachment of the current sheath from the insulator. As a result, only part of the current flows in the plasma focus, which becomes particularly evident as energy in the capacitor bank increases. In megajoule systems, the value of the current flowing in the focus decreases to even less than 50% of the total current registered in the circuit. This phenomenon of current shunting shows that the existing scaling law, which relates the emission of neutrons from the plasma focus to the total current of I_t registered in the system during discharge and shown as $Y_n \sim I_t^4$, should be formulated so as to associate the emission of neutrons with the current I_p, flowing through the plasma in the focus, i.e. $Y_n \sim I_p^4$. We can verify this law if the neutron emission and current I_p are measured simultaneously.

Secondly, the phenomenon of current shunting is associated with electric gaseous breakdown along the insulator and shaping of the current sheath, which should achieve the structure and properties needed to sweep the gas as soon as possible due to its role in gas sweeping. Therefore, the design of the electrode-insulator node should provide a rapid and uniform electrical gaseous breakdown along the insulator, as well as detachment of the current sheath from the surface as soon as possible. This prevents evaporation of impurities which affect the structure of the layer from the surface of the insulator, while changing the sweeping performance. The result is often that a certain amount of working gas remains, and that there is a repeated electric breakdown in the remaining gas in the vicinity of the insulator and aforementioned current shunting. The insulator material should have a high dielectric constant, providing a high capacity for gigahertz frequencies and a high melting point, which prevents its sputtering. Furthermore, the insulator should have a small diameter and a small thickness, matched to the geometry of electrodes.

Research on the electric gaseous breakdown phase for different charging voltages of capacitor banks, both in the megajoule system in Frascati, as well as in smaller systems, have shown that the main reason for a low total emission of neutrons from the focus was a change in the nature of the breakdown which, instead of closing the circuit by a discharge from the anode to the cathode along insulator, closed the circuit in another area between the cathode and the anode (e.g. at the end of electrodes). This results in a very diffuse current sheath of a large volume (weakly formed) and often asymmetrical with respect to the axis of the cylindrical insulator. Such a sheath sweeps gas very poorly during movement along the electrodes

and during compression towards the axis, resulting in a large radius of the plasma focus and a low-density of plasma. Then the current shunting outside the focus (pinch) becomes significant, the current flowing in the focus is small, and the amplitude of the current derivative at the time of the maximum compression of plasma decreases rapidly. Thus, electrical gaseous breakdown between the electrodes outside the insulator, rather than on the surface of the insulator, causes deterioration of parameters of the plasma focus, leading to a decrease in the total emission of neutrons. As Paschen's law shows, this breakdown, in addition to the voltage between the electrodes, also depends on the pressure of the working gas.

These observations resulting from systematic research on many PF systems led to the conclusion that if we want to obtain a plasma focus (pinch) with parameters that ensure high intensity of the fusion reaction (high emission of neutrons) in the final course of the phenomena associated with the formation, structure, and compression of the current sheath on the electrode axis, we should associate the following values for these systems based on similarity, regardless of the PF size:

- Initial pressure of the working gas.
- Capacitor bank charging voltage, which determines the maximum current in a system at a given capacity of the bank.
- The surface area of the insulator, depending largely on its radius.

It has been shown in the second Chapter that there is a matching condition (formula 2.6), which binds these parameters together:

$$\frac{U_0^2\, C_0^2}{r_A^2\, p_0\, l^2} \cong const \quad , \tag{4.1}$$

where C_0, L_0, U_0 – capacitance, inductance and charging voltage of the capacitor bank,

r_A – radius of the anode (or insulator), l – length of electrodes, p_0 – pressure of the working gas, and the amplitude of the current is expressed as $I_m = U_0(C_0/L_0)^{1/2}$.

We can see that changing only one parameter in the matching condition, e.g. the charging voltage, in order to increase the amplitude of the current I_m can lead to deterioration of plasma focus parameters and thus, to reduction of the total emission of neutrons. It is important to note that matching is a necessary but not sufficient condition for optimal operation of the PF. Simultaneous increase of U_0 and p_0 in such a way that meets the matching condition does not necessarily provide for optimal operation of the system with respect to neutron emission. With an increase in the charging voltage and pressure of the working gas in the PF vacuum chamber, conditions of the electric breakdown change, causing the discharge to develop asymmetrically to the surface of the insulator.

Similarly, an attempt to increase the amplitude of the current I_m by increasing the voltage U_0 and reducing the inductance L_0 may result in inferior parameters of the plasma focus, i.e. reduction of neutron emission instead of an increase in capacitance C_0. It has been found

that with a low-induction (very fast) capacitor bank and high charging voltages, the electrical gaseous breakdown does not have to occur at the surface of the insulator, and the formed current sheath is too blurred and distorted. In addition, the matching condition is violated, causing the deterioration of plasma focus parameters, which causes a decrease in the emission of neutrons from plasma.

Experiments conducted on different PF systems, including those with a battery energy of more than 0.5 MJ, in the 1970s and 80s allowed technological systematization of the causes leading to a decrease in the total neutron emission from the plasma focus associated with loss of generation of deuterons with energies of the order of tens of keV, and with a deterioration of plasma parameters in the focus. A number of attempts were made to eliminate these causes by appropriately selecting the material and geometry of the insulator; by adequately setting the working gas pressure, voltage, and geometry of the electrodes; by attempting to pre-ionize gas near the surface of the insulator, etc. Unfortunately, due to closure of the largest PF systems in Los Alamos, Frascati, and Stuttgart, these attempts were aborted before the research was finalized. For this reason, experimental results obtained on the PF-1000 system in IPPLM in Warsaw, at a rated energy of 1.1 MJ, which is currently the only major system in the world where deuterium is used as the working gas, represent an important contribution to the analysis of fusion problems in the PF system. The most important researched problems include:

- The nature of (D,D) fusion in the focus of PF.
- Presence of a large group of deuterons with energies of dozens of keV.
- Breakdown of the law regarding the scaling of neutron emission depending on the amperage in the system.

The remainder of this chapter includes a description of PF-1000, the diagnostics used, and experimental results that show new facts or experimentally confirm the hypotheses adopted on the basis of results obtained on previously mentioned systems operated in the 1970s and 80s.

The analysis aims to examine the nature of the course of fusion of deuterium nuclei in the plasma focus, the effect of ions with a mean kinetic energy of the order of tens of keV, and how parameters of the plasma focus affect emission of neutrons produced in fusion reactions. In addition, it is aimed at relating these parameters to the formation of the current sheath. The conclusions of this analysis will reveal the character of nuclear fusion in a Plasma-Focus system and whether this system has the potential to be a fusion reactor.

4.1 PF-1000 EXPERIMENTAL SYSTEM

The basic design of the Plasma-Focus PF-1000 was made in the late 1970s, and the main elements of the system were made at the Institute for Nuclear Research, Poland, and assembled in the late 1980s at the Institute of Plasma Physics and Laser Microfusion, Poland. The system was commissioned at the beginning of the 1990s, and it was modernized several times during its life time.

The PF-1000 is unique because of its technical parameters and diagnostic equipment. The device consists of the following main modules (Scholz et. al., 2000):

- Capacitor bank.
- Experimental chamber with a collector and high-voltage cables.
- Energy load, or cylindrical coaxial electrodes separated by an insulator.
- A set of measurement systems (i.e. diagnostics) consisting of standard diagnostics and those prepared for specific experiments.

THE CAPACITOR BANK

The capacitor bank of a total capacity C_0 = 1.332 F consists of twelve modules, each of which contains 24 low-inductance, high-voltage (50 kV) capacitors with a capacity of 4.625 μF and inductance of 40 nH each – for a total of 288 capacitors connected in parallel. Capacitors are in special modules arranged on two levels above and below the experimental area (Fig. 4.1). Each capacitor is equipped with a three-electrode, pressurized "*field distortion*" type spark gap which may be filled with dried compressed air at a pressure above atmospheric, providing the resistance of the spark gap to self-breakdown, thus enabling the bank to be charged to a maximum voltage of 40 kV. Spark gaps are started with a small time spread (less than 20 ns) with a special trigger system consisting of 16 fired spark gap. A modern automatic system controls charging of the capacitor bank. This system is coupled with the circuit which controls the jitter of sparks. The capacitor bank can be charged from U_0 = 20 to 40 kV, which enables accumulation of electric energy in the range of 266÷1064 kJ. The rated total inductance of the capacitor bank and the collector is L_0 = 19 nH, and the internal resistance is R_0 = 2.6 mΩ. Tests with a shorted capacitor bank enabled determination of the maximum short-circuit current, I_{SC} = 12 MA; the time to reach the maximum current is $t_{1/4} = 6\mu$s.

Fig. 4.1. The upper part of the PF-1000 capacitor bank. A view of one of the twelve modules containing 24 capacitors. (Scholz et al., 2000)

THE EXPERIMENTAL CHAMBER

The cylindrical chamber (Fig. 4.2) of size Ø = 1.4 m, l = 2.5 m and volume of about 4 m^3 is made of stainless steel and connected to the collector of the current generator (condenser bank), to which low-induction, high-voltage cables are attached that connect the capacitor bank modules to the electrodes of the system through the collector. The axis of the experimental chamber (and electrodes) is located on a horizontal plane approximately 120 cm above the floor level. The vacuum in the chamber is produced by a high-efficiency rotary pump and two turbo-molecular pumps capable of achieving a vacuum at 10^{-4} Pa. The chamber is filled with working gas via a pressure-controlled valve in the range of 1÷100 Pa.

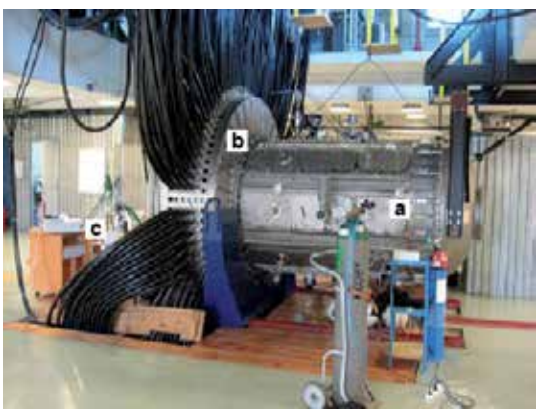

Fig. 4.2. The experimental chamber (a) of PF-1000 with the collector (b), and cables (c) feeding current from the capacitor bank to the electrodes (Scholz et al., 2012)

ELECTRODES OF THE PF-1000 SYSTEM

The system uses two types of electrodes differing in cathode design and anode end (Fig. 4.3). The electrodes enable operation in the full range of capacitor bank energy up to 1 MJ. In the set of type 1 electrodes shown in Fig. 4.3a, the outer electrode (cathode) consists of 24 stainless steel tubes with a diameter of 32 mm each. The tubes are arranged in a circle with a diameter of 400 mm. The inner electrode (anode), with a diameter of 226 mm and a length of 560 mm, is made of pure copper. The anode ends with a head of a diameter which is 10 mm larger than the cylindrical part of the anode, creating a cylindrical protrusion on this edge in the shape of a triangle extending over the cylindrical portion of the anode. The intent of this protrusion was to stop metal vapor during compression of the current sheath to the system axis, but its effect on the plasma focus turned out to be much stronger due to the diffraction of a shock wave on the edge. A hole with a diameter of 30 mm was made in the middle of the head. Electrodes are divided by an Al_2O_3 insulator with a length of 113 mm on the anode.

The cathode in type 2 electrodes (Fig. 4.3b) was changed by using 12 tubes with a diameter of 80 mm. The length of the anode, cathode, and insulator remained unchanged. During further modernization, 4 capacitive voltage probes and 4 probes measuring the current derivative were installed in the collector in order to study the current distribution inside it. In addition, the length of electrodes was shortened by 100 mm, so that the length of the anode and cathode in the final version was 460 mm. The length of the insulator was also reduced from 113 mm to 85 mm.

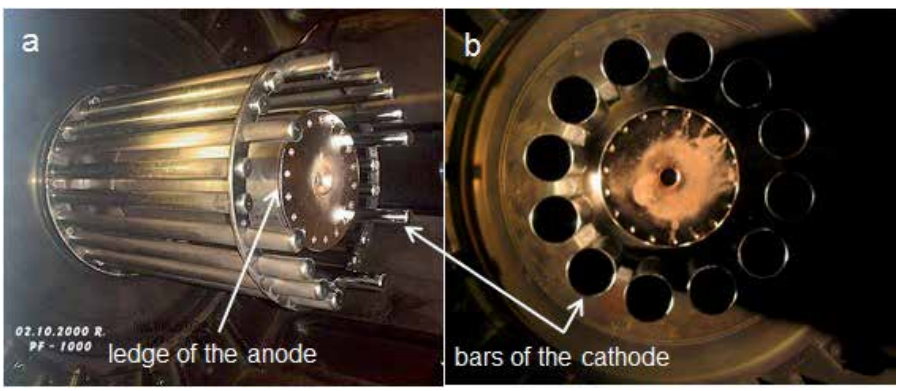

Fig. 4.3. Two types of electrodes used in PF-1000. a) cathode consisting of 24 bars with a diameter of 32 mm. b) cathode consisting of 12 bars with a diameter of 80 mm (Sadowski and Scholz, 2009)

STANDARD DIAGNOSTICS SYSTEM OF THE PF-1000 SYSTEM

Diagnostic equipment consists of electrical probes in the system.

These are:

- Rogowski coil (located in the collector, Fig. 4.4), which is used to measure current during discharge. Calibration factor of the coil is 47 kA/V.
- Four magnetic probes for determining the current derivative, distributed symmetrically at 90° in the collector (Fig. 4.4). First, they are used to determine the nature of the compression of the current sheath by analyzing the depth of the derivative minimum at the phase of maximum compression; second, to determine the time it takes the current sheath to reach the end of the electrodes (the time at which $dI/dt = 0$); and third, to control uniform current distribution in the collector, i.e. the simultaneous discharging of all 12 sections of the capacitor bank.
- Three capacitive probes for measuring voltage, also located in the collector (Fig. 4.4), for determining the voltage induced in the system in the phase of maximum compression, which in the case of the current derivative provides information on the quality of compression. Calibration factor of the probes is 4 kV/V.

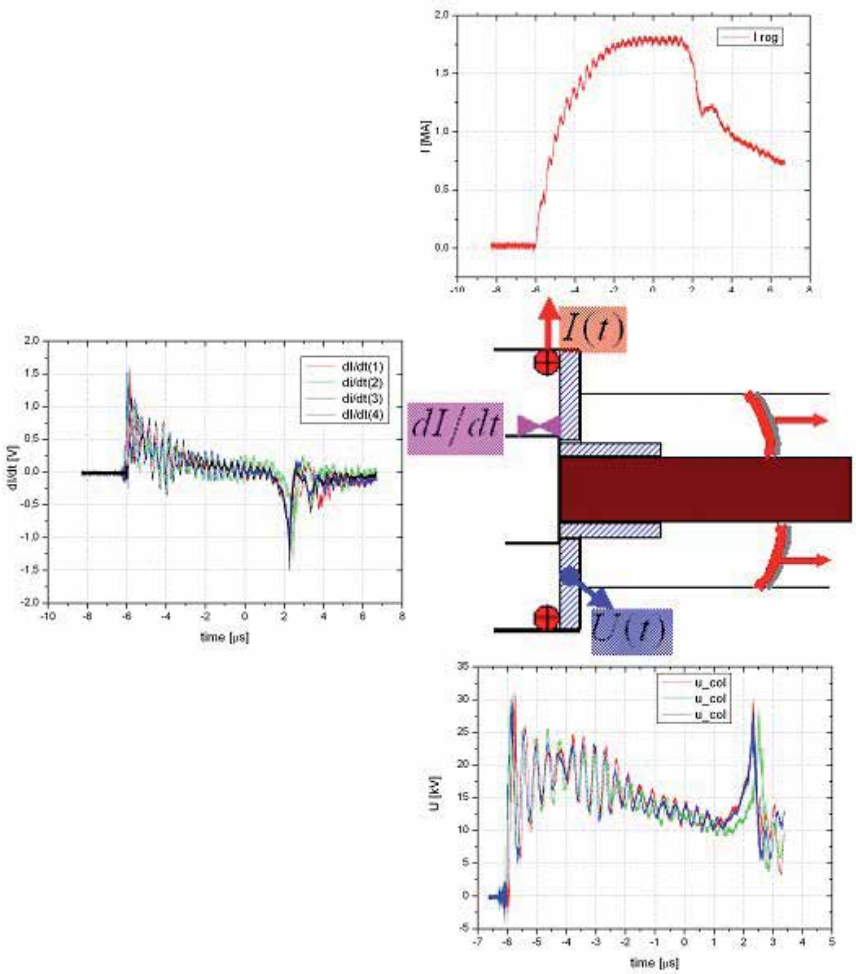

Fig. 4.4. Schematic arrangement of the Rogowski coil I(t), probes dI/dt, and probes U(t) in the PF-1000 collector. Adjacent are sample electrical waveforms from one discharge recorded by these probes (Scholz, 2004)

Standard diagnostics for measuring electrical quantities were supplemented with a silicon detector based on a PIN semiconductor which registers photons of energies in the range of 0.8÷10 keV through a pinhole with a diameter of 100 μm, covered with beryllium foil 10 μm thick. In this optical configuration and counter geometry, the radiation reaches the detector from the plasma focus through the hole and foil. Fig. 4.5 shows the location of the detector at the vacuum chamber in the PF-1000. The detector provided information about the initial time of forming the focus, and was not absolutely calibrated. The emergence of

the first pulse from the detector was taken at time $t = 0$, i.e. the moment of formation of the focus (current sheath reaching the electrode axis).

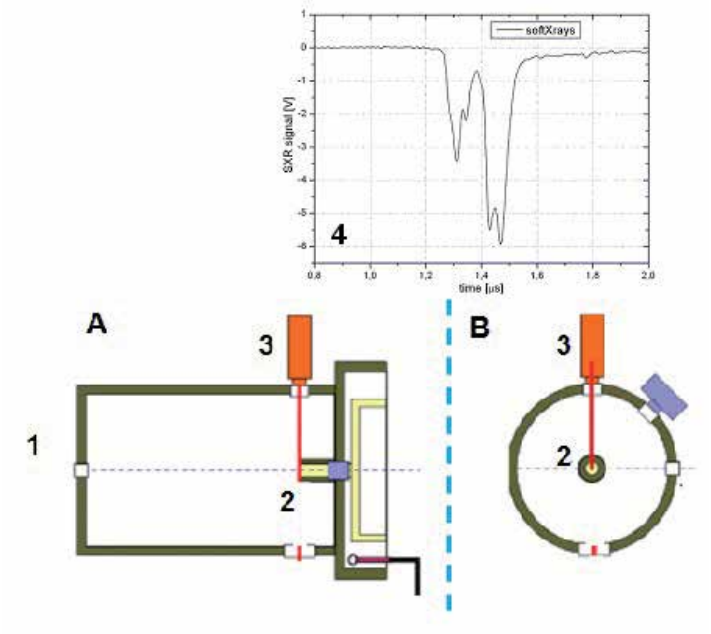

Fig. 4.5. Geometry of the PIN diode on a PF-1000 vacuum chamber with respect to the electrodes. A, B – cross-sectional view of the vacuum chamber; 1 – PF-1000 experimental chamber; 2 – electrodes, 3 – PIN diode, 4 – soft X-ray signal captured by the PIN diode

In addition to standard diagnostics for measuring electrical quantities, the system is equipped with silver activation counters calibrated absolutely using an Am-Be source by rapid "*source removal*" (Gentilini et al., 1980). They are used to measure the total emission of neutrons from the plasma focus. Fig. 4.6 shows the settings of scintillation probe detectors (SPD) in relation to the plasma focus. The standard diagnostic equipment of PF-1000 also includes eight scintillation probe detectors in housings made of boron carbide, paraffin, and lead, but their arrangement in relation to the plasma focus changes depending on the nature of the experiment.

Each probe is located in a mobile Faraday cage with an autonomous system for triggering, power supply, and recording of signals using an oscilloscope (Fig. 4.7). The probes allow the measurement of hard X-ray and neutron signals in different positions relative to the plasma focus.

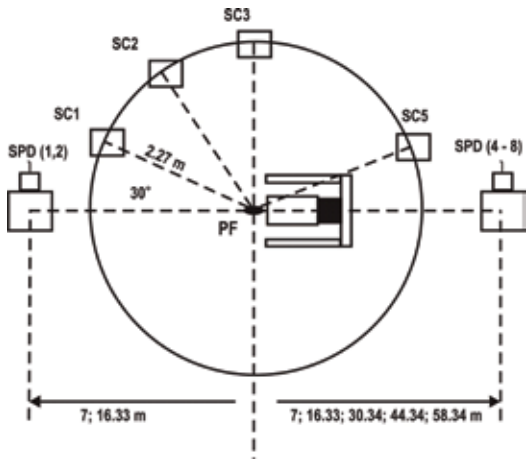

Fig. 4.6. The geometry of the distribution of silver counters (SC) in the PF-1000 in relation to the plasma focus. SC1 ÷ SC5 – silver counters, SPD – scintillation probe detectors (Scholz et al., 2004)

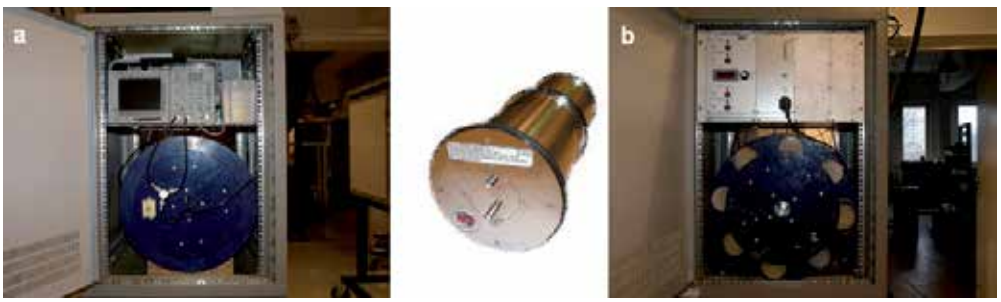

Fig. 4.7. Measuring stand for the detection of hard X-rays and neutrons. Probe located in the housing, a Faraday cage. a) rear view, b) front view. In the middle is a view of the probe with a Bicron® type scintillator with a diameter of 50 mm and a photomultiplier. (Scholz, 2011)

Systems for measuring electrical pulses and for triggering registration and diagnostic systems consist of detectors located on the experimental chamber and a multi-channel system for control, collection, and analysis of signals. In order to avoid any disturbances, the signals from detectors are transmitted to the main control and data collection system using fiber optics, which is located in a mobile Faraday cage with an autonomous power supply (Fig. 4.8) (Tomaszewski et. al., 2002).

Fig. 4.8. Monitoring and control system for PF-1000 diagnostics in a Faraday cage

Measurement signals from the electrical, neutron, and hard X-ray diagnostics can be archived either via an intranet or by means of portable storage media. The numerical values from silver counters are collected separately in the main control room of the PF-1000.

Other diagnostic equipment of the PF-1000 is related to research both on physical processes affecting the evolution of the plasma focus (pinch), and on its parameters and their impact on the nature of the (D,D) fusion process from the viewpoint of the scaling law. This diagnostic equipment has changed in the course of the experiments and some of it has come from other laboratories specializing in plasma diagnostics. This enabled the linking of multiple emission characteristics of the PF-1000 plasma focus in order to better understand the processes occurring in it that lead to fusion in deuterium plasma.

4.2 DIAGNOSTIC EQUIPMENT OF THE PF-1000 SYSTEM

As noted in the previous section, in addition to standard diagnostics related to operational parameters of the PF-1000 such as: current, voltage, current derivative, and neutron counters monitoring the neutron yield from the plasma focus, diagnostics were also used for measurements which enabled study and explanation of problems associated with the scaling law, as well as the nature and course of nuclear fusion reactions in deuterium plasma in the pinch.

There are two diagnostic systems in the PF-1000: those which register signals integrated over time and those which register waveforms in the time expansion. When studying the phenomena occurring in the PF-1000 system, the key problem is time synchronization of this second group of diagnostics with the phenomena occurring in the PF. Synchronization accuracy and the time resolution of registration should be adjusted to the rate of change in physical processes taking place in PF-1000. These processes have different time scales according to which they can be divided and grouped.

The first group consists of processes related to the discharge of the capacitor bank (power source) through the electrodes (load); processes of formation, acceleration, and compression of the current sheath to the electrode axis; and formation of the plasma focus. The time scale of these processes is of the order of microseconds, i.e. the fastest waveforms associated with pulses of current, voltage, and current derivative correspond exactly to this time scale. The diagnostics group corresponding to these processes enables obtainment of information about the course of the entire discharge; that is, about the time of acceleration, and compression. Based on these measurements, we can estimate how the power supplied to the PF system changes over time. In turn, based on the minimum of the current derivative, we can approximate the nature of compression, as well as of the plasma focus. These diagnostics enable optimization of the geometry of electrodes depending on the power source. They played an important role in early research on PF systems, and they are conventionally used in every system today.

The second group consists of magnetohydrodynamic processes taking place in the different discharge phases in the PF. Due to diagnostics set to register such processes, we can separate and characterize these phases. Due to the fact that these phenomena are related to the movement of the center of mass of the medium which moves at a velocity of the order of 10^7 cm/sec at typical distances of the order of centimeters or millimeters, the time resolution and the synchronization accuracy of the diagnosis with the phenomenon should be about 1 ns.

Finally, the third group consists of kinetic processes occurring in the plasma of the PF focus. Their characteristic times are related to the rates of accumulation of micro-instabilities, the course of radiation processes, the frequency of collisions of plasma particles, and characteristic frequencies such as the cyclotron or plasma frequency. These processes require diagnostics with a time resolution at fractions of nanoseconds, or even picoseconds, as well as a spatial resolution at a micron level. The diagnostics described in this paragraph did not have such a time resolution, because only in the last 2 to 3 years has development of technology begun to allow the construction of such metering systems.

Diagnostic systems which enable the recording of information not only at picosecond, but at nanosecond synchronization and time resolution, were used in the experiments whose results shall be described in the next section. In such pulse experiments as those done when studied phenomena in the PF, the individual components of diagnostic equipment must be run at exact times and with precision down to the nanosecond. Such accuracy requires the consideration of all delays, such as pulse propagation time in cables (about 5 ns/m) and in the recording equipment, which means implementing appropriate calibration and corrections. The synchronization system used was designed based on nanosecond plasma radiation detectors, very fast spark gaps, coaxial forming lines, and optical fibres. This provides accuracy in determining the moment in time in relation to the evolution of a phenomenon of not less than 5 ns. The spatial scale of plasma phenomena, in particular of the plasma focus, is calibrated using fixed patterns on the spatial grid, placed on the electrode axis in the center of the anode.

MAGNETIC PROBES

Standard measurements of current, voltage, and current derivative over time, globally in the whole PF system, enable approximate determination of the formation of the plasma focus (see Chapter 2). These values belong to the so-called operating characteristics of the system. In order to examine this process more precisely with the development of measurement techniques, measurements using magnetic probes of local current density began in an effort to explore the structure of the current sheath and its dynamics in the area between electrodes, which are usually placed away from the plasma focus (Gourlan et al., 1978; Borowiecki et. al., 1984; Krauz et. al., 2007; Bruzzone and Grondonaz, 1997).

Measurement with a magnetic probe entails measuring the voltage induced by the time-varying magnetic flux passing through the loop of a given radius (Fig. 4.9). Depending on the setting of the loop with respect to the current sheath in PF, we can measure the change of the magnetic flux over time in relation to the B_θ or B_z component. The value of the magnetic field induction is converted into the current flowing in the sheath by using simple relationships:

$$U_p \sim \frac{dB}{dt} \Rightarrow B \sim \int U_p\,(t)dt \Rightarrow I \sim B \cdot r_p \quad , \tag{4.2}$$

where U_p – voltage induced in a loop with radius r_p by the change of the magnetic field induction vector perpendicular to the surface of the loop over time, B – modulus of magnetic field induction, I – current flowing in the current sheath.

Typically, two independent loops (Fig. 4.9) are used, so that the voltage pulses registered have the same shape and amplitude, but inverted polarity. This way we can ensure that the registered signals come from changes in the magnetic flux, and not from electromagnetic interference.

The measuring element of the probe is enclosed in a metal, ceramic, or glass housing of a given thickness, which allows diffusion of the magnetic field. We should take into account the fact that the measurement is carried out through contact with plasma, thus may interfere with plasma in the current sheath and affect its movement and parameters. In addition, if the current flowing in the sheath is high (greater than 1 MA), the probe is destroyed, so it is a disposable sensor. For this reason, the measurements using probes, as noted previously, were carried out away from the plasma focus (pinch), where the current did not achieve such high values.

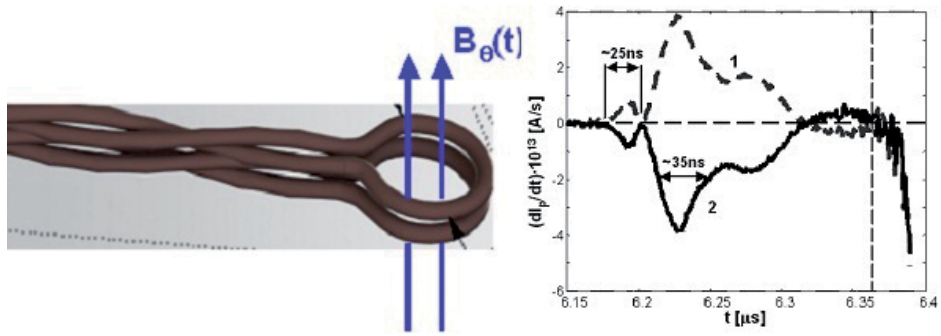

Fig. 4.9. Measurement element of the magnetic probe – a loop which measures changes in the magnetic flux B_θ over time resulting from the current flowing in the current sheath. Adjacent is a sample signal from such a probe located 40 mm from the electrode axis; 1, 2 – the same signal from dB_θ/dt, but with different polarization. (Krauz et al., 2012)

Skilful measurement using the probe provides important information about current in a given location, as well as about the structure of the current sheath. By placing several probes at predetermined distances along the electrodes, we can also determine the velocity of the current sheath (Mather, 1971). In some experiments, the recording element of the probe was additionally equipped with an optical fiber of a small diameter (less than 1 mm) protruding from the ceramic housing at a length of about 1 mm (Fig. 4.10) and connected to the photomultiplier. It recorded the radiation in the visible range emitted from the passing the current sheath at the probe location. Such a probe has also been used to study the structure of the current sheath for early phases of radial compression in the PF-3 system (Krauz et al., 2011).

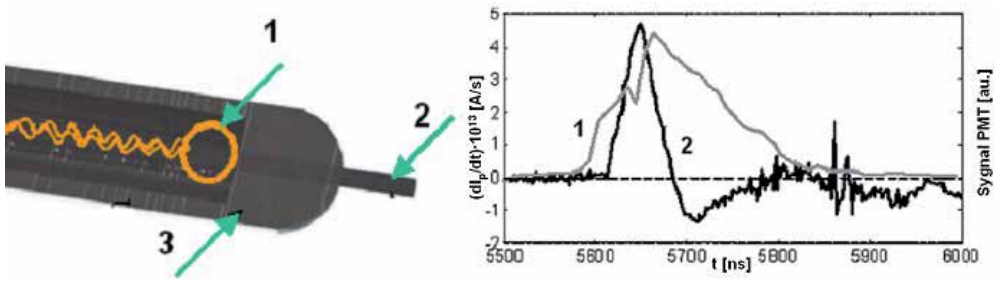

Fig. 4.10. On the left: Sensing element of the magneto-optical probe; 1 – loop which measures changes in the magnetic flux B_θ over time, 2 – optical fiber, 3 – ceramic housing of the probe. On the right: Sample signal from the probe placed 40 mm from the electrode axis; 1 – signal from the photomultiplier (PMT), glow of the current sheath, 2 – signal from dB_θ/dt (Krauz et al., 2012)

For the first time in the history of research on PF systems, a third type of magnetic sensor was used in experiments using the PF-1000, wherein the measuring element has an additional loop to measure the variation in the magnetic flux B_z over time. The recording element of this magnetic probe included two loops perpendicular to each other that registered changes in the flux of B_θ and B_z components of the magnetic field, as well as the optical fiber. Thus, the probe enabled simultaneous registration of radiation from the current sheath, as well as B_θ and Bz components of the magnetic field. The recording element of this new probe is shown in Fig. 4.11.

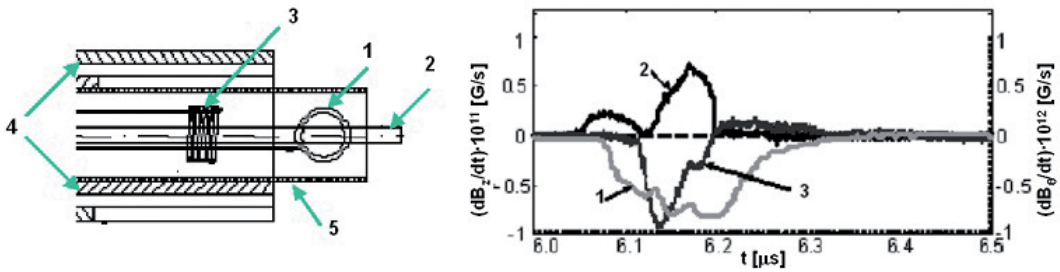

Fig. 4.11. From left to right: The sensing element of the magneto-optical probe for measurement of axial components B_θ and B_z of the magnetic field; 1 – coil for measuring the B_θ component, 2 – optical fiber, 3 – coil for measuring the B_z component, 4 – copper screen with a slot for the axial component of the magnetic field, 5 – dielectric shield. On the right: Sample signal from the probe placed 40 mm from the electrode axis; 1 – signal from the photomultiplier, glow of the current sheath, 2 – signal from dB_z/dt, 3 – signal from dB_θ/dt) (Krauz et al., 2012A)

The probes were prepared and absolutely calibrated in a uniform, time-varying magnetic field of known inductance and change frequency at the Kurchatov Institute using the method described in (Glazyrin et al., 2009).

The sensitivity of the probes was $(1.0 \div 5.0) \cdot 10^{-11}$ Vs/Gs, the accuracy of calibration was at about 5%, and the accuracy of current measurement in plasma at 15÷20%. In the case of probes for the simultaneous measurement of B_θ and B_z, the sensitivity of channel B_θ assumed values in the range of $(0.3 \div 1) \cdot 10^{-10}$ Vs/Gs, and for channel B_z $(0.5 \div 5) \cdot 10^{-10}$ Vs/Gs. Time resolution of the probes was about 1.5 ns.

Probes prepared in this way were placed on the side of the collector very close to the electrode axis, at the place where forms the plasma focus (pinch). The location of probes relative to the PF-1000 electrodes is shown in Fig. 4.12. The recording element of the probe is elevated 0.5 or 1.5 cm above the surface of the anode, as shown in the figure.

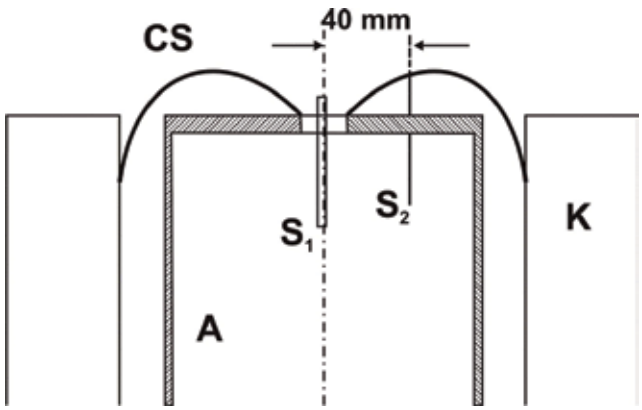

Fig. 4.12. Location of magnetic probes in the PF-1000; A – anode; K – cathode (12 tubes); CS – current sheath; S1 – magnetic probe 0 or 12 mm from the electrode axis; S2 – magnetic probe 40 mm from the electrode axis (Krauz et al., 2012)

A set of high-speed cameras: streak and frame; and then multi-frame interferometry was used in addition to the magnetic probes to study the compression of the current sheath. The frame camera enabled us to determine the geometry of the plasma focus and its change over time. Electron density of plasma in the pinch can be determined based on interferometry, and the streak camera images enabled us to determine the compression speed of the current sheath.

CAMERAS: STREAK; FRAME OPTICAL; AND X-RAY

The Fenix II streak camera is a device which records radiation from plasma in the wavelength range of 700÷900 nm through a slot 0.1 mm wide, positioned perpendicularly to the electrode axis, with an adjustable time expansion of 16.7 to 167 ns/mm. Fig. 4.13 shows the position of the slot relative to the plane of the anode and the image recorded by the camera. A CCD camera with a memory buffer (512×512×8 bit) was used in digital image recording.

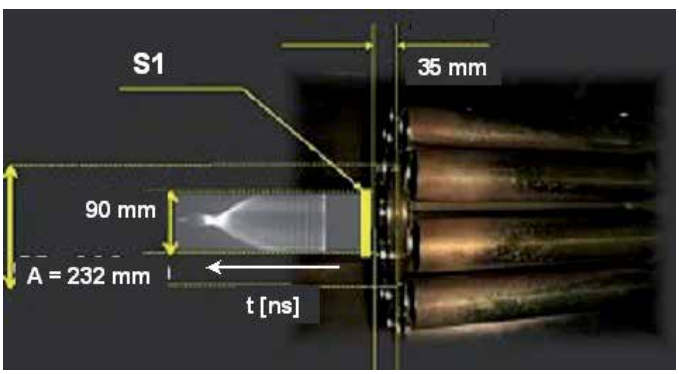

Fig. 4.13. Position of the camera slot relative to the anode and a sample image captured by the streak camera. S1 – slot, A – anode. (Borowiecki et al., 2006)

In addition to the streak camera which recorded the glow of plasma through the slot, the technique of still photography was used in the experiments on the plasma focus. A four-frame camera (QUADRO) with image sensors was used for this purpose. The radiation from plasma was recorded through an interference filter which transmitted only the continuous radiation and cut off linear radiation. Filter parameters: Selected wavelength – 593 nm; transmission – 30%; half of the spectral width – 6 nm. Using gating pulses of high voltage (about 15 kV) enabled obtainment of the exposure time for one frame equal to 1 ns. The time delay between the frames was 10 or 20 ns. Just as in the case of the streak camera, the CCD camera with the memory buffer (512×512×8 bit) was used in digital image recording. The spatial scale on the resulting still images was calibrated with a centimeter grid placed on the electrode axis in the center of the anode. Fig. 4.14 shows an example of a frame from the QUADRO camera overlaid with a centimeter grid in the (*r*,*z*) plane.

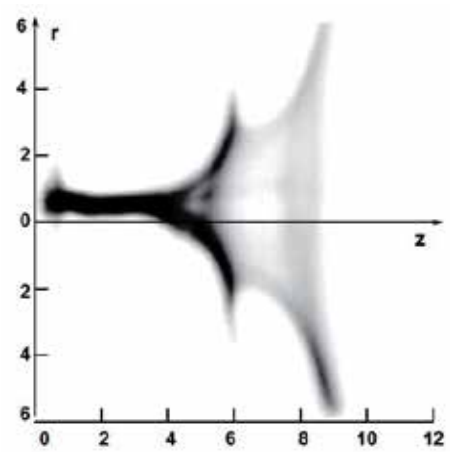

Fig. 4.14. An example of one frame from the QUADRO camera. The figure shows the scale [in cm] in the (r,z) plane. The anode is on the left (not marked).

A set of optical cameras photographing plasma in the visible range was supplemented with a four-frame *camera obscura* (pinhole camera) to record the plasma glow in the soft X-ray range. Unlike the classical pinhole camera, the camera used in the experiments on the PF-1000 includes four holes with a diameter of 230 μm each, arranged symmetrically and covered with polystyrene filters (C_8H_8)n 5.2 μm thick. The principle of operation of such a camera is shown in Fig. 4.15.

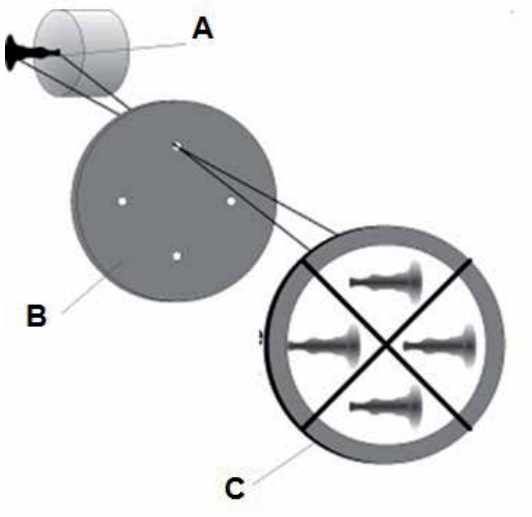

Fig. 4.15. Diagram of a four-frame pinhole camera. A – plasma focus, B – aperture with 4 holes, C – recording element (Tomaszewski et al., 2002)

A *Micro Chanel Plate* (MCP) divided into four electrically isolated sectors of a quadrant shape (Fig. 4.15), behind which a luminescent screen with fiber optics (A), lens (B) and a CCD camera (C) were located (Fig. 4.16), was the recording element used in the pinhole camera.

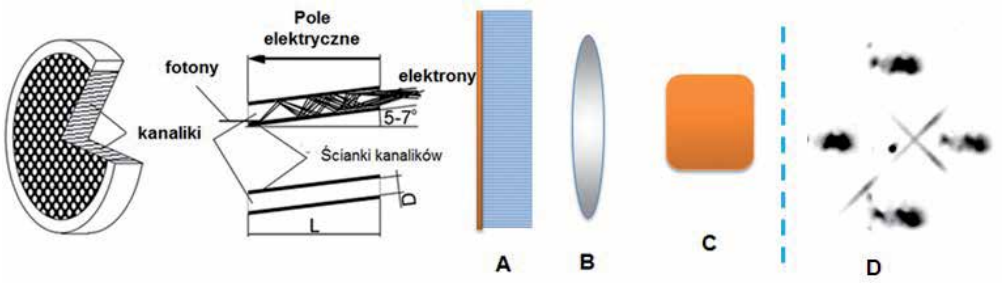

Fig. 4.16. The operation principle of the four-frame pinhole camera Micro Channel Plate (MCP). A – luminescent screen with fiber optics, B – optical system, C – CCD camera, D – sample recording of the plasma focus in the PF-1000 (according to information from K. Tomaszewski).

Each MCP sector was independently gated using a voltage pulse with an amplitude of 5÷6 kV. This enabled us to obtain four frames with an exposure time of 2 ns, and an interval between frames of about 10 ns. Polystyrene $(C_8H_8)n$ filters with a thickness of 5.2 μm have an additional window of quantum transmission in the range of 150÷290 eV, in comparison with a beryllium filter with a thickness of 10 μm. Plasma radiation is intense in this range of quantum energies, and the sensitivity of the Micro Channel Plate is high, which enabled us

to get a clear image of the plasma focus (D) despite a short exposure time (about 2 ns). Fig. 4.17 shows the spectral response of the camera for different materials.

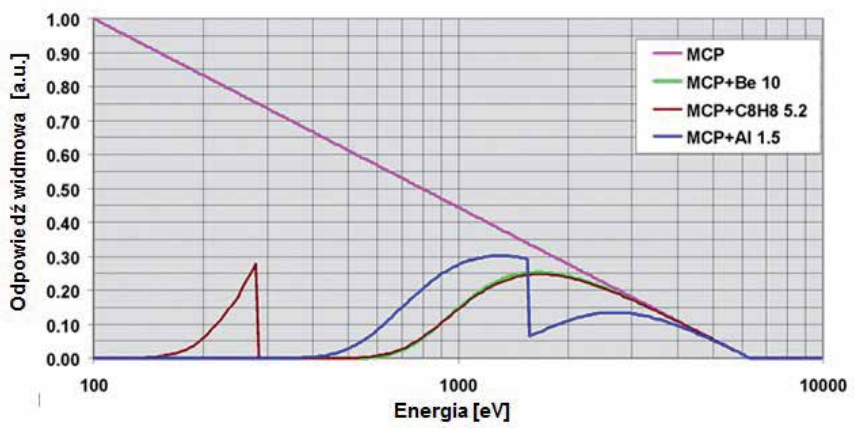

Fig. 4.17. Spectral response of the camera for different filters for the camera holes

The recording element of the pinhole camera was placed at a distance of 100 cm from the electrode axis, and the plate with holes was placed at such a distance that the camera zoom ratio was 1:4. Fig. 4.18 shows the locations of streak, frame, and X-ray cameras in the vacuum chamber of the PF-1000. If the streak camera was placed in one of the measuring paths of the frame camera, only three frames were recorded using the QUADRO camera.

The high-speed four-frame optical camera allowed registration of changes in the image of the plasma focus every 10÷20 ns. In the case of four frames, these changes can be tracked during a single discharge for only 40 to 80 ns. By moving the recording time of the first frame relative to the phenomenon for various discharges, we can trace the whole life time of the plasma focus, which lasts about 200 ns, in the sequence of these four frames.

In such a case, we should have assumed that for the same conditions of the working gas pressure and capacitor bank charge voltage, the evolution of the focus would progress very similarly for the same current measured at the collector, but that assumption was very rough. Furthermore, it was difficult to unquestionably assess the electron and ion density of the plasma based on the image of plasma glow. Therefore, the camera system was replaced by a Mach-Zehnder optical interferometer in subsequent experiments.

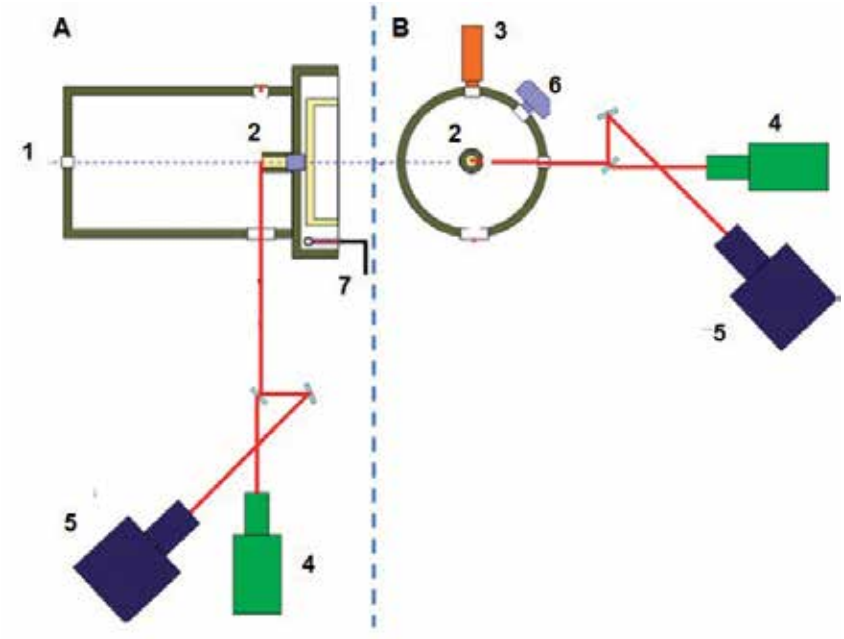

Fig. 4.18. Schematic layout of the streak, optical frame, and X-ray cameras on the vacuum chamber of the PF-1000; the longitudinal (A) and transverse (B) section of the vacuum chamber; 1 – vacuum chamber, 2 – electrodes, 3 – PIN diode, 4 – QUADRO frame camera, 5 – FENIX streak camera, 6 – X-ray frame camera

MACH-ZEHNDER INTERFEROMETER

In this type of interferometer used in the PF-1000 (Fig. 4.19), the laser beam is split in a special delay line (2) into 16 beams that reach the expander system (3) in a specific time sequence. If we assume that the first beam reaches the expander at time 0, the next at 10 ns after the first, the third 20 ns after the second, etc., alternately 10 and 20 ns for each consecutive beam reaching the expander, the last one would reach the expander 220 ns after the first .

After passing through the expander, each beam is separated by a mirror system into two beams (4), each of which passes through the interferometer via a different path. Subsequently, both beams converge at the output of the system. The interference image seen on the screen depends on the phase shift of the two beams, and therefore it is sensitive to the smallest details which can affect the difference in optical paths between the arms of the interferometer. If the beam in one of the interferometer arms passes through the plasma, a transparent object whose refractive index is subject to slight changes over time and space, then the results of these changes are visible in the interference image as a set of interference

fringes (B). This can be used to study subtle heterogeneities in plasma, e.g. the spatial distribution of its density.

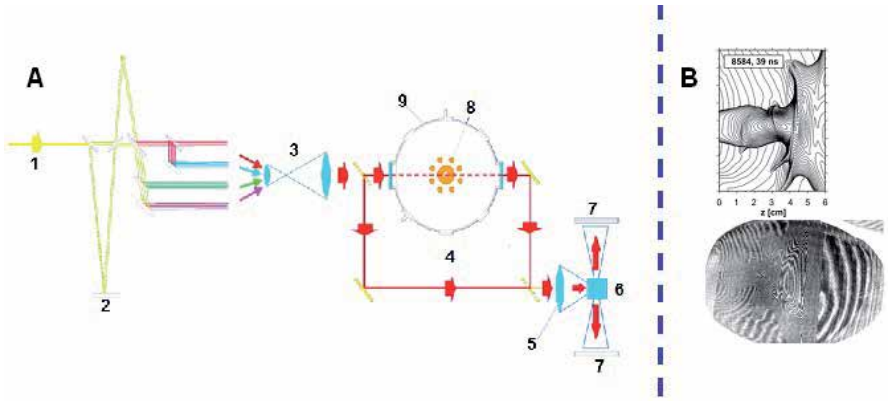

Fig. 4.19. A) Diagram of the 16-frame Mach-Zhender interferometer for the PF-1000; 1 – laser, 2 – optical delay line, 3 – expander, 4 – Mach-Zhender interferometer, 5 – lens, 6 – beam separator, 7 – film, 8 – PF-1000 electrodes, 9 – vacuum chamber. B) A sample interferogram and its reconstruction (T. Pisarczyk) (Zielińska et al., 2011)

Nd:YLF laser emitting radiation with a wavelength of 1.06 μm was used in the interferometer system. The laser was also adapted to operate at the second, third, and fourth harmonic of the radiation frequency. The second harmonic with a wavelength of 527 nm was used for interferometry. At this wavelength, the energy of the laser pulse was 500 mJ with a stability of approximately 7%, and duration of 1 ns. The beam diameter was 12 mm. The laser was equipped with a special trigger system which enabled its synchronization with the phenomenon,, with an accuracy of 1 ns. The optical delay line allowed us to take 16 interferograms in an interval of 0÷220 ns, with spacing between successive frames of 10 and 20 ns alternately. Exposure time for one frame was 1 ns. Recording was done on photographic film, which was then scanned for further digital reconstruction (Fig. 4.19B). The spatial scale on the interferometric image was determined using a cylindrical object with known dimensions placed in the electrode axis of the anode.

The distribution of electron and ion density can be determined based on a reconstructed image of lines (the assumption of *quasi*-neutrality: $n_e \cong n_i$) of plasma in the pinch (focus) of the PF-1000 using the Abel inverse transform procedure shown in (Pisarczyk et al., 2009). Fig. 4.20 shows an example of the distribution of electron density in the plasma focus.

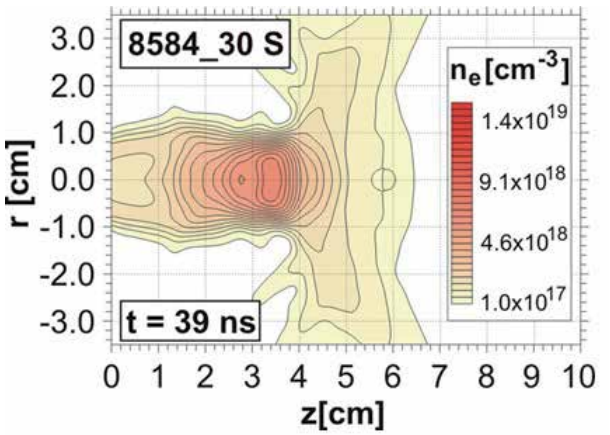

*Fig. 4.20. Distribution of electron density in the plasma focus of the PF-1000. Discharge No. 8584, 39 ns after the maximum compression (*Scholz et al., *2012)*

One of the important parameters of plasma in the focus of the PF-1000, in addition to its electron density, is the electron temperature. Temperature measurements were made using an X-ray spectrometer which allows recording of the X-ray spectrum emitted by helium-like argon ions. Argon was used as an admixture for the working gas, namely deuterium.

BENT-CRYSTAL X-RAY SPECTROMETER

Spectra of soft X-rays with energy of 2÷10 keV integrated over time, but spatially expanded, were recorded on the PF-1000 using a bent-crystal X-ray spectrometer (Faenov et al., 1994). The spectrometer included spherically bent mica crystal (2d = 19.94 Å) with a bend radius of 150 mm. The effective reflective surface of the crystal was 10 × 50 mm^2. Soft X-rays reflected from the crystal were recorded on DEF-5 film of constant sensitivity in the range of 1÷10 keV, shielded with titanium foil (5 μm thick) to protect the film from visible light. The total energy resolution of the spectrometer was $E/\Delta E \approx 800$. Spectra were recorded in a plane perpendicular to the axis of the plasma focus, so the main contribution to the total width of the recorded spectral line was from plasma of 5 mm in size in the radial direction of the plasma focus (pinch). In this configuration, the film was placed outside the Rowland circle, allowing us to get a photograph of the plasma focus in (z, λ) coordinates (Fig. 4.21).

The recorded spectra were used to determine the electron temperature of plasma and the parameters of epithermal electrons in the plasma focus.

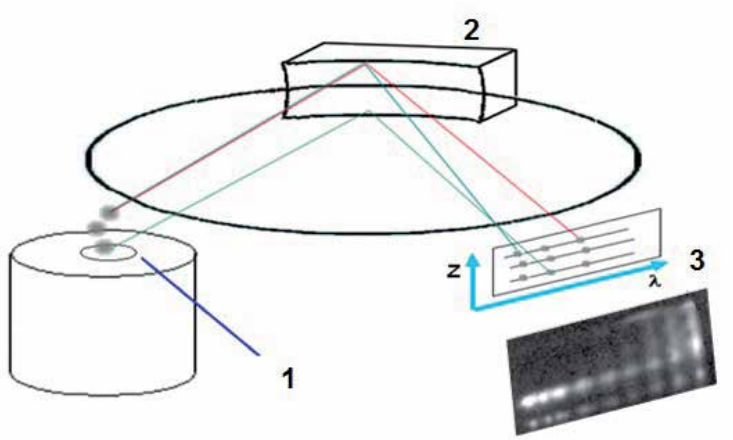

Fig. 4.21. Position of the spectrometer in relation to the plasma focus. 1 – plasma focus, 2 – mica crystal, 3 – an example of the recorded X-ray spectrum (Sadowski and Scholz, 2009)

The last group of diagnostics used in experiments on the PF-1000 was dedicated to measurements of charged particles – electrons and protons from the second channel of (D,D) deuterium fusion. A magnetic beta-ray spectrometer was used to record the energy spectrum of electrons emitted from the plasma focus integrated over time. Measurements were carried out in order to confirm the emission of epithermal electrons from the plasma focus of the PF-1000.

MAGNETIC BETA-RAY SPECTROMETER

The magnetic spectrometer was positioned along the electrode axis of the PF-1000 system from the collector side at a distance of 160 cm from the anode plane. Fig. 4.22 shows the diagram of the spectrometer location and its major components.

As shown in the figure, the spectrometer included a collimator and magnet (Fig. 4.22B - 3, 4) to deflect the electron beam, which was recorded by X-ray film covered with aluminium foil 30 μm thick. The foil transformed the beam into X-rays which were recorded by two overlaid films. The first film was used as a filter which eliminated the effect of saturation (fuzzy maximum of the spectrum), which is often visible on the first film.

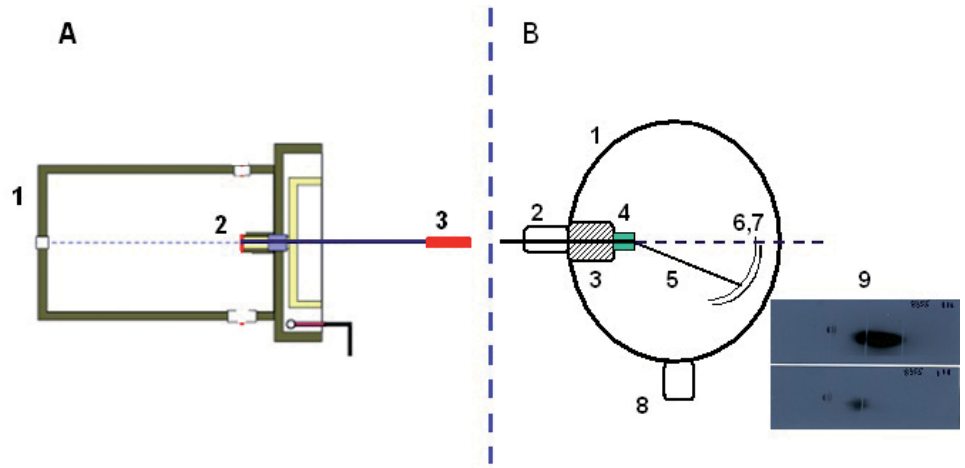

Fig. 4.22. Magnetic electron spectrometer, system diagram. A) Position of the spectrometer relative to PF-1000 electrodes; 1 – experimental chamber, 2 – electrodes, 3 – spectrometer; B) Spectrometer diagram; 1 – housing, 2 – vacuum connections, 3 – collimator, 4 – permanent magnet, 6, 7 – Al foil, X-ray film, 8 – connection to the pump system, 9 – recorded spectrum (Kowalski et al., 2011)

Another diagnostic in this group was directly related to the recording of protons from the second channel of (D,D) fusion, in which a proton with an energy of 3.02 MeV, and a triton with an energy of 1.11 MeV are created. Pinhole cameras with trace detectors were used for this recording.

PINHOLE CAMERAS WITH TRACE DETECTORS

The three cameras used in this experiment were placed at three different angles $\phi = 0°$, 68°, and 90°, and at distances from the center of the anode end respectively equal to 100 cm, 61 cm, and 50 cm (Fig. 4.23). The diameter of the holes in the cameras was 3 mm, which defined the solid angles at which protons could reach the trace detector placed in the camera for a given geometry of the camera settings. These angles were, respectively, $\Omega = 7.07 \cdot 10^{-6}$ sr, $1.90 \cdot 10^{-5}$ sr, and $2.80 \cdot 10^{-5}$ sr. In order to cut off the trace detector from high-energy deuterons, which are capable of reaching it, it was covered with aluminium foil 80 μm thick (Malinowska et al., 2006). A PM-355 detector was used in the experiment. A batch of these detectors was calibrated on a Van de Graaff generator. The calibration graph, or the diameter of the trace versus proton energy depending on the time the detector was etched, is shown in (Banaszak et al., 2005).

Fig. 4.23B shows an example of proton traces recorded by a trace detector placed in the pinhole camera which was positioned at 90° relative to the electrode axis.

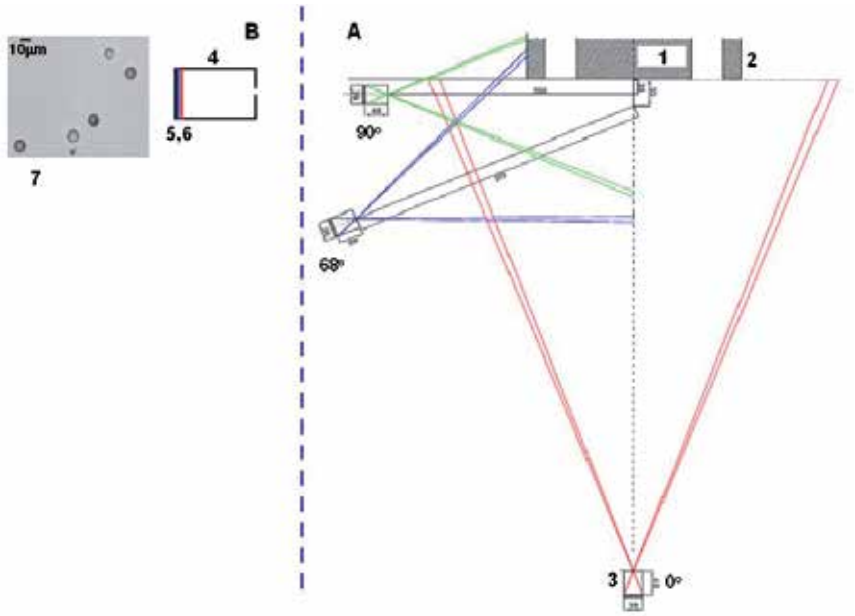

Fig. 4.23. Locations of pinhole cameras with trace detectors. A) Positions of cameras relative to the axis of electrodes of PF-1000; 1 – anode, 2 – cathode, 3 – pinhole camera at 0°; B) Diagram of the camera; 4 – camera housing, 5 – 80 μm aluminum foil, 6 – PM-355 trace detector, 7 – traces recorded in the detector (Courtesy of A. Malinowska)

All of these diagnostic groups were used in the experiments on the PF-1000, always with standard measurements, in particular with the measurement of the current and the total emission of neutrons. Neutron emission measurement determines the yield of the fusion reaction in the plasma focus. In contrast, the scaling law associates amperage with yield, but in order to conclusively prove that this law refers to the current flowing in the plasma focus, measurements were made using magnetic probes, which incidentally led to the discovery that the magnetic field lines in this system are spiral. Magnetic probes also helped answer the question of what the structure of the current sheath is, and how it affects the fusion yield.

Diagnostics of nuclear reaction products, measurements of electron beams, X-ray spectra, and electron concentration were used to explain the nature of nuclear fusion reactions in the focus. Research was carried out to determine whether a nuclear reaction taking place in the focus (pinch) is of a thermonuclear nature, i.e. whether the ion temperature is sufficiently high, or if only some ions have high kinetic energy, and the reaction is of a beam–plasma target nature. Additionally, diagnostics used for imaging of the focus enabled exploration of its geometry, evolution in time, the speed of compression of the current sheath, and the density of plasma.

These diagnostics were used at various times and their use was the result of a given experiment taking place. At the same time, efforts were made to use as much of the measurement systems as possible in one experiment in order to better understand the phenomena occurring during the formation and life time of the plasma focus.

4.3 DESCRIPTION OF THE EXPERIMENTAL RESULTS OBTAINED ON PF-1000

In the third chapter, the experimental scaling law was described, relating the total emission of neutrons to the current in PF systems with relationship $Y_n \sim I^{3.3\div5}$. One can also associate neutron emissions with the total energy stored in the capacitor bank with relationship $Y_n \sim W^2$ (Michel et al., 1974), where the energy of the capacitor bank varied from several kJ to hundreds of kJ (Rager, 1981). The presented experimental relationships clearly show that the yield of fusion in the PF system's pinch (plasma focus) significantly depends on the intensity of the current flowing in the PF circuit, or the energy of the power supply source. This relationship provides a simple indicator of when the energy produced in fusion reactions occurring in the plasma focus exceeds the energy stored in the capacitor bank (the power source of PF).

However, experiments carried out on large systems with the maximum rated energy of the capacitor bank at 1 MJ showed that the total emission of neutrons, despite increasing the energy in the capacitor bank, stopped at about $10^{11} \div 10^{12}$ neutrons/pulse (Gourlan et al., 1979; Herold et al., 1989). It has not been finally decided in the papers presented here whether this inhibition of the increase in neutron emission is associated with physical phenomena occurring in the plasma focus, or rather due to flaws in the general, technical design of PF devices. The explanation of this phenomenon has become a key issue faced by all teams operating PF systems with high-voltage capacitor banks which can accumulate an electrical energy of more than 0.5 MJ. For example, based on measurements of the current distribution (see Chapter 2, Fig. 2.5), it was found in the Frascati system that a part of the current remains at the insulator and does not participate in the compression of plasma and does not flow in the plasma focus. A similar situation was observed in a PF-3 system at the Kurchatov Institute during experiments in which neon was used as the working gas. Measurements of current using absolutely calibrated probes showed that only a part of the total current is involved in the compression of the plasma which forms the plasma focus (pinch) (Krauz et al., 2007).

THE RESULTS OF MEASUREMENT USING MAGNETIC PROBES – CURRENT SHUNTING

The PF-1000 system used miniature, absolutely calibrated probes, also used in PF-3, for measuring changes in the azimuthal component of the induction of magnetic field dB_θ/dt;

and magneto-optical probes for the simultaneous measurement of dB_θ/dt and plasma glow, as described in section 4.2. Experiments were conducted in order to investigate the dependence of the total emission of neutrons from the plasma focus on the total current measured in the system, the current involved in the compression of the current sheath, and the current flowing in the plasma focus. Simultaneous use of magneto-optical probes enabled determination of the structure of the current sheath in the phase just before the maximum compression.

During these experiments, the total emission of neutrons was measured with a silver counter (SC1 in Fig. 4.6) and the total current in the system was measured with a Rogowski coil and probes placed in the collector of the system (see Fig. 4.4). In addition, a neutron probe located 7 m from the plasma focus was used, indicated in Fig. 4.6 as SPD4.

The location of magnetic probes relative to PF-1000 electrodes is shown in Fig. 4.12. The measurement line with probes connected to an oscilloscope was on the anode potential, rendering the measurement difficult. In addition, the probes are disposed of after each experiment (they are damaged during the measurement) and measuring takes place through contact with plasma, which means that disturbances in the plasma structure and the parameters of its movement may occur when the current sheath flows around the probe through the plasma. It was necessary to examine the extent of the disturbance of plasma in the current sheath during supersonic flow around the probe and how quickly it disepears in order to conclude that the proximity of the probe to the plasma focus did not affect its parameters. The Mach-Zhender interferometer described in Section 4.2 was used to investigate this effect. For example, Fig. 4.24 shows the interferograms of the flow around magnetic probes in the flat housing described in section 4.2 (Fig. 4.9).

Based on the research, we can conclude that placement of the magnetic probes close to the plasma focus does not affect its final characteristics, and the impact is less in the case of a miniature flat probe than that of a cylindrical housing (Krauz et al., 2012). Moreover, the presence of probes does not affect the total emission of neutrons. Therefore, it can be assumed that measurements of the current and structure of the current sheath around the plasma focus using probes did not affect the course of the phenomenon. They reliably reflect the current and the structure of the current sheath.

The first experiments using probes were carried out on a system which has passed so-called "insulator training" and is operated regularly with a total emission of neutrons above 10^{10} neutrons/pulse. In order to maintain repeatability of the current in the system and the neutron emissions obtained, this study was done at fixed values of capacitor bank charging voltage and deuterium pressure in the chamber. The discharge, wherein the measurement with a probe was performed and during which it was damaged, was followed by the exchange of gas in the chamber.

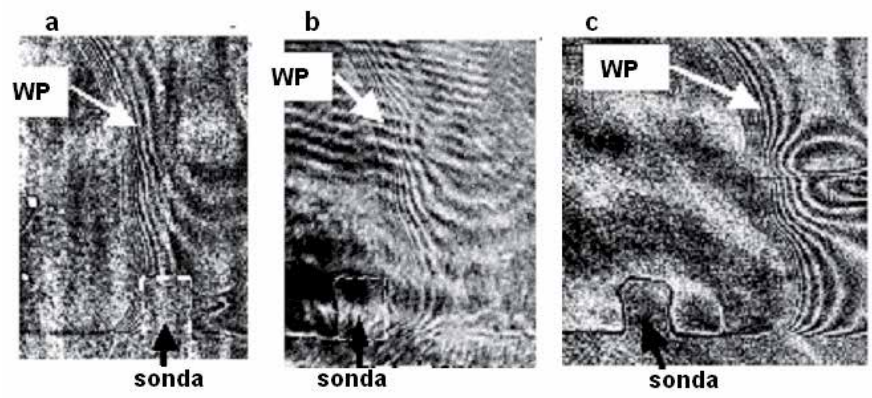

Fig. 4.24. Interferograms showing movement of the current sheath in the area of the magnetic probe with a flat housing positioned 4 cm from the electrode axis in the PF-1000, recorded at different points in time from the beginning of the discharge: a) 5824 ns, b) 5844 ns, c) 5884 ns. Discharge No. 9120: D_2, $p_0 = 240$ Pa, $U_0 = 24$ kV, $W_0 = 384$ kJ, $Y_n \approx 1.3 \cdot 10^{11}$ n/pulse (Krauz et al., 2012)

Fig. 4.25 shows the derivative of the current as a function of time, measured by the S2 magnetic probe situated at a distance of $r = 4$ cm from the electrode axis in the PF-1000 (a) and the calculated amperage value (b). The signal appears after 6.2 μs from the beginning of the discharge and has a well-defined maximum whose width at half the height was approximately 35 ns in this case. As can be seen from the figure, both loops show a symmetrical signal during the first 200 ns. This means that both signals come from the change in magnetic flux over time. When the signal symmetry was disturbed (see Fig. 4.25a outside the vertical dashed line), it was thought that one of the loops was destroyed and the signals were not analyzed beyond that point.

The current flowing in the current sheath was determined based on the registered current derivative. It reached a maximum value of about 1.7 MA. Furthermore, Fig. 4.25b shows the intensity of the total current flowing in the circuit measured with the Rogowski coil, I_{tR}, and magnetic probes, I_{t1}, placed in the collector of the PF-1000. You can see that the current measured at the collector was equal, within the confines of measurement uncertainties, to the current measured with the probe near the plasma focus. Slight differences in values obtained from the probes located in the collector are the result of non-uniform current distribution in the collector of the PF-1000.

The maximum value of the signal measured using the S2 probe, achieved when the current sheath passes through its area, and under conditions of a small change in intensity of the total current measured at the collector, corresponds to the passage of the whole sheath current to an area within a radius less than 4 cm from the electrode axis. From its peak until the destruction of the probe, the waveform of the current measured by the S2 probe corresponds to changes in intensity of the total current in the PF-1000 circuit measured at the collector (Fig. 4.25b).

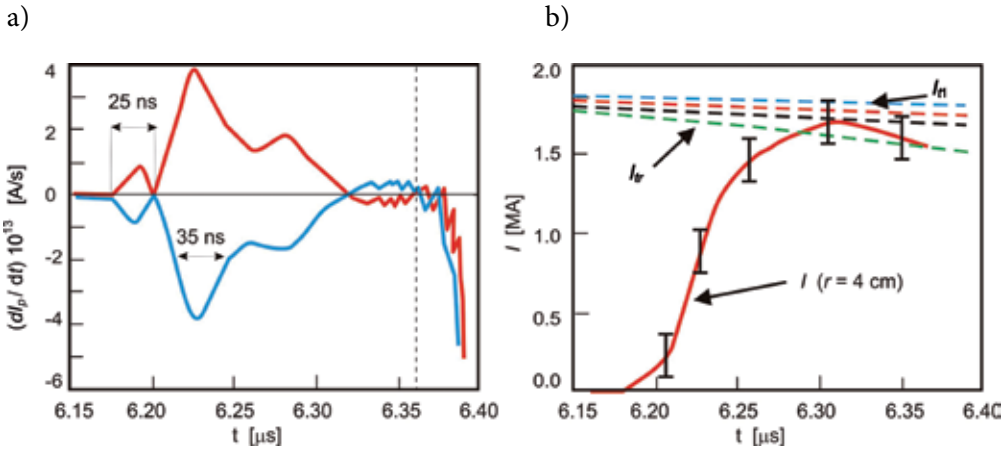

Fig. 4.25. The results of measurements of the current derivative from the S2 magnetic probe, dI/dt (r = 4 cm) in the current sheath, and the amperage at the collector:
a) Derivative of the current flowing in the sheath measured by the S2 probe located r = 4 cm from the electrode axis, elevated 10 mm above the surface of the anode; the vertical dotted line shows the damage point of the probe.
b) Current measured with the S2 probe, I, current measured using the Rogowski coil, I_{tR}; current measured using probes at the collector, I_{t1}.
Discharge No. 8220; D_2, p_0 = 400 Pa, U_0 = 27 kV, W_0 = 485 kJ, Yn ≈ 1.24·1011 n/pulse
(Krauz et al., 2012)

For example, Fig. 4.26 shows electrical waveforms measured at the collector of the PF-1000 during the entire time of discharge No. 8220, as shown in Fig. 4.25.

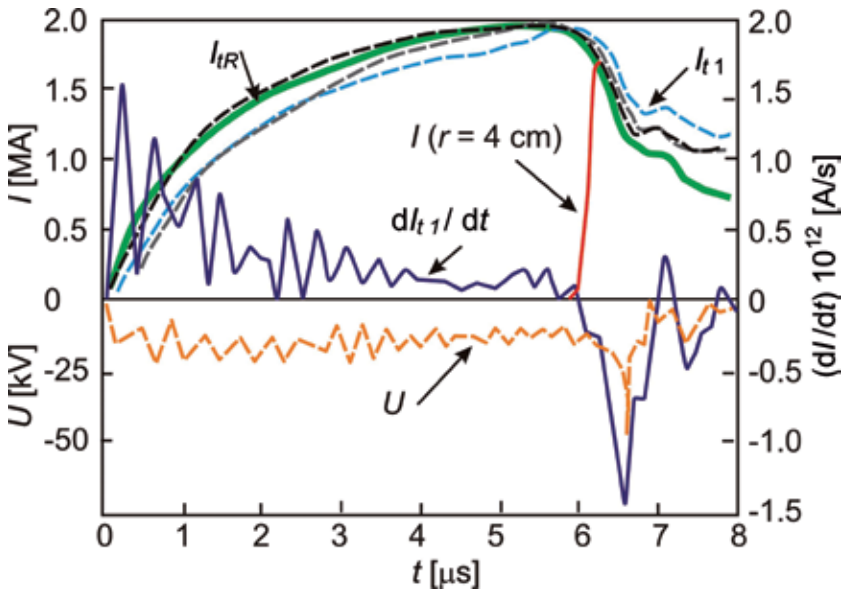

Fig. 4.26. Results of current measurements using the S2 probe I (r = 4 cm), discharge current measured using the Rogowski coil I_{tR}, and magnetic probes at the collector I_{t1}, voltage measured using one of the capacitance probes placed in the collector U, and derivative of the total current measured at the collector dI/dt. (Based on the results of experimental session on the PF-1000 10/2009, elaborated by K. Mitrofanow, S. Krauz, M. Scholz)

The current waveform shown in Fig. 4.25b, measured in the vicinity of the PF, shows that a high total emission of neutrons above 10^{10} n/pulse, illustrating the yield of the fusion reaction, is associated with the lack of current shunting in the circuit of the PF.

The effect of current shunting on the total emission of neutrons from the focus is shown in Fig. 4.27, which shows waveforms of current versus time measured with the S2 probe in the vicinity of the PF (r = 4 cm), as well as current waveforms in the circuit measured at the collector of the PF-1000. The measurements were performed for different capacitor bank charging voltages U_0 = 20 ÷ 24 kV, which correspond to the energy stored in the bank W_0 = 260 ÷ 380 kJ, and a fixed pressure of deuterium in the experimental chamber p_0 = 267 Pa. Part of the experiments was carried out with the new Al_2O_3 alundum insulator, which allowed determination of how the total emission of neutrons is affected by the so-called „training" (or degassing) process of the insulator, as mentioned in Chapter 3.

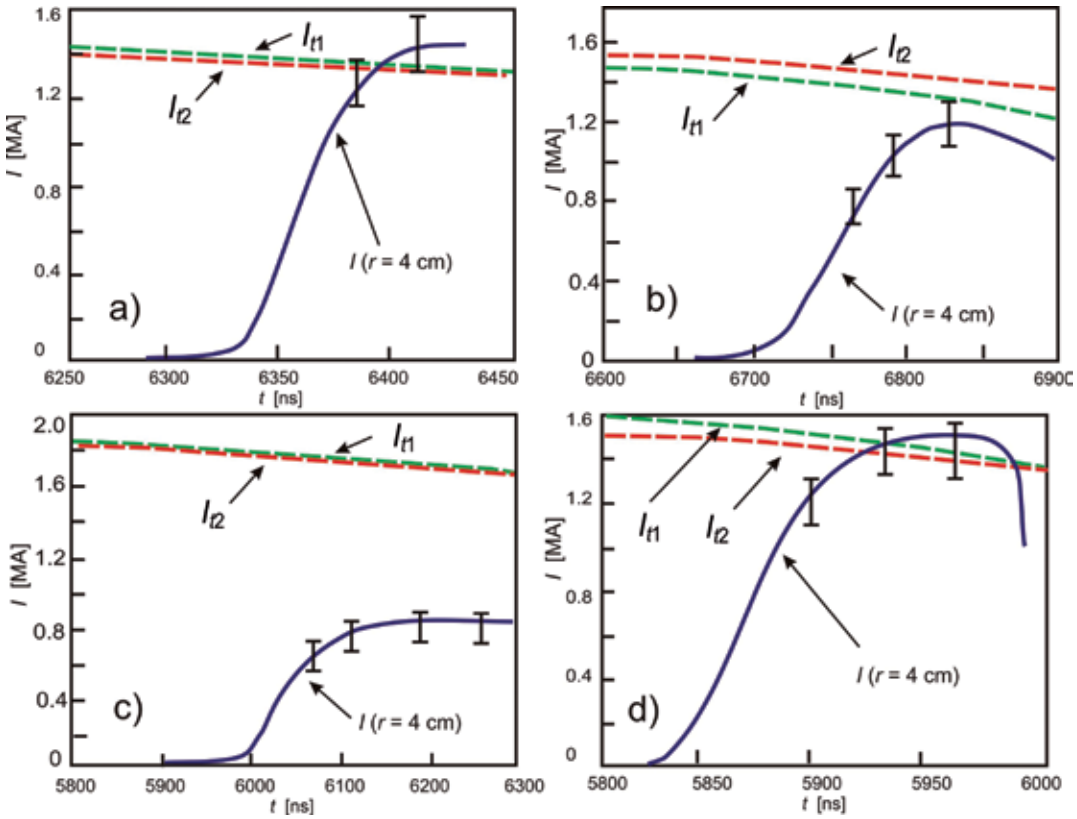

Fig. 4.27. Waveforms of electric current in the circuit measured at the collector (I_{t1}, I_{t2}) and calculated by measuring dI/dt from the S2 magnetic probe, I (r = 4 cm).
a) Discharge No. 8464: D_2, p_0 = 267 Pa, U_0 = 20 kV, W0 = 266 kJ, $Y_n \approx 6.3 \cdot 10^{10}$ n/pulse;
b) Discharge No. 8465: D_2, p_0 = 267 Pa, U_0 = 20 kV, W0 = 266 kJ, $Y_n \approx 5.1 \cdot 10^{9}$ n/pulse;
c) Discharge No. 8466: D_2, p_0 = 267 Pa, U_0 = 24 kV, W0 = 383 kJ, $Y_n \approx 1.5 \cdot 10^{8}$ n/pulse;
d) Discharge No. 8479; D_2, p_0 = 267 Pa, U_0 = 23 kV, W0 = 352 kJ, $Y_n \approx 1.0 \cdot 10^{11}$ n/pulse
(Based on the results of experimental session on the PF-1000 10/2009, elaborated by K. Mitrofanow, S. Krauz, M. Scholz)

Fig. 4.27a shows the current waveforms obtained for the charging voltage U_0 = 20 kV, where the total emission of neutrons was $Y_n \approx 6.3 \cdot 10^{10}$ n/pulse. The signal from the probe appears after 6260 ns from the start of a discharge, and the amperage reaches a value of about 1.3 MA within approximately 150 ns. Taking into account the uncertainty of measurements using the S2 probe (10÷20%), we can say that, in this case, the total current in the PF circuit (measured at the collector) reaches the region $r < 4$ cm around the plasma focus.

Current waveforms as a function of time shown in Fig. 4.27b indicate that for a discharge taking place under the same initial conditions as shown in Fig. 4.27a (p_0 = 267 Pa, U_0 = 20 kV), but for a gas in which impurities remained that were released from the insulator and electrodes during an earlier discharge, the maximum amperage measured with the S2

probe at point $r = 4$ cm was 1.2 MA. This represents 85% of the total current in the PF circuit, which results in a total emission of neutrons in this discharge of only $Y_n \approx 5.1 \cdot 10^9$ n/pulse, which is one order of magnitude less than in the case shown in Fig. 4.27a.

If the insulator has not undergone training, the increased charging voltage of the capacitor bank usually results in an increase of the total current in the PF circuit and, consequently, an increase in the amount of impurities released from the insulator and electrodes. Fig. 4.27c shows the current waveforms for such a discharge. The capacitor bank charging voltage was higher here, $U_0 = 24$ kV, which caused the total current measured at the collector to reach its maximum value of about 1.8 MA. In contrast, the current measured by the magnetic probe in the vicinity of the focus was approximately 0.8 MA, which represents 45% of the total current in the circuit. The remaining current flowed outside the area, limited by a radius of 4 cm from the electrode axis. The current measured by the probe dropped from about 0.8 to about 0.3÷0.4 MA. Thus, 75÷80% of the total current flowed outside the plasma focus. The total emission of neutrons was only $Y_n \approx 1.5 \cdot 10^8$ n/pulse, which was less by two orders of magnitude as compared to the discharge, where the total current was 1.3 MA (Fig. 4.27a).

Fig. 4.27d shows current waveforms measured in the discharge, which was carried out after the "training" of the insulator. The discharge was carried out for $U_0 = 23$ kV. The current measured by probe S2 increases from 5.8 μs from the beginning of the discharge, and within 150 ns reaches a maximum value of about 1.4 MA, which corresponds to the total current in the PF circuit. A clear drop in the current measured with the S2 probe is associated with the final stage of pinching the plasma focus, and the beginning of the processes of energy dissipation of the magnetic field in the plasma. The total emission of neutrons was $Y_n \approx 1.0 \cdot 10^{11}$ n/pulse.

The current waveforms in Fig. 4.27, correlated with the total emission of neutrons, clearly show that for the scaling law (3.2) for those systems, there should be current flowing in the plasma focus I_p, but not the total current in the PF circuit I_t.

Total current shunting may explain why there is a violation of the scaling law if we formulate it in relation to the current in the circuit. The conditions of the experiment, or the presence of impurities due to a new insulator, have confirmed that one of the reasons for shunting may be inappropriate structure of the current sheath, which causes inefficient sweeping of the working gas (see Chapter 3). The presence of impurities, while having an impact on the electrical breakdown of the working gas, as the experimental practice has shown, worsens the efficiency of gas sweeping. Distribution of the plasma density and current within the current sheath in the final stage of discharge and compression significantly affects the stability of the plasma focus, as well as the processes responsible for energy dissipation of the magnetic field in the plasma parameters of the focus, and thus also affecting the yield of deuterium fusion reactions.

RESULTS OF INTERFEROMETRIC AND MAGNETIC PROBES MEASUREMENTS

Fig. 4.28 and 4.29 show the results of measurements made with a set of miniature magnetic probes (with a flat tip) located at distances of $r = 4$ cm (S2 probe) and 1.3 cm (S1 probe) relative to the electrode axis (see Fig. 4.12). Measurements using probes were correlated with results obtained from a sixteen-channel Mach-Zhender interferometer (see. Fig. 4.19), and with soft X-ray signals received by the PIN diode (0.6÷15 keV range) (see Fig. 4.18). The experimental results were obtained for fixed pressure conditions of the working gas (deuterium) $p_0 = 240$ Pa and capacitor bank charging voltage $U_0 = 24$ kV ($W_0 = 384$ kJ).

Fig. 4.28 shows that the current sheath reaches the S2 probe ($r = 4$ cm) after 6.15 μs from the beginning of the discharge, and reaches S1 probe after another 165 ns ($r = 1.3$ cm). Based on the transition time between these two points, we can estimate the average velocity of the current sheath $v_r \approx (1.3 \div 1.6)\cdot 10^7$ cm/s. We can also see that the half width of the pulse of derivative $\mathrm{d}I_p/\mathrm{d}t$ decreases for S2 from 34 ns to 18 ns right on the S1 axis. The instantaneous velocity of the sheath when passing through the probe region, calculated based on this data, is $v_r \approx (1.8 \div 1.9)\cdot 10^7$ cm/s for the probe located further from the axis, and $v_r \approx (0.7 \div 0.8)\cdot 10^7$ cm/s for the probe located closer to the axis.

Knowing the average velocity of the sheath between the two probes, and waveforms I_p and $\mathrm{d}I_p/\mathrm{d}t$, we can use the formula:

$$\delta_{skin} \cong v_r \frac{I_p}{dI_p/dt} \quad , \tag{4.3}$$

to estimate the thickness of the skin layer present in the current sheath.

In the experiment shown in Fig. 4.28, the width of the skin layer decreases in the current sheath from about 0.8 cm for $r = 4$ cm, to about 0.3 cm for $r = 1.3$ cm.

Selected interferograms recorded at different times (red dots in Fig. 4.28) show the formation of the plasma focus (t_2) and the development of instability m = 0 over the entire length of the plasma focus and the formation of a neck at the anode (t_5).

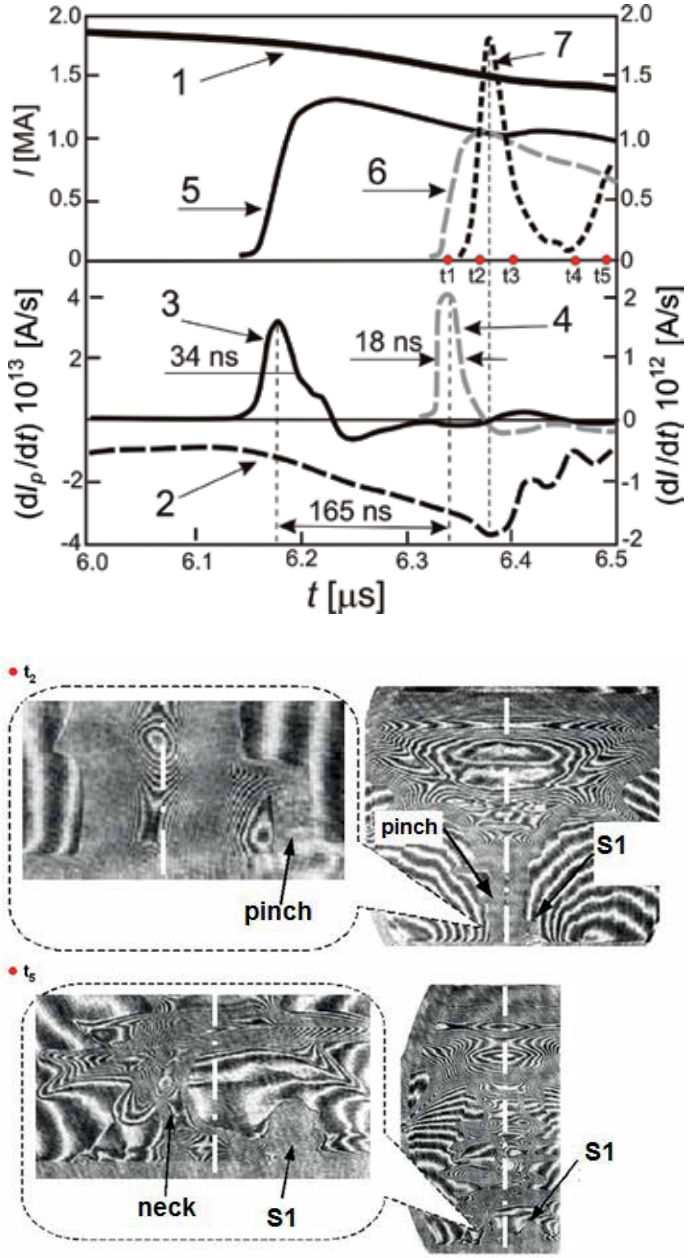

Fig. 4.28. The results of measurements made using probes S1 and S2, a probe at the collector, the Rogowski coil, and a PIN diode correlated with interferometric measurements: 1 – current intensity measured using the Rogowski coil; 2 – derivative dI/dt from the probe at the collector; 3, 4 – derivative dI_p/dt from probes S2 and S1; 5, 6 – amperage from probes S2 and S1; 7 – X-ray pulse measured by the PIN-diode in the range of 0.6÷15 keV.

Red points – the points in time of frames from the interferometer: t_2 = 6369 ns, t_5 = 6489 ns.
Discharge No. 9363: D_2, p_0 = 240 Pa, U_0 = 24 kV, W_0 = 384 kJ, $Y_n \approx 2.9 \cdot 10^{10}$ n/pulse
(Mitrofanov et al., 2014)

We can see that at t_2 probe S1 registered the crossing through the most dense parts of the current sheath, and the current reached approximately 1 MA, corresponding to the current registered by probe S2. This means that current flowing in the plasma focus at maximum compression of the plasma represented about 66% of the total current measured at the collector (Fig. 4.28, waveforms 1,5,6). The result was low neutron emission $Y_n \approx 2.9 \cdot 10^{10}$ n/pulse. During discharges with high emission of neutrons (of the order of $Y_n \approx 1.0 \cdot 10^{11}$ n/pulse), the current flowing in the region below probe S2 (r = 4 cm) was 90÷100% of the full current measured at the collector (see Fig. 4.27d) (Krauz et al., 2012).

The diameter of the plasma focus was about 1.8 cm in this case, and the soft X-ray pulse reached the maximum at its beginning (Fig. 4.28, 7 – signal from the PIN diode). The falling edge of the pulse corresponds to the expansion and breakup of the plasma focus. The second X-ray pulse occurred at the moment of formation of a neck at the surface of the anode (Fig. 4.28, t_5).

Another example, shown in Fig. 4.29, shows that the nature of the waveforms measured by probes S1 and S2 is very similar to those shown in Fig. 4.28.

In this case, the current sheath reached S2 probe after about 6.13 μs from the beginning of the discharge, and the S1 probe after another 180 ns. The average velocity of the current sheath was about $v_r \approx 1.5 \cdot 10^7$ cm/s, and the thickness of the skin layer in the current sheath, estimated from formula (4.3), varied from $\delta_{skin} \approx 1.2$ cm at r = 4 cm, to $\delta_{skin} \approx 0.2$ cm at r = 1.3 cm. The current at the moment t_1 of the creation of the plasma focus measured by probe S1 was about 1.2 MA. This represented 85% of the total current measured in the circuit, and was higher than in the previous discharge (No. 9363, Fig. 4.28). This resulted in a higher total neutron emission $Y_n \approx 4.5 \cdot 10^{10}$ n/pulse. At time t_1, the signal from the soft X-rays reached a maximum, and the diameter of the plasma focus was less, i.e. 1.1 cm. As in the previous case, a neck formed (t_3) at the surface of the anode. Its size was comparable to the thickness of the skin layer, δ_{skin}, which means that all of the sheath current flowed through it. A noticeable decrease in current measured by probe S1 indicated dissipation of magnetic field energy at the neck, which caused, among other things, another increase in the soft X-ray signal.

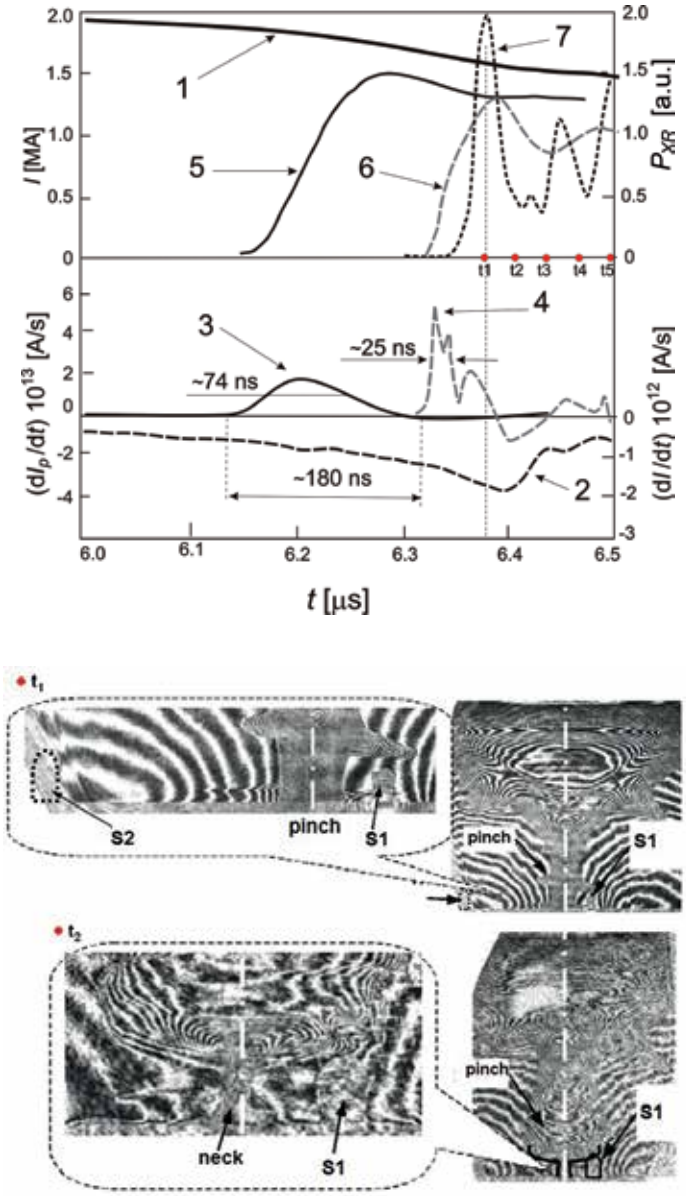

Fig. 4.29. The results of measurements made using probes S1 and S2, a probe at the collector, the Rogowski coil, and a PIN diode, correlated with the interferometric measurements. 1 – current intensity measured using the Rogowski coil; 2 – derivative dI/dt from the probe at the collector; 3, 4 – derivative dI_p/dt from probes S2 and S1; 5, 6 – amperage from probes S2 and S1; 7 – X-ray pulse measured by the PIN-diode in the range of 0.6÷15 keV.
Red points – the points in time of frames from the interferometer: t_1 = 6377 ns, t_5 = 6437 ns.
Discharge No. 9364: D_2, p_0 = 240 Pa, U_0 = 24 kV, W_0 = 384 kJ, $Y_n \approx 4.5 \cdot 10^{10}$ n/pulse
(Mitrofanov et al., 2014)

The results shown in Figures 4.27 to 4.29 indicate that the value of current flowing in the current sheath, and then in the plasma focus (pinch), significantly impacts the total emission of neutrons. Frequently, this current value is different from the total current flowing in the PF circuit. This phenomenon is caused by improper formation of the structure of the current sheath, which leads to poor sweeping of the working gas therefore, a portion thereof remains outside the sheath. This causes the electric current to flow outside the sheath as a result of repeated breakdown.

An ideally shaped current sheath has the characteristics of a "snow plow," with a clear separation of the shock wave from magnetic piston area in which the entire sheath current flows. In a real situation, the magnetic field often penetrates the area of the shock wave, worsening the sweeping of gas and compression of plasma in the pinch (focus).

In order to illustrate these effects, Fig. 4.30 and 4.32 show the signals from probes S1 and S2 correlated, as before, with results obtained from a sixteen-channel Mach-Zhender interferometer. The results shown in these figures were obtained for fixed pressure conditions of the working gas p_0 = 160 Pa and capacitor bank charging voltage U_0 = 24 kV (W_0 = 384 kJ).

In the magneto-optical probes used, the signal from the optical channel increases when the shock wave passes through the probe. This is because the light intensity is proportional to n^2_e (see Fig. 4.30, t_1). In contrast, the signal from the loop to measure the derivative of the magnetic field (the so-called "magnetic channel") occurs when the magnetic piston passes through the probe.

By using magneto-optical probes S1 and S2 (Fig. 4.30, 4.31), correlated with interferometric measurements, the structure of the current sheath as it reached the axis of the system was determined. Fig. 4.30 shows that at time t1, the current measured by probe S2 (r = 4 cm) reached a maximum value of about 1.2 MA, and the whole current sheath passed through the probe. Based on the interferogram recorded at time t_1, the widths of the magnetic piston $\delta_{TM} \approx 1.5$ cm and shock wave $\delta_{FU} \approx 0.8$ cm were determined. We can see that at time t_1 = 5781ns, the current sheath had not yet reached the S1 probe.

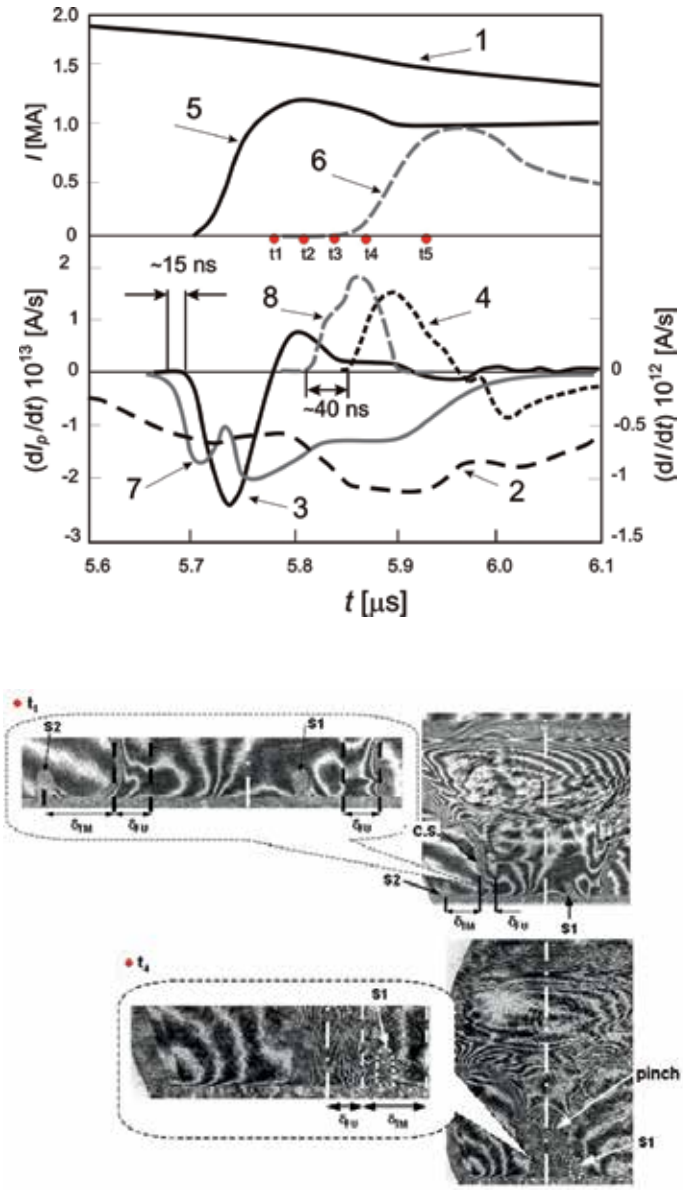

Fig. 4.30. The results of measurements made using probes S1 and S2, a probe at the collector, and the Rogowski coil, correlated with the interferometric measurements. 1 – current intensity measured using the Rogowski coil; 2 – derivative dI/dt from the probe at the collector; 3, 4 – derivative dI_p/dt from probes S2 and S1; 5, 6 – amperage from probes S2 and S1; 7, 8 – radiation signals from the current sheath (in the visible range) recorded by probes S2 and S1.
Red points – the points in time of frames from the interferometer t_1 = 5781 ns, t_4 = 5871 ns.
Discharge No. 9373: D_2, p_0 = 160 Pa, U_0 = 24 kV, W_0 = 384 kJ, $Y_n \approx 3.2 \cdot 10^{10}$ n/pulse
(Mitrofanov et al., 2014)

The rapid increase of the signal coming from the lighting of the layer in the shock wave area (curve 8, Fig. 4.30) at times t_2 = 5811 ns and t_3 = 5841 ns indicated the approach of the shock wave to the area of probe S1; that is, to a distance of 1.3 cm from the axis of the system. At the same time, probe S1 recorded virtually no signal from changes of the magnetic field (curve 4, Fig. 4.30). At the next moment t_4 = 5871 ns, the shock wave reached the axis of the system, and probe S1 registered the increase of the signal related to the magnetic field. The plasma focus (pinch) created as a result of compression can be seen on the interferogram recorded at this time.

The current measured by the S1 probe peaked at about 1 MA, and then decreased (curve 6, Fig. 4.30). This decrease was much larger than the decrease in total current in the system, measured by the Rogowski coil (curve 1, Fig. 4.30). This may indicate that a part of the current began to flow outside the area of radius r = 1.3 cm (position of the S1 probe). In addition, Fig. 4.30 shows that the time between the arrival of the shock wave and of the magnetic piston in the area of probes S1 (signals 4, 8) and S2 (signals 7, 3) changes during the approach to the electrode axis.

Estimation of the average velocity of the current sheath passing through area of probes S1 and S2 shows that the sheath had a velocity $v_r \approx 1.8 \cdot 10^7$ cm/s at a distance of 4 cm from the axis of the system, and reached a value of $v_r \approx 0.8 \cdot 10^7$ cm/s at a distance of 1.3 cm from the axis. This is the compression of plasma, and the slowing down of the current sheath as it approaches the axis of the system.

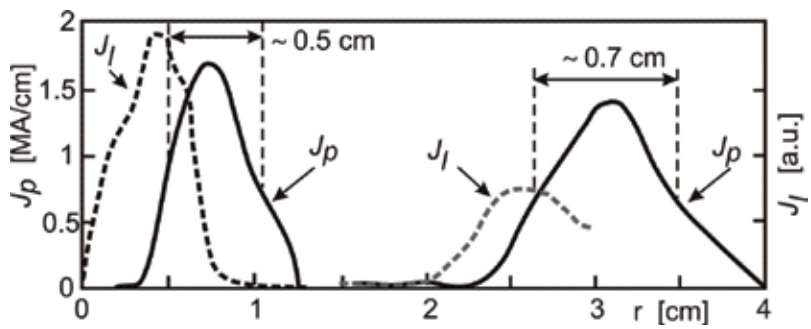

Fig. 4.31. The radial distribution of the linear current density J_p, and optical lighting of the current sheath J_l when passing through area of probes S1 and S2 at velocities of $v_r \approx 0.8 \cdot 10^7$ cm/s (S1) and $v_r \approx 1.8 \cdot 10^7$ cm/s (S2).
Discharge No. 9373: D_2, p_0 = 160 Pa, U_0 = 24 kV, W_0 = 384 kJ, $Y_n \approx 3.2 \cdot 10^{10}$ n/pulse (Krauz et al., 2012)

Assuming that, when the current sheath passes through the probe area, both the total current in the sheath and the lighting of the sheath change little, we can further assume that their signals will be determined primarily by the velocity of the current sheath v_r, and the radial distribution of the linear current density and lighting from the sheath. Taking this into account, we can determine this distribution based on formula $J(r) = (\mathrm{d}I/\mathrm{d}t)/v_r$, which enables us to determine radial distributions of linear current density and lighting from the

current sheath when it passes through area of probes S1 and S2. Fig. 4.31 shows such distributions for discharge No. 9373. The results from the magneto-optical probes and interferometric measurements for this discharge are shown in Fig. 4.30.

Another example shown in Fig. 4.32 demonstrates that, as it gets closer to the axis of the system, the sheath structure changes in such a way that the width of the sheath (i.e. the width of the shock wave area and the width of the magnetic piston), decreases when the layer reaches the electrode axis of the PF system. At the same time, the linear density of current increases. In this example, the total emission of neutrons from the plasma focus reached a higher value of $Y_n \approx 9.4 \cdot 10^{10}$ n/pulse, despite the same pressure conditions and capacitor bank charge voltage as for discharge No. 9373 (see Fig. 4.30). In this discharge (No. 9365), the maximum current measured with probe S1 at time t_1 = 6440 ns was 1.4 MA, which accounted for approximately 95% of the total current in the PF-1000 system.

The interferometric image (Fig. 4.32) at time t_1 shows a visible expansion of the plasma focus, with pinch instabilities beginning to appear in the background. This leads to the creation of an area of increased plasma compression, the so-called neck, at the anode of the PF, which can be seen on the interferogram recorded at time t_2. At this point, the radius of the neck is roughly equal to the thickness of the skin layer, which means that the current is uniformly distributed in the neck area, and the current density can be evaluated using the relationship $j(r) = I(r < 1.3 \text{ cm})/\pi r^2$, which yields 3 MA/cm^2. At the following instants, t_3 and t_4, the current in the area inside radius r = 1.3 cm (position S1) dropped rapidly with a relatively small change in the total current, measured by the Rogowski coil.

As in the previously described discharge (No. 9373), radial distributions of linear current density and lighting from the current sheath at the time of passage through probes S1 and S2 can be determined. Fig. 4.33 shows such distributions for discharge No 9365. The results of this discharge from the magneto-optical probes and interferometric measurements are shown in Fig. 4.32.

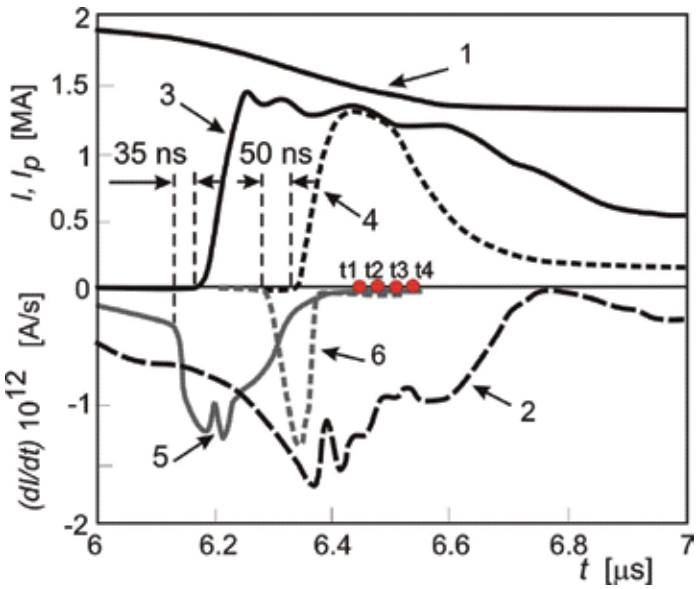

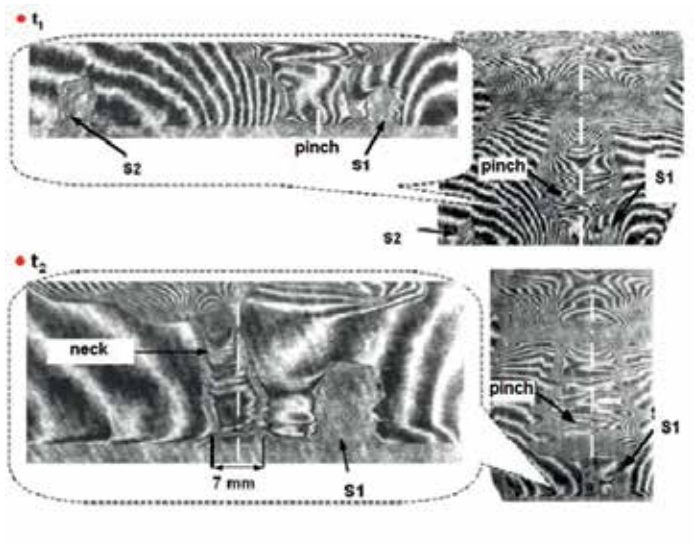

Fig. 4.32. The measurement results of sensors S1 and S2; the probes in the collector and the Rogowski coil correlated with interferometric measurements; 1 – amperage from the Rogowski coil, 2 – derivative dI/dt from the probe at the collector, 3, 4 – amperage from probes S2 and S1, 5, 6 – radiation signals from the current sheath (in the visible range) registered by probes S2 and S1. Red points – the points in time of frames from the interferometer: t_1 = 6440 ns, t_2 = 6470 ns. Discharge No. 9365: D_2, p_0 = 160 Pa, U_0 = 24 kV, W_0 = 384 kJ, $Y_n \approx 9.4 \cdot 10^{10}$ n/pulse (Mitrofanov et al., 2014)

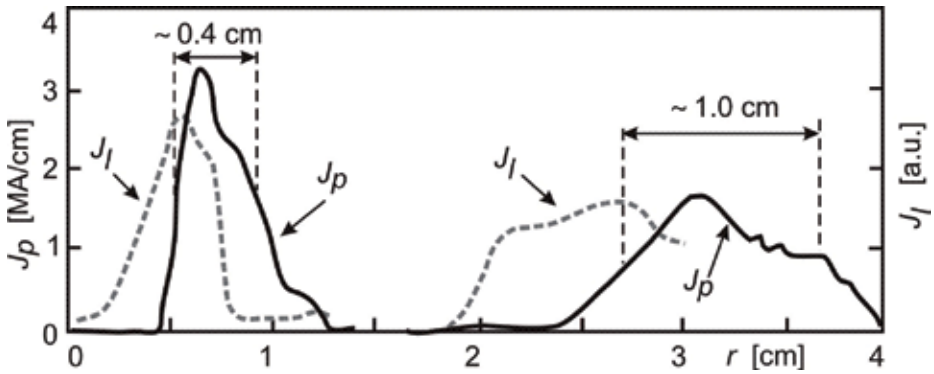

Fig. 4.33. The radial distribution of the linear current density J_p, and optical lighting of the current sheath J_I when passing through probes S1 and S2 at velocities of $v_r \approx 0.8 \cdot 10^7$ cm/s (S1) and $v_r \approx 1.9 \cdot 10^7$ cm/s (S2).
Discharge No. 9365: D_2, $p_0 = 160$ Pa, $U_0 = 24$ kV, $W_0 = 384$ kJ, $Y_n \approx 9.4 \cdot 10^{10}$ n/pulse
(Krauz et al., 2012)

Fig. 4.33 shows that the sheath width, i.e. the width of the shock wave area and the width of the magnetic piston area close to the electrode axis, decreases with the increase of the linear density of the current. When comparing the values of the linear density of the current for the two discharges shown (Fig. 4.31 and 4.33), we can see that the total emission of neutrons increases along with an increase in linear density of the current measured close to the electrode axis.

MEASUREMENTS BY MAGNETIC PROBES NEAR THE AXIS OF THE SYSTEM – THE SCALING LAW

Measurements made with probes near the axis of the system call for a re-evaluation of the scaling law associating total emission of neutrons with current actually flowing around the plasma focus at the time of its maximum compression.

Shown in Fig. 4.34 is the comparison of relationships between Y_n and amperage I_p measured using the S2 probe (r = 4.0 cm) and the S1 probe placed near the plasma focus (r = 1.3 cm), at the time of a minimum current derivative dI/dt, associated with the maximum compression of plasma. The curves shown by a dotted line correspond to relationship $Y_n = k \cdot I_p^4$, where k assumes values of 1.5, 2.0, 3.0. The result confirms the scaling law $Y_n \sim I^4$ for the intensities of currents flowing through the plasma focus (pinch). For comparison, Fig. 4.35 shows the relationship between Y_n and the intensity of the total current flowing in the PF system at the minimum dI/dt associated with the maximum compression of plasma.

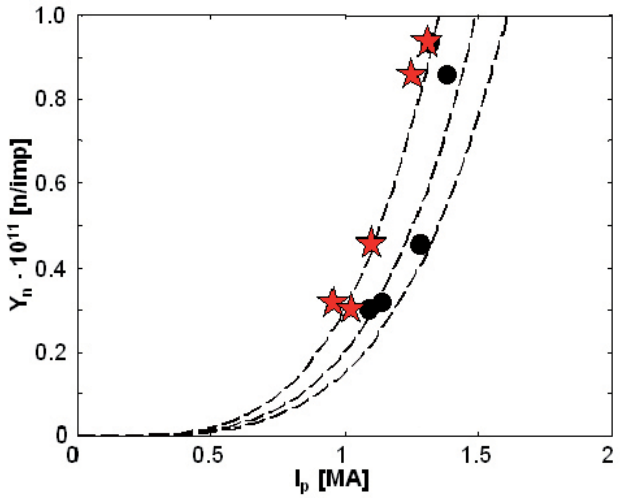

Fig. 4.34. Relationship between the total emission of neutrons Y_n and the current in the plasma focus (I_p). A red star indicates the currents measured by probe S1 (r = 1.3 cm), and a black dot indicates currents measured by probe S2 (r = 4.0 cm). Dashed lines: the function $Y_n = k \cdot I_p^4$ for k = 1.5, 2.0, 3.0 (Mitrofanov et al., 2014)

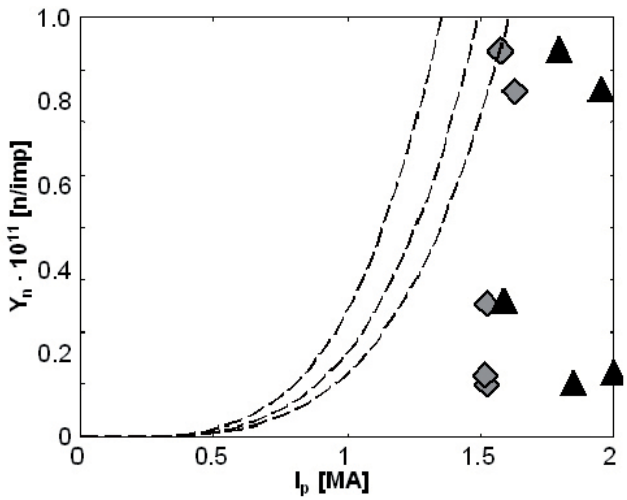

Fig. 4.35. Relationship between the total emission of neutrons Y_n, and the total current measured by the Rogowski coil (gray diamonds) and magnetic probe at the collector of the PF-1000 system (black triangles). Dashed lines as shown in Fig. 4.34. (Mitrofanov et al., 2014)

The measurement results shown in Fig. 4.35 do not show the characteristic relationship of the scaling law $Y_n \sim I4$, which suggests that current shunting plays a role in the system.

Direct measurement of the current around the plasma focus in the PF-1000 using the S1 probe located 1.3 cm from the electrode axis was performed on the PF-1000 for the first time in the history of such systems; and it clearly shows that the scaling law associating the total emission of neutrons with the current intensity in the fourth power is confirmed when we apply it to the current flowing in the plasma focus.

This confirms the hypothesis based on Bennett relationship that the efficiency of (D,D) fusion in the PF is due to thermal movements of plasma ions, which means that this is a

thermonuclear fusion reaction. However, the results of measurements of neutron energy using scintillation probes on long bases show the existence of a Doppler shift in the energy of neutron pulses measured by the probes arranged along the electrode axis of the PF-1000 system at angles of 0° and 180° (relative to the plate of the anode), (Chapter 3, Fig. 3.4). This indicates the movement of the center of mass of reacting deuterons, which can be interpreted as the movement of the plasma focus directed along the electrode axis, wherein the fusion reactions take place in accordance with the "moving boiler" model.

Another interpretation of this phenomenon is based on the assumption that the development of MHD instabilities and energy dissipation of the magnetic field lead to the acceleration of a group of deuterons which react with ions in a plasma focus. The nature of the nuclear fusion the PF has been described using the GPM model discussed in Chapter 3, or the so-called diode model described in (Scholz et al., 2002; Gribkov and Scholz, 2007).

Each of these models was subject to experimental verification. In the "moving boiler" model we should see a certain volume of plasma moving at a high speed along the electrode axis of the PF with a fast camera in visible light or X-ray, or by means of interferometry. The average velocity of the plasma "boiler" calculated based on the measured Doppler shift of the energy of emitted neutrons should be about 10^8 cm/s. In addition, hard X-rays ($E_\nu >$ 100 keV) accompanying the neutron emission indicate the presence of epithermal electrons which should be accompanied by highly energetic ions in case the *quasi*-neutrality of the plasma in the focus is broken. The presence of such electrons indicates the validity of the GPM model or the diode model.

MEASUREMENTS OF THE EPITHERMAL ELECTRON BEAM

The results of measurements made with an electron spectrometer (see. Fig. 4.22) (Scholz et al., 1999; Kowalski et al., 2011) and X-ray spectrometer (Fig. 4.21) (Abdallah et al., 1999; Zając et al., 2010) confirm the presence of epithermal electrons in the focus of the PF-1000.

Fig. 4.36 shows the densitograms obtained by using the electron spectrometer for discharge No. 8361 in the PF-1000. The electron spectrum which was integral in time has been reconstructed based on these densitograms.. We can see that electrons emitted from the PF-1000 have an energy distribution ranging from 80 to about 400 keV. The maximum for this distribution occurs for an electron energy of about 160 keV. If the acceleration processes are caused by the same difference in potentials as in a virtual plasma diode, the deuterons should have a very similar distribution of energy.

The size of the group of epithermal electrons in relation to the total number of electrons in the plasma focus was determined by analyzing the spectrum of helium-like argon ions recorded by an X-ray spectrometer in discharges, in which the working gas was a mixture of argon and deuterium. Fig. 4.37 shows sample images of the plasma focus from a high-speed

X-ray camera (Fig. 4.16), the spectrogram, and the resulting four spectra corresponding to the emission of soft X-rays from four different areas of the plasma focus.

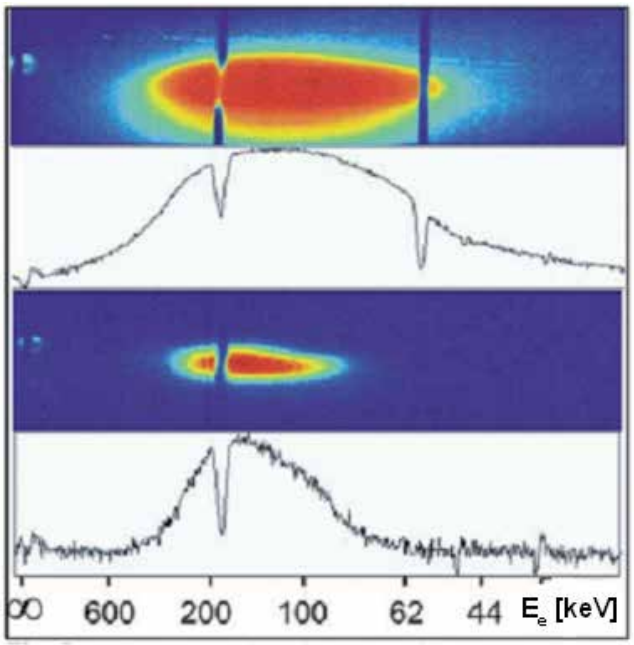

Fig. 4.36. Densitograms from the electron spectrometer set in the z direction at a distance of 74 cm beyond the anode plane, and the resulting energy distribution of electrons emitted from the plasma focus. Local minima correspond to the position of tungsten fibres indicating the energy range in the spectrometer. Discharge No. 8361: $Y_n \approx 2.5 \cdot 10^{11}$ n/pulse (Kowalski et al., 2011)

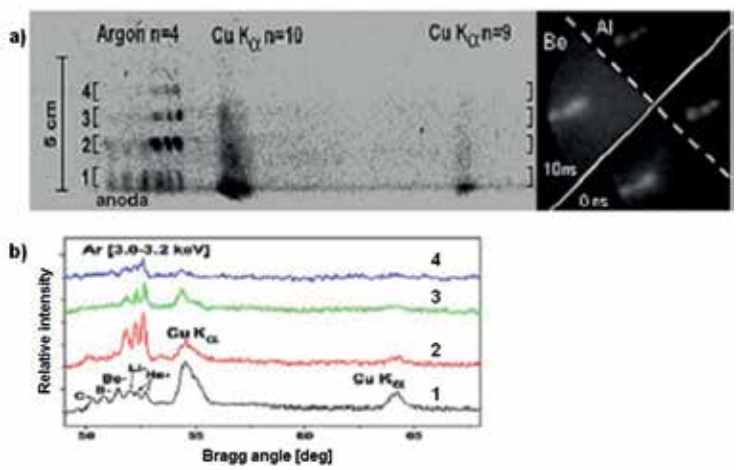

Fig. 4.37. a) X-ray spectrogram of the continuum radiation, and the characteristic lines of argon and copper (left side) in the PF-1000. Frames recorded by a fast X-ray camera for the two selected times with two filters – 10 μm Be and 3 μm Al. b) High-resolution X-ray spectra of the radiation emitted from different areas of the plasma focus as a function of the Bragg angle (1 – denotes the area closest to the anode) (Zając et al., 2010)

The experimentally obtained spectrum was compared with the spectrum calculated using the FLYCHK code (Chung et al., 2005), based on the model of radiative-collision global thermodynamic equilibrium. This code takes into account two electron temperatures, the higher corresponding to the epithermal electron beam modifying the structure of the X-ray spectrum. The electron beam is determined by the energy and the ratio of the number of electrons in the beam to the total number of electrons in the plasma focus f. Precise determination of values of the f ratio is difficult due to its variability in time. Nevertheless, experimental data related to the large width of the Cu K_α spectral line and the relatively flat character of the continuous radiation observed in the area of medium Bragg angles suggest that the value of f in the case of the PF-1000 is very large, $10^{-3} \div 10^{-2}$, as shown in (Abdallah et al., 1999).

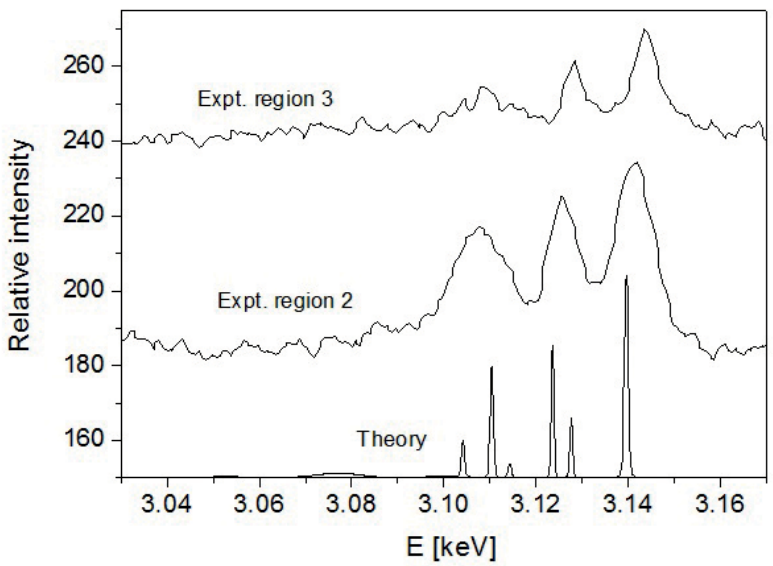

Fig. 4.38. Comparison of the experimental X-ray spectra from areas 1 and 2 of the plasma focus with the spectrum calculated using the FLYCHK model (T_e = 320 eV, $n_e = 10^{19}$ cm^{-3}, $f = 5 \cdot 10^{-3}$) (Zając et al., 2010)

Fig. 4.38 shows for comparison the spectra obtained experimentally in the first and second area of the focus (see Fig. 4.37), as well as the spectrum calculated based on the FLYCHK model, assuming that the plasma electron temperature is $T_e \approx 320$ eV, concentration $n_e \approx 10^{19}$ cm^{-3} (as indicated in the interferometry data), and $f \approx 5 \cdot 10^{-3}$. These spectra of energy of epithermal electrons and X-ray spectra are integrated over time.

In addition, it can be concluded from the analysis of X-ray spectra that the electron temperature in the plasma focus is larger for areas further from the anode plane and may reach approximately 700 eV in the outermost region (see Fig. 4.37a) (Zając et al., 2010).

MEASUREMENTS FOR TIME CORRELATION OF NEUTRON EMISSION, ELECTRON BEAM, AND HARD X-RAY

Correlating the presence of epithermal electrons with the emission of neutrons requires correlated of the neutron emission in time with the emission of an electron beam and hard X-rays. In addition, the association of the moment of neutron emission with the dynamics and distribution of plasma density and lighting of plasma in the PF pinch may answer the question of whether we should reject the "moving boiler" model for the diode model, supplemented to some extent by the GPM model.

Fig. 4.39 shows a typical set of signals recorded with different diagnostics, with the correlation of different types of radiations from the plasma focus.

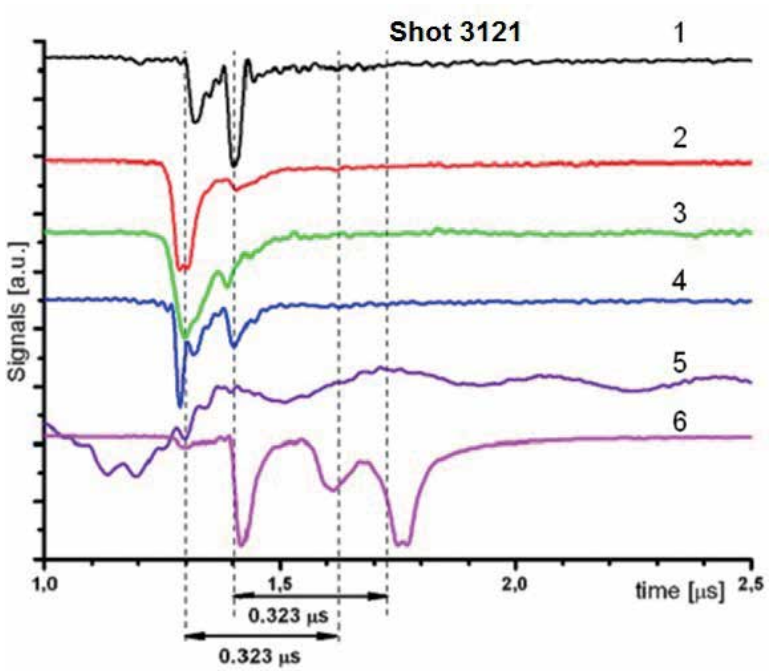

Fig.4.39. The set of signals recorded using different diagnostics, showing the correlation of different types of radiations from the plasma focus; 1 – Hard X-rays (8 ÷ 30 keV); 2 – Soft X-rays (3 ÷ 8 keV); 3 – Soft X-rays by the PIN diode (0.8 ÷ 4 keV); 4 – Epithermal electrons by Cherenkov detector; 5 – Current derivative by the probe in the collector; 6 – Hard X-rays (over 80 keV) and the neutron signal obtained from the scintillation probe placed at an angle of 90° relative to the electrode axis. Discharge No. 3121: D_2, p_0 = 465 Pa, U_0 = 35 kV, W_0 = 825 kJ, $Y_n \approx 3.4 \cdot 10^{11}$ n/pulse. (Scholz et al., 2004)

All signals, except for those from the neutrons, make allowance for delays associated with: the arrival time of the radiation at the detector; equipment delay times; and sometimes the travel time of the signal along cables of different lengths; etc. The signal from scintillation probes is shifted in time, taking into account equipment delays and time of flight hard X-rays registered together with the neutron pulse.

Collected signals correlated in the time, shown in Fig. 4.39 and obtained from various diagnostics in the same discharge, enable determination of the sequence of phenomena which occur in the plasma focus, and their association with the course of (D,D) fusion.

It follows from the presented signals that the first pulse of neutrons occurs 323 ns after the maximum pulse of soft X-rays, which is associated with the arrival time of neutrons with energies of 2.45 MeV from the plasma focus at the scintillation probe. This means that the first neutron pulse corresponds to the maximum compression of plasma in the focus. The second neutron pulse is correlated with the pulses of hard X-rays and electrons. Hard X-rays in the energy range of 8÷30 keV (curve 1), generated by escape electrons, reflect the first electron pulse from a Cherenkov detector (curve 4). Other pulses from this detector correspond to hard X-rays (over 80 keV), also registered by the neutron probe (curve 6) and thus, are correlated with emission of neutrons from the plasma focus.

Similarly, we can compare the evolution of the plasma focus recorded using the Mach-Zhender interferometer with the neutron pulse measured via scintillation probe versus time, and after taking all delays into account. Fig. 4.40 shows the distributions of electron concentration in the PF-1000 focus captured for different times and neutron signals with registration moments of a given frame marked with a red line. We can see that the main neutron emission from the focus occurs in the expansion phase of plasma in the focus, at the moment when a neck associated with instability m = 0 is created.

Similar to Fig. 4.32, which shows the interferometric image, the expansion of the plasma focus is visible in the distribution of electron concentration reconstructed on the basis of the interferogram, with instabilities of the plasma focus (pinch) beginning to appear in the background. This leads to the formation of an area of increased plasma compression, the so-called neck. At this point, the radius of the neck is roughly equal to the thickness of the skin layer, which means that the current is uniformly distributed in the neck area. In the following instant, the electron concentration in the neck drops rapidly with a relatively small change in the total current in the system, as measured by the Rogowski coil. We can assume on these grounds that the diode mechanism is triggered, which replaces the conductive current with a current of beams of electrons, and then ions, accelerated in the diode in the absence carriers (electrons) in this area of the plasma focus.

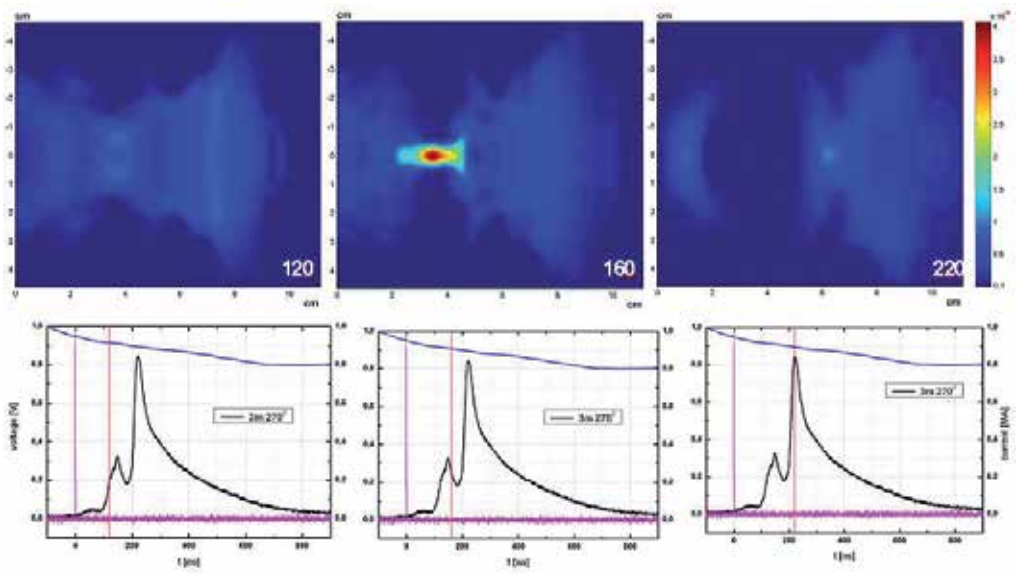

Fig.4.40. Distributions of electron concentrations reconstructed based on interferograms recorded at different points in time: 120; 160; and 220 ns after reaching the minimum of the current derivative dI/dt registered by the probe at the PF-1000 collector (top figure). Neutron pulses recorded by the scintillation probe positioned perpendicularly to the electrode axis at a distance of 3 m (lower figure). The red vertical line in lower figures corresponds to the moment of registration of the upper interferogram. Discharge No. 8406: D_2, p_0 = 240 Pa, U_0 = 24 kV, $Y_n \approx 9.0 \cdot 10^{10}$ n/pulse (Scholz et al., 2011)

The overview of experiments and their results described in this chapter was aimed at providing understanding of two basic topics related to thermonuclear fusion in the plasma focus of the PF-1000, namely:

- Why the scaling law $Y_n \sim I^4$ breaks?
- What physical phenomena observed in the plasma focus affect the performance of nuclear reactions occurring in them?

Measurements of the current in the focus using absolutely calibrated magnetic probes clearly demonstrated what the cause of violate the scaling law was, and showed that it is still valid as long as the total current in the PF system flows inside the plasma focus (pinch). It was also shown that the plasma temperature does not affect the course and nature of (D,D) fusion in the PF to such an extent that we should identify the nature of the reaction as thermonuclear. Nevertheless, the analysis of the conditions under which (D,D) nuclear reactions occur enables us to describe the physical phenomena which may be responsible for the relationship of $Y_n \sim I^4$.

5

THE NATURE OF THE FUSION REACTION IN THE PF SYSTEM – SUMMARY

In the previous chapter, we presented the results of measurements of the basic parameters of the plasma focus, and their changes during neutron emission. Our reflections on the process of nuclear fusion in deuterium plasma generated in the PF-1000 system will begin by assessing the possibility of explaining total neutron emission based on an assumption about the thermonuclear nature of this emission. Experimental data suggest that the first neutron pulse is emitted when the current sheath moving at a velocity of the order of 10^7 cm/s reaches the electrode axis, forming the plasma focus. A properly shaped focus is roughly the shape of a cylinder with a height of approximately 6 ÷ 8 cm and diameter of the order of 1 cm. The maximum concentration of plasma particles on the axis of the focus, as shown by the interferometric data, is approximately 10^{19} deuterons per cm^3, and the lifetime of this quiet phase is about 120 ns.

Ion temperature in the focus is the result of both the heating of ions at the shock front which is moving at a velocity of $v_r \sim 10^7$ cm/s, and the adiabatic heating of plasma, according to the formula $(T_1 / T_0) = (n_1 / n_0)^{\gamma-1}$, where T_0 - temperature of ions heated at the shock front, n_0 – initial density of deuterium corresponding to the pressure of deuterium in the vacuum chamber, and γ for deuterium is equal to 5/3. Given that the deuterium pressure in

the chamber p_0 = 240 Pa, n_0 would be about 10^{17} particles per cm^3, the compression about 100, and $T_1 \cong 21.5\ T_0$. If the velocity of the shock wave at the time it reaches the axis is of the order of 10^7 cm/s, the deuterium ion at the shock front acquires a thermal energy T_0 of the order of 40 eV. Thus, at the time of emission of the first neutron pulse at the plasma focus, we get: focus concentration $n_i \cong 10^{19}$ cm^{-3}; temperature $T_i \cong 0.86$ keV; radius of the focus $r_p \cong 0.5$ cm; and length of the focus $l_p \cong 8$ cm. This quiet stagnation phase lasts about $\tau \cong 100$ ns. If we assume that the emission in the first neutron pulse is of fusion nature, then by using the formula:

$$Y_n = \frac{n_D^2}{4}\langle\sigma v\rangle_{DD}\pi r_p^2 l_p \tau \quad , \tag{5.1}$$

for the parameters of the focus, we obtain emission value $Y_n \cong 2{\cdot}10^9$ n/pulse. The estimated value of the total emission is about 50 ÷ 100 times smaller than the measured value of approx. 10^{11} n/pulse, which roughly matches the data obtained using scintillation probes, where the first pulse is about 20 ÷ 80 times smaller than the second one.

The main neutron pulse appears approx. 160 ns after the formation of the plasma focus, and its maximum occurs in the phase of plasma expansion and the formation of a neck associated with an instability m = 0 (see Chapter 4, Fig. 4.40).

Let's assume as before that, in the case of the second pulse, the emission is also of thermonuclear nature. Here, emission can occur from the neck, or the rest of the plasma focus. Of course, this affects the values, which must be plugged into equation (5.1). If neutrons are emitted from the plasma neck, the concentration of deuterons is approximately $5{\cdot}10^{18}$ cm^3, and its radius and length as determined based on the interferogram is: $r_p \cong 0.4$ cm; and $l_p \cong 2$ cm (see, e.g. Chapter 4, Fig. 4.40). However, if the emission comes from the rest of the plasma focus, its size and the concentration of deuterons will be, respectively: $r_p \cong 2$ cm; $l_p \cong 4$ cm; and the concentration of ions will be approximately 10^{18} cm^{-3}. For these plasma parameters, if we want to obtain experimentally measured emissions at 10^{11} n/pulse from formula (5.1), regardless of the area of neutron emission, we should assume that the ion temperature has increased and remained at $T_i \geq 4$ keV.

The ion temperature of plasma is the hardly measurable and was not measured in experiments on the PF-1000. Aside from this, the results of its measurements in other PF systems were questionable and not very reliable. Therefore, we should check if the ion temperature $T_i \geq 4$ keV determined from the reaction rate based on formula (5.1) - for concentrations of plasma and neutron emission in the second pulse - measured in the experiment has a valid value. We can do this by estimating, for example, the mean free path for the ion–ion collision in the plasma focus expressed by the formula:

$$l_{ii} = 3 \cdot 10^{18}\frac{T_i^2}{n_i} \quad , \tag{5.2}$$

where l_{ii} is expressed in [cm], T_i in [keV], and n_i in [cm^{-3}].

For plasma focus parameters during the emission of the first neutron pulse, l_{ii} is of the order of 0.2 cm, which means that the mean free path of ions is less than the size of the plasma focus. Similarly, we can determine the mean free path of ions in the second pulse by assuming the temperature of ions to be 4 keV, and the plasma concentration to be $3 \cdot 10^{18}$ cm^{-3}, which results in a value of the order of several centimeters. In this case, the free path of ions greatly exceeds the size of the focus, and the plasma becomes collisionless due to the route of ions.

Similarly, by using the classical formula for the effective time between ion collisions:

$$\tau_{ii} = 2.95 \cdot 10^7 \frac{T_i^{3/2}}{n_{pl}\lambda} \quad , \tag{5.3}$$

where $n_{pl} = n_i = n_e$ is the plasma concentration in [cm^{-3}], T_i – ion temperature in [eV], and λ – Coulomb logarithm,

we can calculate this time throughout the maximum compression and stationary phase of the plasma focus (stagnation phase) during the emission of the first neutron pulse, as well as when plasma is expanding and a neck is created at the time of the development of instability m = 0. In the stagnation phase, for plasma concentration of the order of 10^{19} cm^{-3} and ion temperature of approximately 0.86 keV, the time of ion–ion collisions is about 7 ns, which is significantly shorter than the lifetime of this phase (about 100 ns). This confirms that the ionic component in this phase reaches thermal equilibrium. The electron temperature of plasma at the focus estimated from the measured X-ray spectrum of the helium-like argon ions (see Chapter 4) is lower than the ion temperature because mainly ions are heated, first in the shock wave, then as a result of adiabatic compression. The time it takes to reach thermal equilibrium between electrons and ions, as compared to the time for just ions, should be $(m_i/m_e)^{1/2} \cong 60$ times longer. This also means that the electrons do not reach the temperature of ions in the phases of the first compression and then stagnation.

For the second neutron pulse and the parameters of the focus during its lifetime, based on the value of ion temperature estimated using formula (5.1), we can determine the effective time of the ion–ion collision of the order of 0.25 μs based on formula (5.3), which exceeds the maximum lifetime of the plasma focus.

To sum up, we can say that the emission of the first pulse can be of thermonuclear nature as a result of the heating of ions with the shock wave and the adiabatic compression of plasma. However, as indicated by the analysis of characteristic collision times, the emission of the second neutron pulse is not of thermonuclear nature, and plasma is not in thermal equilibrium during this emission. The explanation of the nature of this emission requires a different perspective on the nature of fusion reactions in the plasma focus, as well as analysis of experimental data in terms of phenomena associated with the acceleration of ions to an energy of the order of dozens or even more than a hundred keV. Let us see what phenomena associated with the evolution of the plasma focus and current flow occur just before and during the emission of the second neutron pulse.

The experimental data presented in the previous chapter show that the emission of the second neutron pulse is accompanied by expansion of the plasma focus, during which instability m = 0 develops. As a result, the neck area, with a high compression of plasma, appears near the PF-1000 anode, which is reflected on the interferogram recorded at t_2 (see Chapter 4, Fig. 4.32). At this point, the radius of the neck is almost equal to the thickness of the skin layer, which means that the current is uniformly distributed therein. In the following instants, the current in the area inside a radius of r = 1.3 cm (position S1) drops rapidly with a relatively small change in the total current in the system, as measured by the Rogowski coil. In the area of a neck, the concentration plasma rapidly drops, reaching the level of the surrounding background. The second neutron pulse reaches the maximum at this moment. The decay of the conductivity current in the plasma focus, accompanied by a decrease in the plasma concentration around the anode in the vicinity of the electrode axis, with a simultaneous slight change of the total current flowing in the system, shows that the current flow changes the nature in the focus (pinch). In addition, a voltage pulse is observed at this time that amplitude of the pulse exceeds the charging voltage of the capacitor bank recorded in the PF system using the capacitive voltage probe. This may indicate that an area is formed in the plasma focus where streams of electrons and ions are generated and accelerated, i.e. a bipolar plasma diode is formed. Current is generated in this diode, first as an electron beam I_e, and then after stopping the electrons in the magnetic field, is maintained with the current of the ion beam - in this case, deuterons I_{wD}, with energies significantly higher than the mean thermal energy of deuterons in the plasma focus. Thus, the electron beam interacting with the plane of the anode is accompanied by the emission of hard X-rays in such a magnetically insulated plasma diode, and a beam of deuterons penetrating the plasma focus appears after the magnetization of electrons. We will try to demonstrate that a beam of deuterons generated in the diode, while interacting with the rest part of the plasma focus as a target, may be responsible for the second neutron pulse in the Plasma-Focus system.

To this end, we will try to estimate the size of the measured neutron emission. The mean distance travelled by the deuteron in a beam with an energy of E_{wD}, before the creation of a neutron as the result of fusion with a deuteron in the plasma target, is equal to:

$$L_{wf} = \frac{1}{\sigma(E_{wD}) n_{iD}} \quad , \tag{5.4}$$

where n_{iD} is the plasma concentration of deuterons in the focus, and $\sigma(E_{wD})$ - is the collision cross-section for the fusion reaction given in the formula (Huba, 2009):

$$\sigma(E_{wD}) = \frac{482}{E_{wD}\left[exp\left(47.88 E_{wD}^{-1/2}\right)-1\right]\left[(1.177-3.08\cdot 10^{-4} E_{wD})^2+1\right]} \cdot 10^{-24} \quad [\mathrm{cm}^2] \quad , \tag{5.5}$$

where E_{wD} is expressed in [keV].

In contrast, the maximum distance a deuteron in the beam can cover in the focus in the direction of its axis is equal to its length l. Thus, a deuteron in the beam is capable of generating l/L_{wf} neutrons in the plasma target as a result of the fusion reaction. The number of deu-

terons in the beam can be estimated based on knowledge of deuteron current in the beam:

$$N_D = I_{wD}\frac{\Delta\tau}{e} \quad , \tag{5.6}$$

where $\Delta\tau$ is the time of the existence of a plasma diode in which beams are generated, and e is the elementary charge.

Therefore, the total emission of neutrons in the second pulse will be:

$$Y_n = \frac{\Delta\tau}{e} I_{wD}\frac{l}{L_{wf}} \quad . \tag{5.7}$$

Replacement of the electron beam with the deuteron beam occurs simultaneously with the process of trapping electrons in the magnetic field in the area of the diode, which becomes possible if the cyclotron radius of the deuterons r_{cD}, accelerated in the diode, is larger than the distance between the virtual anode and the cathode of the diode ($r_{cD} > d$). In this way, first the current of the electron beam, and then the current of the deuteron beam, replaces the conduction current flowing in the plasma focus when the radius of the neck at the anode (Chapter 4, Fig. 4.32) reaches the thickness of the skin layer.

The cyclotron radius of accelerated deuterons can be expressed by the following formula:

$$r_{cD[cm]} = \sqrt{\frac{E_{wD}m_D}{2}}\frac{c^2 r_p}{eI_p} = \sqrt{\frac{m_D U}{2e}}\frac{c^2 r_p}{I_p} = 13{,}7\,\frac{r_{p[cm]}\sqrt{U_{[kV]}}}{I_{p[MA]}} \quad , \tag{5.8}$$

where r_p – radius of the of the plasma focus at the moment of maximum compression, I_p – amperage in the focus, c, m_D i e – speed of light, deuteron mass, and elementary charge, respectively. It is assumed that the energy of the deuteron in the beam is $E_{wD} = eU$, where U – the maximum value of the voltage amplitude measured by the capacitance probe (see e.g. Chapter 2, Fig. 2.3).

For experiments on the PF-1000, with the emission of neutrons at $Y_n \cong 10^{11}$ n/pulse, it is typical that $r_p \cong 0.4$ cm, $U \cong 50$ kV and $I_p \cong 1.4$ MA. Hence, the cyclotron radius of deuterons in the beam is $r_{cD} \cong 27.7$ cm, which is not only considerably more than the distance d, which is usually close to the diameter of the focus, but also the size of the plasma focus (pinch).

Since the condition $r_{cD} > d$ is true for the characteristic values occurring in the experiments on the PF-1000, we can assume that I_{wD} can replace the conductivity current I_p. Thus, we can use formula (5.7) to estimate the value of the emission of neutrons. Let's assume based on interferometric measurements that at the moment of the second neutron pulse, the concentration of deuterons in the focus is $n_D \cong 10^{18}$ cm^{-3}, and the focus length $l \cong 8$ cm, and as before, in experiments on the PF-1000 with an emission of neutrons at 10^{11} n/pulse, that the $I_p = I_{wD} \cong 1.4$ MA, and $E_{wD} = eU \cong 50$ keV. We can assume time $\Delta\tau$ by estimating the duration of the emission of the second pulse of neutrons at approximately 80 ns. For deuteron energy

$E_{wD} \cong 50$ keV, the collision cross section for the fusion reaction expressed by formula (5.5) is $\sigma(E_{wD}) \cong 4.71 \cdot 10^{-3}$ barn; therefore, $L_{wf} \cong 4.24 \cdot 10^{7}$ cm. By plugging these values into formula (5.7), we obtain:

$$Y_n \cong \frac{8 \cdot 10^{-8}}{1.60 \cdot 10^{-19}} 1.4 \cdot 10^{6} \frac{8}{4.24 \cdot 10^{7}} \cong 1.32 \cdot 10^{11} \quad , \tag{5.9}$$

The estimated value of the emission in the second neutron pulse based on the assumed diode model matches the experimental values in the order of magnitude. This means that the bipolar diode model used in (Scholz et al., 2002) to estimate the emission of deuteron streams from the focus, which was further developed in (Gribkov and Scholz, 2007), seems to explain the size of the primary neutron emission from the focus of the PF system, and thus the nature of the emission.

The results prompted us to examine the hypothesis about the role of the non-thermal component of deuterium ions which, when interacting with the plasma focus as a target, causes a high emission of neutrons, proving to the high yield of the nuclear fusion reaction in plasma. These epithermal ions occur when the current conductivity decreases in the focus (see Chapter 4, Fig. 4.32), which is related to the evolution of the plasma focus, i.e. the appearance of the neck at the PF system anode. According to the experimental results, we can see that the decrease in conductive current in the focus is time-related to the appearance of a second, primary neutron pulse. Analysis of the phenomena accompanying this decrease, often called „current disruption", has many features in common with the plasma diode model.

Based on this model, we can attempt to explain the character of (D,D) reactions in the PF focus, as well as determine the scaling law associated with the relationship between neutron emission, and the current flowing in the system. To this end, let us consider the energy propagation in the PF system. Knowing the following measured relationships: changes of current over time $I(t)$; voltage in the collector area $U(t)$; and inductance $L(t)$, we can find the total electromagnetic energy $W_c(t)$ supplied to the system during discharge. Let us write the energy balance equation, assuming that the total energy is lost to the magnetic field energy stored between the electrodes, the collector of the PF system, and the moving current sheath, and to the work done on the current sheath:

$$W_c(t) = \int_0^t I(\tau)U(\tau)d\tau = W_m(t) + W_{pl}(t) = \frac{1}{2}L(t)\,I^2(t) + [W_k(t) + W_{wew}(t)] \,, \tag{5.10}$$

where the energy consumed to perform work on the current sheath is lost to the kinetic energy W_k of the sheath, and its internal energy W_{wew}.

This energy balance shows that the energy stored in the magnetic field is the power source for the ion current beam, which is described by the Lorentz force law, meaning that the magnetic field tries to maintain its flow during the decaying of the conductivity current. This energy, proportional to the square of the current flowing in the focus, is passed on to the deuteron beam, and it is then expended on the production of neutrons in the process of

fusion of deuterium nuclei.

The second factor which contributes to the emission of neutrons from the focus is the concentration of deuterons in the plasma target which interacts with the beam. The concentration of plasma deuterons in the focus during gas sweeping, and then its confinement in the focus, depends in a similar way on the square of the amperage, and has a direct impact on the emission of neutrons, as can be seen in relationships (5.4 and 5.7).

Thus, we can conclude that in the deuterium fusion in the plasma focus is beam of ions which draws energy from the magnetic field proportional to I^2, and interacts with the plasma target, where the concentration of deuterons is also a function of I^2. Hence the simple conclusion that, as with neutron emissions of a fusion nature, we are dealing with the scaling of this emission in the fourth power of the current, $Y_n \sim I^4$.

The beam - plasma target interaction takes place in some types of tokamak systems, in which a beam of neutral deuterium (or tritium) atoms with energies of the order of 100 keV is shot into plasma produced in the tokamak. However, due to the long plasma confinement time in such devices, atoms of deuterium shot after the resonant charge exchange with plasma ions can not only react in fusion, but also transfer their energy to plasma electrons, and these in turn to ions, as the result of Coulomb collisions. This is a process of heating plasma to a temperature at which fusion reactions take place intensively.

Let us see how the process of heating the plasma target with the deuteron beam can affect the emission of neutrons from the PF system. As we know, a deuteron beam with an energy of E_{wD}, such that the following condition is satisfied:

$$\frac{m_e}{m_D}\frac{E_{wD}}{T_e} \ll 1 \quad , \tag{5.11}$$

where m_e, m_D, - the mass of the electron and deuteron, respectively, and T_e – electron temperature expressed in [eV],

is subject to braking, and loses its energy mainly by collisions with the electrons of the plasma target. The braking time of deuterons as a result of these collisions is given by the formula:

$$\tau_s^{i/e} = 6.25 \cdot 10^8 \frac{\mu T_e^{3/2}}{n_e Z^2 \lambda_{ie}} \quad , \tag{5.12}$$

where n_e – electron concentration in [cm^{-3}], T_e – temperature in [eV], Z – ion charge, λ_{ie} – Coulomb logarithm (typically assumed as $\lambda_{ie} \cong 10$ for these plasma parameters), and μ - the ratio of ion mass to the proton mass.

Using equation (5.12), we can determine the deuteron stopping distance with the energy E_{wD} in the plasma target of the electron concentration given by the formula:

$$l_s^{D/e} = \left(\frac{2E_{wD}}{m_D}\right)^{1/2} \tau_s^{D/e} \quad . \tag{5.13}$$

For the experimental conditions in the PF-1000 with the emission of neutrons at 10^{11} n/pulse, and plugging in values $T_e \cong 300$ eV, $n_e \cong 5 \cdot 10^{18}$ cm^{-3}, and $E_{wD} \cong 50$ keV to formulas (5.12) and (5.13), we obtain the value of the stopping distance: $l_s^{D/e} \cong 28.4$ cm. This value is much larger than the characteristic size of the plasma focus in experiments on the PF-1000; hence, we can neglect the stopping of the ion beam in the focus and its effect on the increase of the electron temperature in the first approximation. This means that heating the plasma target in these conditions with an ion beam has little effect on the emission of neutrons from the focus (pinch).

Given that the yield of the fusion in the plasma focus of the PF depends on two factors - the beam of accelerated ions, and the plasma target – it is appropriate to ask which one plays a major role in the production of neutrons from the fusion reaction. In the case of an ion beam, what counts is its energy (about 50 keV here) and the quantity relative to the total number of deuterons at the focus, which can be estimated from the relationship:

$$\xi = \frac{I_{wD}(\Delta\tau/e)}{n_{iD}\pi r_p^2 l} \quad , \tag{5.14}$$

where l and r_p is the length and radius of the focus, n_{iD} – concentration of plasma deuterons in the focus, I_{wD} – ion beam current, and $\Delta\tau$ – lifetime of the plasma diode.

For the above-mentioned experimental conditions in the PF-1000, the ratio ξ=1.3810^{-2}, which approximately matches the results of estimation of the ratio between the number of accelerated electrons, to the total number of electrons in the plasma focus carried out using the FLYCHK code based on measurements of the soft X-ray spectra for doping with helium-like argon ions from the focus.

However, in the case of the plasma target, the rate of the reaction depends on the concentration of plasma particles, the electron temperature, and the distance travelled by the accelerated deuteron in the target. Temperature of the target and electron concentration significantly affect the stopping distance of ions, and the transfer of energy to electrons, which could result in a rise in the temperature of plasma (both ions and electrons), and an increase in the share of fusion reactions in the total neutron emissions from the focus. In turn, the magnetic field may affect the distance in the target, and by causing the cyclotron motion of deuterons, this field can significantly increase its length in relation to L_{wf}.

Unfortunately, despite the fact that all of these factors can affect the yield of the fusion reaction, we cannot control them. However, we should be aware that, irrespective of the nature of the fusion reaction in the plasma focus, the reaction yield increases in the fourth

power of the amperage and, as shown by experiments on the **Z** system in the Sandia National Laboratories, USA, this relationship is maintained for an amperage of several MA (Coverdale et al., 2005).

A lot of attention was paid in Chapter 1 to the physical conditions which fuel should meet in a thermonuclear system in order to produce net energy. It is important to maintain the plasma in thermal equilibrium for a certain period of time, with the yield of fusion being such that the resulting energy produced is higher than the energy used for the production, heating, and confinement of the plasma at a given fuel density and temperature of the order of several dozens of keV .

This approach led to the conclusion that all systems based on the simple principle of an accelerated, external beam of ions (deuterons or tritons) with a plasma target have no future as reactors from the viewpoint of energy production. However, the research that we conducted on large PF systems lead to the conclusion that, under certain conditions, fast ions can appear directly in the same plasma as a result of accelerator mechanisms related to the development of instability. In addition, if the plasma electron temperature is sufficiently high, then the internal injection of fast ions leads to a sharp increase in the efficiency of nuclear fusion reactions. Such a situation exists in Plasma-Focus systems. Of course, we should not regard PF systems as fusion reactors, if only due to the fact that we cannot really control and influence the course of some processes in such pulse systems. However, the scaling law of the reaction yield with the current is maintained over a wide range of amperage values, and we now know why deviations from this law were observed in previously researched systems.

Future researchers might be interested in discovering the conditions under which we can best realize the following scheme: *an accelerated beam in plasma interacting with the plasma target at a high electron temperature*, as well as what kind of technical implementation of such a scheme is possible - not necessarily as a reactor but, for example, as a source of fast, high-intensity neutrons. Such research of PF systems in the future can provide much information necessary for this purpose.

LITERATURE

1. **Ananin, S.I., Vikhrev, V.V., Filippov, N.V. 1978.** Structure of the current shell in a Z pinch. *Sov. J. Plasma Phys. (United States, Engl. Transl.)*. 1978, Tom 4:2.

2. **Anderson, O.A., Baker W.R., Colgate, S.A., Ise J., Pyle R.V. 1958.** Neutron Production in Linear Deuterium Pinches. *Phys. Rev.* 1958, Vols. 110, Issue 6, p. 1375-1387.

3. **Arcymowich, L.A. 1963.** *Upravlaiemyie termoiadiernyie reakcji.* s.l.: Fizmatgiz, 1963. p. 143-214.

4. **Banaszak, A., Szydlowski, A., Sadowski, M.J., Jaskola, M., Korman, A., Paduch, M., Scholz, M., Schmidt, H. 2005.** Measurements of Fusion Protons Emitted from High-temperature Plasma by Means of Solid-state Nuclear Track Detectors. *Plasma 2005, Opole.* 2005.

5. **Basque, G., Jolas, A., Watteau J.P. 1968.** Comparision of a two-dimensional snowplough model with experiment. *Phys. Fluids.* 1968, Vol. 11, p. 1384-1386.

6. **Bennett, W.H. 1934.** Magnetically Self-focussing Streams. *Phys. Rev.* 1934, Vol. 45, p. 890.

7. **Bernard, A., Bruzzone, H., Choi, P., Gribkov, V., Herrera, J., Hirano, K., Krejci, A., Lee, S., Luo, C., Mezzetti, F., Sadowski, M., Schmidt, H., Ware, K., Wong, C.S., Zoita, V. 1998.** Scientific status of plasma focus research. *J. Moscow Phys. Soc.* 1998, Vol. 8, p. 93-170.

8. **Bernard, A., Coudeville, A. 1976.** Structure of Current Sheath and Fast-particle Beams in the Focus Experiment. *6th Int. Conf. on Plasma Phys. and Contr. Nuclear Fusion*. 1976, Vol. 3.

9. **Bernard, A., Coudeville, A., Garqonnet, J. P., Genta, P., Jolas, A., Landure, Y., de Mascureau, J., Nail, M. and Vezin, R. 1975a.** Microinstabilities Connected with Neutron Emission and Electromagnetic Radiation in the Plasma Focus. *Proc. of 7th European Conf. on Controlled Fusion and Plasma Physics. Lausanne, Switzerland, 1-5 Sept. 1975*. 1975, Vol. 1, p. 60.

10. **Bernard, A., Coudeville, A., Jolas, A., Launspach, J. and de Mascureau, J. 1975.**

Experimental Studies of the Plasma Focus and Evidence for Nonthermal Processes. *Phys. Fluids.* 1975, Vol. 18, p. 180-194.

11. **Bernstein, M.J., Hai, F. 1970.** Evidence for Nonthermonuclear Neutron Production in a Plasma Focus Discharge. *Phys. Letters.* 1970, Vol. 31A, p. 317.

12. **Bernstein, M.J., Meskan, D.A.,van Paassen H.L.L. 1969.** Space, Time and Energy Distribution of Neutrons and X-Rays from Focused Plasma Discharge. *Phys. Fluids.* 1969, Vol. 12, p. 2193-2202.

13. **Borowiecki, M., Czekaj S., Denus, S., Koziarkiewicz W., Socha R., Tomaszewski K., Zadrożny M. 1984.** The dynamics and plasma sheath structure in the plasma-focus device. *J. Tech. Phys.* 1984, Vol. 25, 3-4, p. 457-473.

14. **Borowiecki, M., Czekaj, S. Denus, S., Koziarkiewicz, W., Skrzeczanowski, W., Socha, R., Tomaszewski K., Zadrozny, M., Kaliski, S. 1985.** Influence of Insulator on Plasma-Focus Discharge. *Proc. of the 4th Int. Workshop on Plasma Focus and Z-pinch Research, 9-11 Sept., 1985, Warsaw, Poland.* 1985, pp. 86-89.

15. **Bostick, W.H., Grunberger, L., Prior, W. 1969.** Neutron Production by Vortex Annihilation in the Plasma Focus. *Proc. of the 3rd European Conf. on Controlled Fusion and Plasma Physics, Utrecht, The Netherlands, 23-27 June, 1969.* 1969, p. 120.

16. **Braginski, S.I. 1963.** Javlienia pierienosa v plazmie. *Voprosy Teorii Plazmy.* 1963, Tom 1, str. 183.

17. **Braginski, S.I., Migdal, A.B. 1958.** *Fizika Plazmy i Probliema Upravlaiemych Tiermojadiernych Reakcji.* 1958, Vol. 2, p. 20-25.

18. **Bruzzone, H., and Grondona, D. 1997.** Magnetic probe measurements of the initial phase in a plasma focus device. *Plasma Phys. Control. Fusion.* 1997, Vol. 39, p. 1315.

19. **Brzosko, J.S., Robouch, B. V., Klobukowska J. 1987.** A Macroscopic Study of the Neutron, Gamma- and X-ray Emissivity in the Frascati Plasma Focus. *Fusion Technology.* 1987, Vol. 12, p. 71.

20. **Coverdale, C.A., Deeney, C., Ruiz, C., et. al. 2005.** *32 IEEE International Conference on Plasma Science, Monterey, CA, 18-23 June. 2005*, p. 273.

21. **Czekaj, S., Koziarkiewicz, W., Skrzeczanowski, W., Socha, R. 1981.** Line radiation of highly ionized impurities in a plasma produced in the plasma-focus devices. *J. Tech. Phys.* 1981, Tom 22, 4, p. 455-462.

22. **Decker, G., Wienecke R. 1976.** Plasma focus devices. *Physica B+C.* 1976, Vol. 82, p. 155-164.

23. **Denus, S., Kaliski, S., Kasperczuk, A., Kowalski, S., Pokora, L., Sadowski, M. and Wereszczyński, Z. 1977.** Application of multiframe laser interferometry to the study of plasma dynamics in a plasma-focus device. *J. Tech. Phys.* 1977, Vol. 18, p. 381-394.

24. **Dyachenko, V.P., Imshennik, V.S. 1974.** Dvumierna magnetogidrodina-miczeskaia model plazmiennovo fokusa Z-pincha. *Voprosy Teorii Plazmy.* 1974, Tom 8, p. 164.

25. **Faenov, A. Ya., Pikuz, S.A., Erko, A.I., Bryunetkin, B.A., Dyakin, V.M., Ivanenkov, G.V., Mingaleev, A.R., Pikuz, T.A,. Romanova, V.M., Shelkovenko, T.A. 1994.** High-prformance x-ray spectroscopic device for plasma microsources investigations. *Physica Scripta.* 1994, Vol. 50, p. 333.

26. **Filippov, N.V. 1983.** Plasma-Focus Experiments at the Kurchatov Institute Moscow (Review). *Fizika Plasmy.* 1983, Vol. 9, 1, p. 25-44.

27. **Filippov, N.V., Filippova, T.I., Vinogradov, V.P. 1962.** Dense, high-temperature plasma in a noncylindrical 2-pinch compression. *Nuclear Fusion Supplement.* 1962, Tom Pt2, p. 577.

28. **Gamow, G., Teller E. 1938.** The Rate of Selective Thermonuclear Reactions. *Phys. Rev.* 1938, Vol. 53, p. 608-609.

29. **Glazyrin, I.V., Grabovski, E.V., Zukakishvili, G.G., et al. 2009.** *Problems of Atomic Science & Engineering (PASE), Ser. "Thermonuclear Fusion" (Rus. J.).* 2009, Tom 2, p. 67-82.

30. **Gourlan, C., Kroegler H., Maisonnier Ch., Rager J.P., Robouch B.V. and Gentilini A. 1979.** Recent Progress in 1-MJ Plasma Focus Dynamics and Scaling for Neutron Production. *Proc. 7th Int. Conf. on Plasma Physics and Controlled Nuclear Fusion Research, Innsbruck, Austria, 23-30 August 1978.* Nuclear Fusion suppl., 1979, Vol. II, IAEA-CN-37, p. 123-134.

31. **Gourlan, C., Kroegler, H., Maisonnier, C., Rager, J.P., Oppenlaender, T. 1978.** Measurement of current density distribution in a megajoule plasma focus device. *Proc. 8th European Conf. on Controlled Fusion and Plasma Physics, Prague, Czechoslovakia, September 19-23, 1977.* Ceskoslovenska Vedecko Technicka Spolecnost, 1978, Vol. 2, Invited and Supp. Papers, p. 247.

32. **Gribkov, V.A., Filippov, N.V. 1979.** *Preprint FI AN Sov. Union.* 1979, Vol. 94.

33. **Gribkov, V.A., Scholz, M. 2007.** Ustanowka plazmienogo fokusa mejzerowskoj geometriej eliektrodow PF-1000 dlia prowierki massztabirowanija osnownych proceccow w PF na megadżoulnom urownie enrgii. *Enciklopedia nizkotemperaturnoj plazmy.* 2007, Tom IX-3, Gława 4: Ustanowka plazmienogo fokusa, p. 145-175.

34. **Herold, H., Jerzykiewicz A., Sadowski M. and Schmidt H. 1989.** Comparative analysis of large plasma focus experiments performed at IPF, Stuttgart, and IPJ, Świerk. *Nuclear Fusion.* 1989, Vol. 29, 8, p. 1255-1266.

35. **Huba, J.D. 2009.** *NRL Plasma Formulary.* Washington : Beam Physics Branch, Plasma Physics Division, Naval Research Laboratory, 2009. p. 45. Vol. DC 20375.

36. **IPPLM. 1996.** IPPLM Report No 4183. 1996.

37. **Jäger, U. and Herold H. 1987.** Fast Ion Kinetics and Fusion Reaction Mechanism in the Plasma Focus. *Nuclear Fusion.* 1987, Vol. 27, 3, p. 407-423.

38. **Kasperczuk, A. 1984.** *Interferometric investigations of physical processes of generation and disintegration of the pinched plasma column in the PF-150 device.* Warszawa: Praca doktorska, IFPiLM, 1984.

39. **Khautiev, E. Yu., Krauz, V.I., et al. 1999.** Mechanizm of the Current Sheath Formation in the Plasma Focus Discharge. *Proc. XXIV Int. Conf. on Phenomena in Ionized Gases, July, 11-16, 1999, Warsaw, Poland.* 1999, Vol. V, p. 89-90.

40. **Kolesnikov, Yu.A., Filippov, N.V. and Filippova, T.I. 1966.** *Proc. of the 7th Int. Conf. on Ionisation Phenomena in Gases, Beograd.* Beograd, Gradevinska Knjiga Publishing House, 1966, Vol. 2, p. 833-837.

41. **Krauz, V., Mitrofanov, K., Scholz, M., Paduch M., Karpiński, L., Zielińska, E., Kubes, P. 2012.** Experimental study of the structure of the current heath on the PF-1000 facility. *Plasma Phys. Contr. Fusion.* 2012, Vol. 54, p. 02510.

42. **Krauz, V.I., Mitrofanov, K.N., Myalton, V.V., Khautiev, E.Yu., Mokeev, A.N., Vinogradov, V.P., Vinogradova, Yu.V., Grabovsky, E.V. and Zukakishvili, G.G. 2007.** Studies of Dynamics and Structure of Current Sheath on Plasma Focus Facility PF-3. *ECA, Proc. 34th EPS Conference on Plasma Phys. Warsaw, 2007.* 2007, Vol. 31F, p. P-1.018.

43. **Krauz, V.I., Mitrofanov, K.N., Myalton, V.V., Vinogradov, V.P., Vinogradova, Yu.V., Grabovsky, E.V., Koidan, V.S. 2011.** Dynamics of the Structure of the Plasma Current Sheath in a Plasma Focus Discharge. *Plasma Phys. Report.* 2011, Vol. 37, p. 742.

44. **Krauz, V.I., Mitrofanov, K.N., Scholz, M., Paduch, M., Kubes, P., Karpinski, L., and Zielinska, E. 2012a.** Experimental evidence of existence of the axial magnetic field in a plasma focus. *Europhysics Letters.* 2012, Vol. 98, p. 45001-1 - 45001-6.

45. **Lawson, J.D. 1957.** Some Criteria for a Power Producing Thermonuclear Reactor. *Proc. Phys Soc.* 1957, Vol. B70, p. 6.

46. **Lehner, G., Pohl, F. 1967.** Reaktionsneutronen als hilfsmitel der Plasma diagnostik. *Zeit. f. Physik.* 1967, Vol. 207, p. 83.

47. **Malinowska, A., Szydłowski, A., Malinowski, K., Sadowski, M., Scholz, M., Paduch, M., Ivanova-Stanik, I., Kubes, P. 2006.** Investigation of fusion-reaction protons from PF-discharges. *Czech. J. Phys.* 2006, Vol. 56 Suppl. B, p. B303-B308.

48. **Malinowska, A., Szydłowski, A., Sadowski, M.J., Żebrowski, J., Scholz, M., Paduch, M., Jaskóła M., Korman A. 2008.** Measurements of fusion-produced protons by means of SSNTDs. *Radiat. Meas.* 2008, Vols. 43, Suppl., p. S295-S298.

49. **Mather, J.W. 1965.** *Phys. Fluids.* 1965, Vol. 8, p. 366.

50. **—. 1971.** Dense Plasma Focus. *Methods of Experimental Physics.* 1971, Vol. 9, p. 187.

51. Maxon, S., Edellman, J. 1978. Two-dimensional magnetohydrodynamic calculations of the plasma focus. *Phys. Fluids.* 1978, Vol. 21, p. 1856.

52. Michel, L., Schonbach, K.H., Fisher, H. 1974. Neutron emission from a small 1 kJ Plasma Focus. *Appl. Phys. Letters.* 1974, 24, p. 57-59.

53. Mitrofanov, K.N., Krauz, V.I., Kubes, P., Scholz, M., et al. 2014. Study of the fine structure of the plasma current sheath and magnetic fields in the axial region of the PF-1000. *Plasma Physics Reports.* 2014, 40, p. 623.

54. Paduch, M., Socha, R., Tomaszewski, K. and Wereszczyński, Z. 1992. Optical diagnostics of a plasma-focus device. *Optical Engineering.* 1992, Vol. 31, 3, p. 453-457.

55. Pietrov, D.P. Filipov, N.V, et al. 1958. *Fizika Plazmy i Probliema Upravlaiemyh Tiermoiadiernyh Rieakcji.* 1958, Vol. 4, p. 170-181.

56. Pisarczyk, T., Paduch, M., Kasperczuk, A., Chodukowski, T., Scholz, M., Zielińska, E., Pisarczyk, P. 2009. Methodology of interferometric measurements for the elektron density determination in PF-1000 device. *Kudowa School of Plasma, 21 -25/09/2009.* 2009.

57. Pokora, L. 1980. *Based on laser diagnostics investigations of the dynamics of a plasma generated in laser-target experiments and in plasma-focus discharges.* Warszawa: Praca doktorska, 144 str., 1980.

58. Potter, D.E. 1971. Numerical studies of the plasma focus. *Phys. Fluids.* 1971, p. 1911.

59. Rager, J.P. 1981. The Plasma Focus. *Com. Naz. Energ. Nucl. Centr. Frascati.* 1981, 81.19/cc.

60. Sadowski, M., Scholz, M. 2008. The main issues of research on dense magnetized plasmas in PF discharge. *Plasma Source Sci. and Technology.* 2008, Vol. 17.

61. Sadowski, M.J., Scholz, M. 2009. Megajoule Plasma-Focus experiment; status and prospects. *Wykład zaproszony na ICPIG/Workshop on DMP, Cancun, July 2009.*

62. Schmidt, H., Kubes, P., Sadowski, M.J., Scholz M. 2006. Neutron Emission Characteristics of Pinch Dense Magnetized Plasma. *IEEE Trans Plasma Science.* 2006, p. 2363.

63. Schmidt, R., Herold, H. 1987. A Method of Time Resolved Spectroscopy on Short Pulsed Neutron Sources. *Plasma Phys. Contr. Fusion.* 1987, Vol. 29, p. 523.

64. Scholz, M. Bieńkowska, B., Ivanova-Stanik, L.M., Karpiński, L., Paduch, M., Tomaszewski, K., Zielinska, E., Kravarik, J., Kubes, P., Banaszak, A., Jakubowski, L., Sadowski, M., Szydłowski, A., Schmidt, H., Vitulli, S. 2004. Correlation between pinch dynamics, neutron, and X-ray emission from megajule plasma focus device. *Vacuum.* 2004, Vol. 76, p. 361-364.

65. Scholz, M. 2008. Megajoule Plasma-Focus Facility as a Generator of Intense Fast

Neutron Pulses. *Dense Z-pinches 2008, Alexandria, VA, USA, August 17-21, 2008.*

66. **—. 2011.** Progress of the MJ Plasma Focus Research. *Wykład zaproszony na konferencji Plasma 2011*, Warszawa. 2011.

67. **—. 2004.** The Physics of a Plasma Focus. *Wykład zaproszony na konferencji 21 SPPT 2004, Prague.* 2004.

68. **Scholz, M., Bieńkowska, B., Gribkov V. 2002.** Dense Plasma Focus for applications in PET. *Czech. Journal of Phys.* 2002, Vol. 52, D85.

69. **Scholz, M., Bieńkowska, B., Ivanova-Stanik, I., Karpiński, L., Miklaszewski, R., Paduch, M., Stępniewski, W., Tomaszewski, K., Sadowski, M.J. 2004.** The Physics of a Plasma-Focus. *Czech. Journal of Phys.* 2004, Vol. 54, Issue 3 Supp., p. C170-C185.

70. **Scholz, M., Karpiński, L., Krauz, V., Kubes, P., Paduch, M., Sadowski, M.J. 2012.** Progres in MJ plasma-focus research at IPPLM. *Nukleonika.* 2012, Vol. 57, p. 183.

71. **Scholz, M., Miklaszewski, R., Gribkov, V, Mezzetti F. 2000.** PF-1000 device. *Nukleonika.* 2000, Vol. 45, p. 155.

72. **Scholz, M., Stępniewski, W., Bieńkowska, B., Ivanova-Stanik, I., Miklaszewski, R., Paduch, M., Sadowski, M.J. and Tomaszewski, K. 2005.** Progres in Numerical Modelling of Plasma-Focus Discharge. *PLASMA 2005: Int. Conf. on Research and Applications of Plasmas, 6-9 September 2005 Opole-Turawa, Poland.* AIP Conf. Proc. 812, 2005, p. 57-63, doi:http://dx.doi.org/10.1063/1.2168798.

73. **Skrzeczanowski, W. 1990.** *Study on the structure and dynamics of a current sheath in a PF-20 device.* Warszawa: Praca doktorska, 191 str., 1990.

74. **Stępniewski, W. 2004.** MHD numerical modeling of the plasma focus phenomena. *Vacuum.* 2004, Vol. 76, p. 51.

75. **Tomaszewski, K., Miklaszewski, R., Kasperczuk, A., Paduch, M., Pisarczyk, T., Scholz, M. 2002.** Experimental arrangement for the plasma-focus PF-1000 device studies. *Czech. Journal of Physics.* 2002, Vol. 52 Suppl. D, D133.

76. **Vihriev, V.V., Braginski, S.I. 1980.** *Voprosy teorii plazmy.* 1980, Vol. 10, p. 251-318.

77. **Vlad, M. 1984.** A Time Resolving Spectrometry Method for Particles Emitted in Intense Burst. *Nucl. Instrum. Meth. in Phys. Res.* 1984, Vol. 227, p. 327.

78. **Volobuyev, I.V., Gribkov, V.A., Denus, S., Kalachev, N.V., Kozlova, T.A., Krokhin, O.N., Śledziński, S., Starcev, S.A., Czekaj, S. 1988.** Comparative soft X-ray emission characteristics of the Mather-geometry plasma-focus devices (in Russian). *Fizika Plazmy.* 1988, Vol. 14, p. 682-688.

79. **Zadrożny, M. 1990.** *Experimental and theoretical investigation on a discharge current division in a plasma-focus run-down and implosion chase.* Warszawa: Praca doktorska, 198 str., 1990.

80. Zielińska, E., Paduch, M., Scholz, M. 2011. Sixteen frame interferometer for a study of a pinch dynamics in PF-1000 device. *Contrib. Plasma Phys.* 2011, Vol. 51, p. 279.

ISBN 978-83-63542-56-6